A MEMORY-OPTIMIZED ARCHITECTURE FOR ECG SIGNAL PROCESSING

By

CHUNG-CHING PENG

A DISSERTATION PRESENTED TO THE GRADUATE SCHOOL
OF THE UNIVERSITY OF FLORIDA IN PARTIAL FULFILLMENT
OF THE REQUIREMENTS FOR THE DEGREE OF
DOCTOR OF PHILOSOPHY

UNIVERSITY OF FLORIDA

2011

I dedicate this dissertation to my parents, Chien-Feng Peng and Chiu-Chen Cheng, and my loving wife, Hsiao-Hsiang Hsu.

ACKNOWLEDGMENTS

I thank my advisor Dr. Jih-Kwon Peir for his unlimited support and encouragement both professionally and personally starting even before I came to USA. Under his guidance, I learned so much about research and academia in general and specifically computer architecture. During the darkest time of my journey, he reminded me to remain optimistic and never give up. I am eternally grateful.

My committee Dr. Harris, Dr. Wheeler, and Dr. Li, helped me throughout my research by providing valuable feedback. I am especially grateful for Dr. Harris's support during the difficult time when I changed my research direction.

Many labmates and friends in both CISE and ECE have helped me throughout the long period of time I spent at UF. Seonho Huang who graduated in 2007 taught me everything about ASIC design flow. Dr. Hong Yu who graduated in 2010 showed me the power of persistence on many occasions. Pawan Sabharwal, who was the co-author of many of my publications, helped me revise paper drafts and drew some of my chip layout. Zhiming Xiao, Chun-Ming Tang, Deepak Bhatia, Qiuzhong Wu, and Tanuj Aggarwal have helped me complete several chip designs and testing.

TABLE OF CONTENTS

page

LIST OF TABLES

LIST OF FIGURES

Abstract of Dissertation Presented to the Graduate School
of the University of Florida in Partial Fulfillment of the
Requirements for the Degree of Doctor of Philosophy

A MEMORY-OPTIMIZED ARCHITECTURE FOR ECG SIGNAL PROCESSING

By

Chung-Ching Peng

May 2011

Chair: Jih-Kwon Peir
Major: Electrical and Computer Engineering

Given an increasing demand for wearable personal healthcare devices, automatic heart beat monitoring device along with wireless interconnection is vital for providing real-time heart diagnostics and services. This dissertation investigates low-cost, automatic real-time architecture for electrocardiogram (ECG) beat classification. Based on the nature shape of human heart beat, Euclidean distance is used to detect and cluster the heart beats. The proposed architecture using a Heart Beat Cache, establishes a small table to dynamically capture and record recent heart beats. The information recorded in the cache provides necessary matching attributes to clustering the heart beats. To adapt the dynamic change of heart beat shapes, proper merging and aging of the recorded heart beats in cache increase the detecting accuracy as well as reduce the space requirement. With a small number of recorded heart beats, the proposed Heart Beat Cache consumes low power and can fit into small medical devices.

The proposed architecture was simulated in Matlab using the *MIT-BIH Arrhythmia Database*. We found that all the major beat types were successfully clustered and recognized. Based on the simulation results, the classification of normal beats shows consistent performance throughout 48 patients' data sets, with good average sensitivity (95.83%) and predictivity (89.92%). Among all abnormal beat types, premature ventricular contractions (PVCs) yield more

inconsistent results due to their larger shape variation and the possibility of PVCs in some records containing more than one shape type. Finally, the RTL implementation is developed and described. A cycle-based timing diagram for accessing the Heart Beat Cache is also analyzed.

CHAPTER 1
INTRODUCTION

The demand for wearable personal healthcare devices has recently risen significantly due to the advances in biomedical engineering, nanotechnology and microelectronics, and also due to the need for timely access to healthcare, medical information and medical resources. Wearable devices allow the monitoring of vital signs at home, and enable wirelessly transmitting of physiological data to a remote diagnostic center. Vital signs could include an electrocardiography (ECG) data, heart rate, temperature (skin or ambient), breathing rate, and both diastolic and systolic blood pressure.

Studies have shown that the number of people suffering from heart disease is rising [1]. In this work, we focus on monitoring the ECG signal, which is a crucial tool for cardiologists to diagnose the condition of a heart. For patients with heart problems, the occurrence of irregular heartbeats (arrhythmia) is an indication of potential heart failure requiring immediate treatment. Prevention of heart failure relies on constant tracking of the patients' vital signs and receiving a professional diagnosis based on those measurements in timely manner.

Traditional ECG holter systems record the signals continuously for to only 48 hours maximum, and only then the data is retrieved for analysis. Any events occurring outside these monitoring periods are missed. Also, the data is analyzed only after a considerable delay. To achieve a faster diagnosis and treatment, any cardiac event recorded should be forwarded automatically over the internet to physicians who have been immediately alerted by the system. Thus, it is necessary to design a system to recognize arrhythmia characteristics in real time. The identification of an arrhythmia event involves detecting heart beats automatically, discriminating abnormal beats from normal beats, and identifying the type of arrhythmia. Therefore, wireless

monitoring devices should integrate functions of signal sensing, real-time ECG signal processing and telemetry to other centralized devices that are connected to network.

Figure 1-1 demonstrates a next-generation wireless vital sign monitoring system. Devices can be either integrated with adhesive ECG sensor pads that are attached to the chest or implanted underneath the skin for measuring additional signals (such as blood pressure records). To reduce the power consumption for wireless transmission, bandwidth reduction, which only transmits the most important results, is required. The extracted signals can then be transmitted wirelessly to a larger handheld device containing more complex algorithms and wireless protocols. The handheld device processes several other vital signs' signals simultaneously, and in turn forwards necessary extracted information to the surrounding wireless network. Devices targeted for implantation have additional requirements for safety, reliability, and cost effectiveness. Most importantly, the devices need to have ultra-low power dissipation for a long battery lifetime and minimum size for wearability.

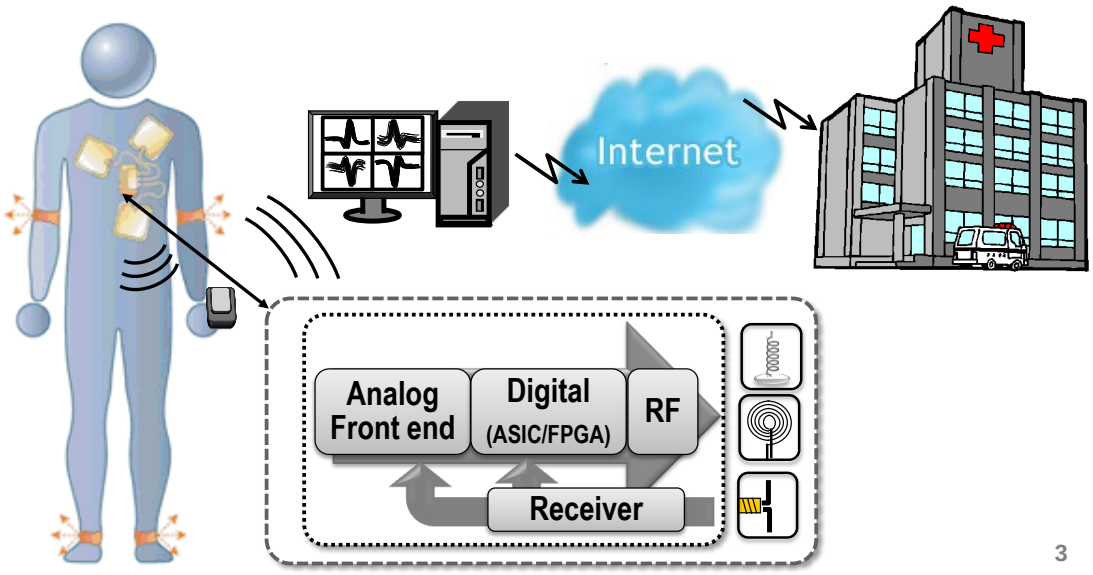

Figure 1-1. Block diagram of a wireless vital signs monitor system.

1.1 The ECG Signal

The electrocardiogram (ECG) measures the electrical activity of the heart, and is probably the most representative and noninvasive test to diagnose cardiac disorders. As Figure 1-2 shows, the ECG signal consists of a number of diagnostic critical segments or waves: the P-wave, the QRS complex, and the T-wave [2-5]. The P- wave is generated during the atrial depolarization, which occurs when the blood is squeezed from the atria to the ventricles.

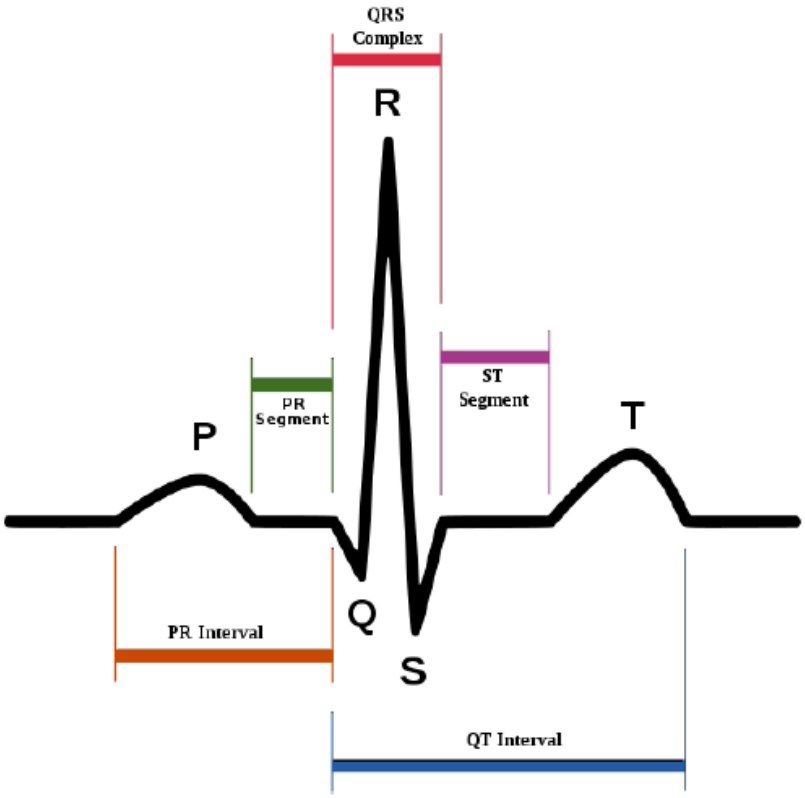

Figure 1-2. Schematic representation of normal ECG signal in sinus rhythm. Reproduced from [3].

The QRS complex, which can be decomposed into Q-, R-, and S-wave segments, is generated when the ventricles depolarize and squeeze the blood from the right ventricle to the aorta. The QRS complex has a period between 80ms and 120ms (longer than P-wave). However, not every QRS complex actually contains a Q-wave, an R-wave, and an S-wave; from Figure

1.3, it is clear that there are many variations of a QRS complex. The problem of QRS complex detection has been studied for several decades. A review of existing methods can be found in [6]. Finally, the T-wave is generated during the period of time when the ventricles repolarize in preparation for the next heart beat.

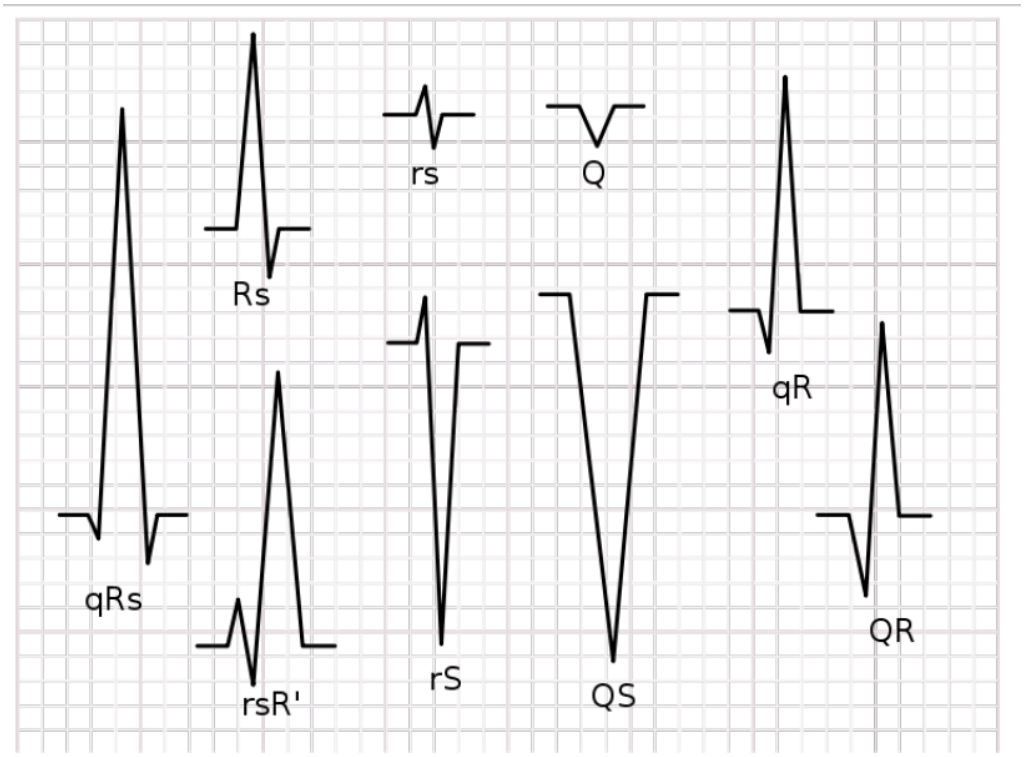

Figure 1-3. Nomenclature for different morphologies of QRS complexes. Reproduced from [3].

Critical information about the heart is obtained by studying the shape and size of the waves, the time between each wave, and the beat rate. In addition to these three basic waveforms, other segments and certain time intervals shown in Figure 1-2 also contain important information about heart conditions. The ST segment lasts from the end of the S-wave to the beginning of the T-wave, and corresponds to the period of ventricular depolarization. The PR segment represents the atrioventricular conduction time, which is used as a reference for

comparison with the ST segment. The QT interval represents the time of ventricular systole, and is measured between the beginnings of the Q-wave to the end of the T-wave [7].

1.2 Arrhythmia Recognition

An arrhythmia is an irregular heartbeat or abnormal heart rhythm and real-time diagnosis is crucial for high-risk cardiac patients. There are four main types of arrhythmias – premature beats, supraventricular arrhythmias, ventricular arrhythmias, and bradyarrhythmias [7]. Premature beats is the most common type of arrhythmias (Figure 1.5) and can be categorized into premature ventricular contraction (PVC) and atrial premature beat (APB), depending on their origin. With ECG data, PVC is characterized by abnormally shorter spacing between subsequent waves, while APB can usually be characterized by an early P-wave. In rare cases, an APB, just like a PVC, can trigger a more serious arrhythmia such as an atrial flutter or atrial fibrillation.

Rhythm	ECG Characteristics	Example
Normal Sinus Rhythm (NSR)	**Rate:** 60-100 per minute **Rhythm:** R-R – **P waves:** Upright, similar **P-R:** 0.12 -0 .20 second & consistent **qRs:** 0.04 – 0.10 second **P:qRs:** 1P:1qRs	

Figure 1-4. Normal heart beat [8].

Supraventricular arrhythmia is a fast heart rate that originates in the upper chambers (atria). The most common are atrial fibrillation or flutter and atrioventricular nodal reentry tachycardia. Likewise, ventricular arrhythmia is a fast heart rate originating in the lower chambers (ventricles). Bradyarrhythmia is a slow heart rate due to problems with the SA node's pacemaker ability, or else an interruption in electrical conduction through the natural electrical pathways of the heart.

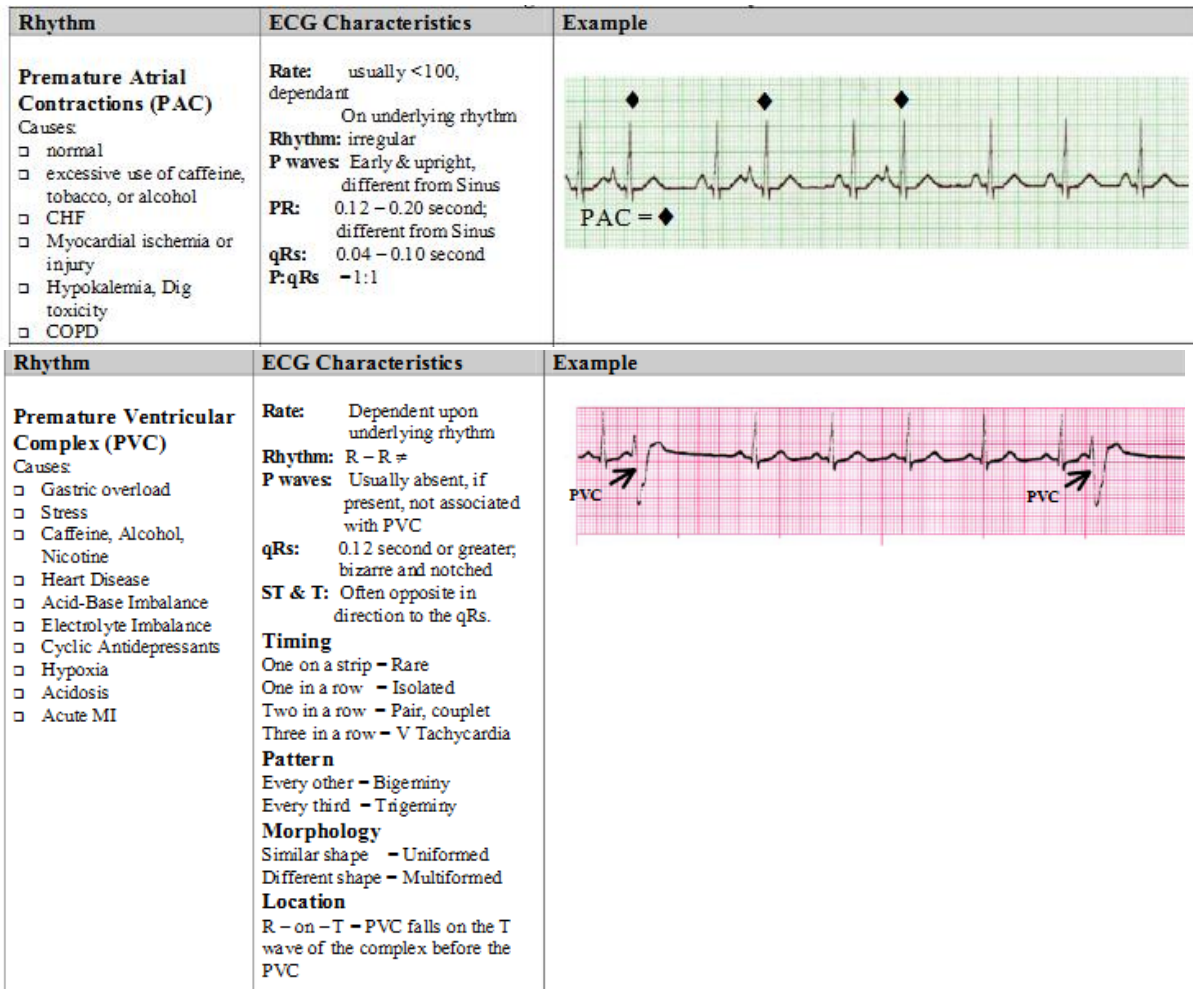

Figure 1-5. Examples of arrhythmia [8].

1.3 Current State-of-the-Art in Automatic Beat Classifier

Armato *et al*. have proposed a feasibility study and development of an arrhythmia recognition system using Kohenen Self-Organizing Map, a neural network method [2]. The algorithm was implemented into Xilinx Virtex-4 FX12, and used 90% of the FPGA resource. One drawback of their architecture is the large memory space required (estimated to be 73 KB). Another disadvantage is the need for offline training. Approximately 70% of the data sets from the *MIT-BIH Arrhythmia Database* were used for training, and the remainder was used for classification. Because training is not always an option for long-term vital signs monitoring in the home environment, another solution needs to be found.

Freescale Semiconductor and *Monebo Technologies* have jointly proposed an "ECG-on-a-chip" solution with the *Monebo* ECG software and *Freescale*'s microcontroller series combined [10]. The *Monebo* algorithm is able to handle a wide range of ECG applications, and targets various commercial platforms from workstations to microcontrollers. The minimum memory size required is 18 KB. In the hierarchy of next-generation vital signs monitoring systems, this solution can serve as part of the centralized processing unit in a handheld device, and thus provide in-depth analysis whenever abnormal beats are detected.

Besides the above-mentioned hardware approaches, there are many existing software algorithms for automatic beat classification, including linear discriminants [11], back-propagation neural networks [12], and learning vector quantization [13]. However, they are usually used for the clinical instruments, where the high computation complexity and the large memory capacity are available.

1.4 Motivation

Although clinical instrument allows more sophisticated algorithms to improve the accuracy, it is becoming increasingly necessary to use the portable medical devices with stringent power constraint. This is because rising healthcare costs combined with a more longer-living population has created demand for new applications and therapies relying on portable medical devices that are wirelessly linked to base stations. However, there are several challenges in the development of automatic beat classification algorithms and their implementations, the most critical one being the trade-off between algorithmic complexity and power consumption.

The leakage power becomes increasingly significant in deep sub-micron technologies. With the low operating frequency typical for ECG processing applications, the dynamic power is not as dominant as the leakage power. Static random access memory (SRAM) often contributes a

large part to the leakage power consumption; therefore a memory-optimized architecture is essential to reduce the total power consumption.

Another challenge of automatic heart beat classification is the variability in ECG readings between people, and even different measurement form the same person. Although different types of arrhythmias have characteristics which are common to all patients, a training process is still required for most of the algorithms to accommodate the inherent variability. Still, an unsupervised ECG monitoring system is preferred for the home environment.

The goal of this work is thus to design a memory-optimized architecture for next-generation wireless ECG telemetry, that does not require supervised training. In the previous sections we have seen that a digital ECG processor plays an important role in wearable healthcare devices. The cornerstone of this work is to transform complicated beat classification algorithms (usually implemented in software) into hardware-friendly operations.

This study has three aims. First, we seek to develop a low-power, real-time online digital beat classification architecture that not only achieves transmission bandwidth as low as the QRS detector, but also enables on-chip real-time ECG data analysis. Second, we investigate the nature of ECG signals and outline the required hardware properties for a fully unsupervised and automated ECG processor implementation. Third, we attempt to provide an ECG signal processing platform capable of partially identifying heart failure symptoms based on beat classification.

1.5 Dissertation Structure

The dissertation proposal is organized as follows. Chapter 2 provides the introduction and performance comparison for both fixed-threshold algorithm and Pan-Tompkins algorithm for QRS detection.

Chapter 3 observes the clustering properties of heart beats through analytical tools such as Euclidean distance distribution and PCA. Then, the temporal properties of the heart beat shape changes is demonstrated.

Chapter 4 explores energy saving architectures for online beat classification that do not sacrifice performance. A low-power architecture for real-time online beat classification is proposed. It does not require any training period and has the capability to quickly respond to changing beat shapes.

Chapter 5 presents an implementation of a single-channel self-contained ECG processing architecture which consists of the QRS spike detector and beat classifier presented in Chapters 2 and 3. The proposed VLSI architecture was implemented in register transfer level (RTL) and functionally verified using ECG data sets.

Chapter 6 gives conclusive comments and the direction for future works that can further improve the performance of the proposed single-channel ECG processor architecture.

CHAPTER 2
QRS COMPLEX DETECTION

2.1 QRS Complex

For an automatic ECG diagnosis algorithm, retrieving characteristic points is essential. The QRS complex is the most significant characteristic waveform set of the cardiac cycle and corresponds to the depolarization of the ventricles in the heart. The position, duration and shape of the QRS complex provide important information about the performance of the heart. The accuracy of a QRS complex detection algorithm is determined by the number of correctly detected beats (as opposed to false positives or missed beats). False detections can result in an incorrect diagnosis (such as heart rate variability). This is a significant problem since ECG recordings may contain noise, sudden changes in QRS amplitudes, and muscle artifacts [32].

Many algorithms have been proposed for QRS complex detection; an overview and comprehensive performance evaluations are described in [6]. General approaches employ techniques such as threshold crossing, single derivatives, digital filters, adaptive and matched filters, template correlation, frequency domain analysis, *maximum a posteriori* (MAP) estimation methods, and the hidden Markov model. For real-time analysis, derivative-based algorithms, with relatively inexpensive computations, are often preferred. These algorithms do not require

Table 2-1. Overview of the QRS detection algorithms in the literature [6].

Algorithm Types	Most Referred Works (Software)	Implementation (Hardware)	Computation Complexity
Threshold-Crossing	Miller *et al*. (1971)	Zemva (2007) --*Xilinx Virtex II*	Low
Derivative-Based	Pan-Tompkins (1985) Hamilton-Tompkins (1986)	Shukla (2008) --*Xilinx Spartan*	Low
Wavelet-Based	Mallat & Hwang (1992)	In *et al*.(2008) --*Xilinx SysGen*	Medium
Neural Network	Hu *et al*.(1993)	De Rossi(2009) --*Xilinx Virtex-4*	High
Hidden Markov Models	Briller *et al*.(1990)		High

training or modifications specific to each patient. Other algorithms borrow ideas from pattern recognition and neural network field [33]. More recently, wavelet transform methods have been used for QRS detection in recent years [11], which exploits the time-frequency properties of each ECG wavelet. The disadvantages of wavelet methods are poor performance due to the sensitivity to the onset and the offset step.

Real-time QRS detector can be considered to be the first step toward an automatic ECG analysis system. In this work, we seek to adopt a QRS detection algorithm from the literature with low hardware complexity and reasonable detection accuracy. Table 2-1 categorized different QRS detection approaches including the representative works as well as their hardware implementation. Only until recent years, people started to implement these software algorithms into hardware [60-61]. It is clear that threshold-crossing and derivative-based approaches have lower hardware complexity compared to others. Therefore, the purpose of this chapter is to compare the performance of the representative works from these two approaches and discuss the tradeoff between performance and hardware cost.

In threshold crossing approach, we used an algorithm *Thresholding* with the threshold being the mean value of the signals added with 3 times of standard deviation value. In derivative-based approach, we used a well-established QRS detection algorithm *Pan-Tompkins* proposed by Pan and Tompkins in 1985 [43]. The *Pan-Tompkins* algorithm has a high accuracy for various beat morphologies, and has been widely used in the past decades [6].

The *MIT-BIH Arrhythmia Database* is a popular choice for evaluation of QRS complex detection algorithms because of its ease of use and popularity [59]. We will use the same ECG data sets from this database to simulate both the *Thresholding* and *Pan-Tompkins* algorithms in Matlab. Then, the performance comparison will be carried out.

2.2 QRS Detection System

For both *Thresholding* and *Pan-Tompkins* algorithms, there are two stages in the algorithmic structure: a preprocessing feature extraction stage and a decision stage. The first stage includes linear filtering and a nonlinear transformation, while the second stage includes peak detection and a set of decision logic for QRS detection. A basic flow diagram is given in Figure 2.1.

2.2.1 Preprocessing Feature Extraction Stage

During the preprocessing stage the signal is filtered, its derivative is calculated, it is squared and then integrated by a moving-window algorithm. The preprocessing formulas listed in this section are taken from the *Pan-Tompkins* algorithm [43], as they are commonly used signal processing techniques. The output waveforms from each processing step are generated using Matlab and shown in Figure 2.3.

A heart beat is defined between two R-waves. The typical frequency range of the QRS complex is from 10 Hz to 25 Hz. To suppress other signal components and noise sources (such as power-line interference), a band-pass filter is required prior to the actual detection. The band-pass filter consists of a high-pass filter and a low-pass filter. The high-pass filter reduces the presence of P- and T- waves and baseline drift, while the low-pass filter removes artifacts.

The transfer function of the second-order low pass filter is

$$H(z) = \frac{1}{32}\frac{(1-z^{-6})^2}{(1-z^{-1})^2}.$$

and its difference equation is

$$y(n) = 2y(n-1) - y(n-2) + \frac{1}{32}[x(n) - 2x(n-6) + x(n-12)].$$

The cutoff frequency is about 20Hz and the gain is 36, and the filter processing delay is 6 samples.

The transfer function of the high pass filter is

$$H(z) = z^{-16} - \frac{1}{32}\frac{(1-z^{-32})}{(1-z^{-1})}.$$

while its difference equation is

$$y(n) = y(n-1) + x(n) - x(n-32).$$

The low cutoff frequency of this filter is about 5 Hz and the gain is 32.

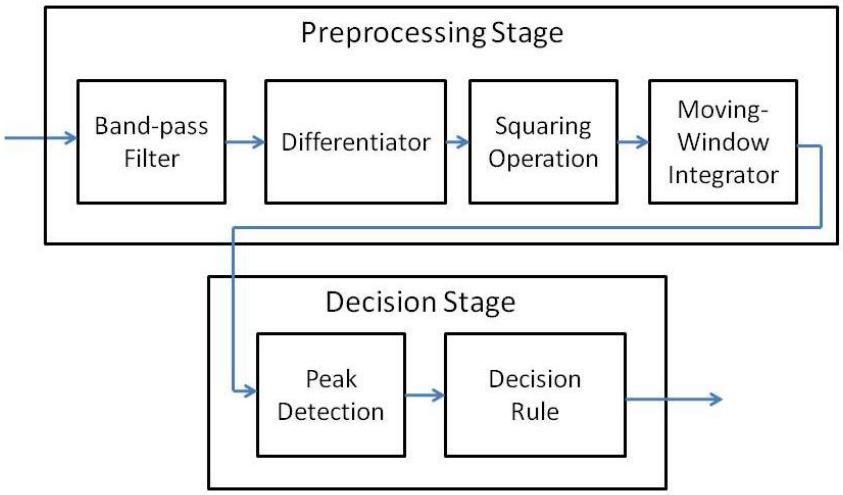

Figure 2-1. Basic flow diagram for *Thresholding* and *Pan-Tompkins* algorithms.

The differentiator further suppresses the low-frequency P- and T-waves, and provides a large gain to the high-frequency components arising from the steep slopes of the QRS complex.

The transfer function of the five-point differentiator is

$$H(z) = \frac{1}{8}(-z^{-2} - 2z^{-1} + 2z^{1} + z^{2})$$

Its difference equation is

$$y(n) = \tfrac{1}{8}[2x(n) + x(n-1) - x(n-3) - 2x(n-4)].$$

Squaring is a nonlinear operation that forces a positive result and emphasizes large differences resulting from the QRS complexes. In addition, small differences from P- and T-waves are suppressed.

$$y(n) = x(n)^2.$$

Multiple peaks are generated from the previous derivative-based operation within the duration of a single QRS complex. Integration smoothes these peaks with a moving-window integration filter.

$$y(n) = \frac{1}{N}[x\big(n-(N-1)\big) + x\big(n-(N-2)\big) + \cdots + x(n)].$$

2.2.2 Decision Stage

For the *Threhsolding* algorithm, the decision stage simply compares the band-pass filtered signal with the previously calculated threshold, which is defined to be the mean value of the signals added with three times of standard deviation value.

For the *Pan-Tompkins* algorithm, there are more steps involved. The peak detector compares the signal with two adaptive thresholds (T1 and T2), which are updated after each detected beat based on some criteria. T1 is set for the filtered ECG, and T2 is set for the signals produced by the moving window integration. Thresholds T1 and T2 are continuously updated after every beat to adapt to the rises and falls of the R-wave peak amplitudes. Processing delays are considered when estimating the average R-R intervals. If an R-wave is not detected after the maximum time interval, the algorithm will repeat the search to find a possible R wave candidate by using a new set of lower thresholds. More details are given in [43] about how to configure the two thresholds and implement the decision rules algorithms using a Matlab simulation.

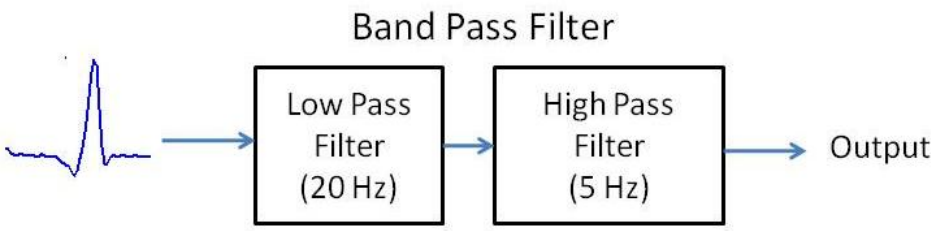

Figure 2-2. Block diagram of the band pass filter.

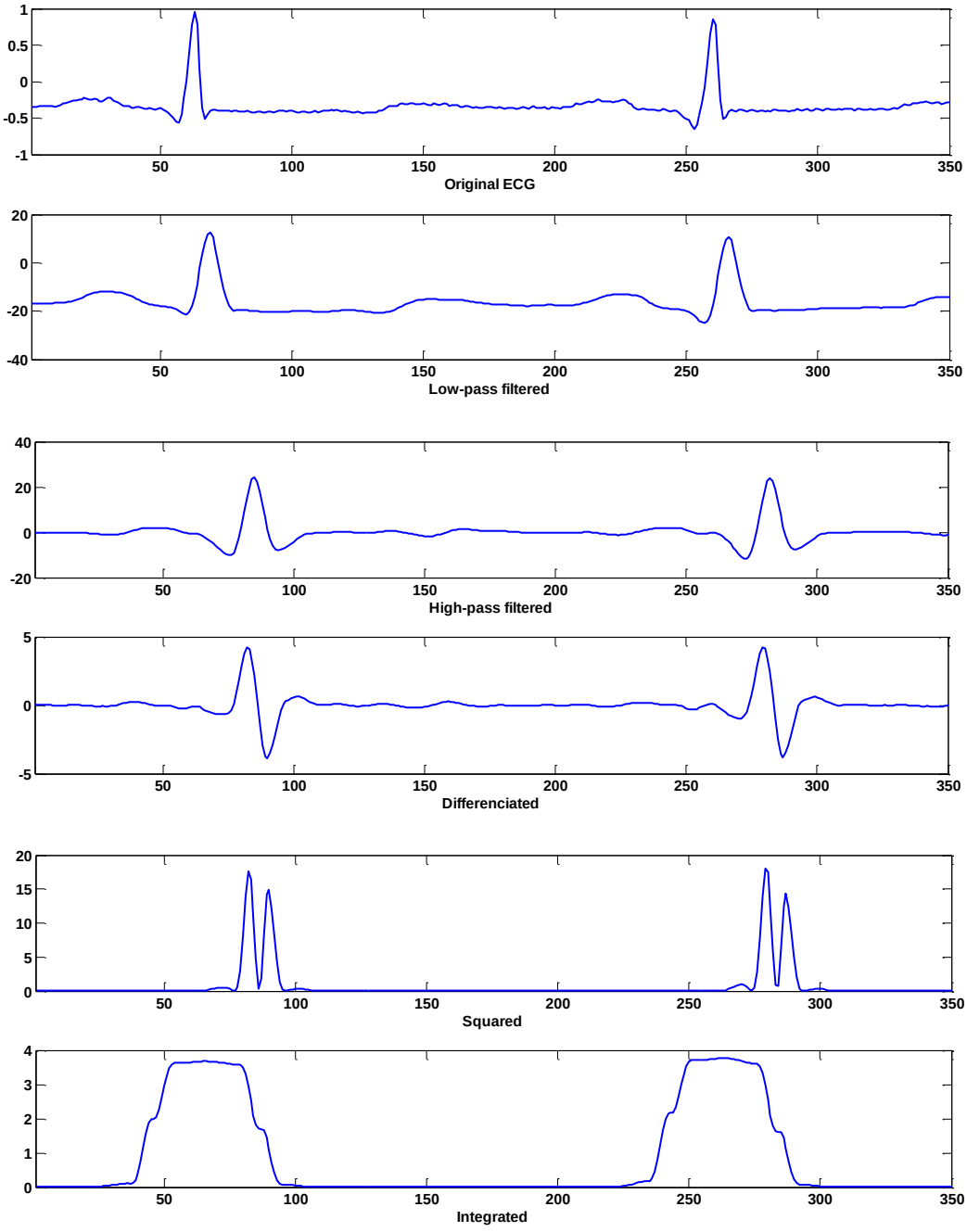

Figure 2-3. Matlab simulation results of the preprocessing stage using *MIT-BIH Arrhythmia Database*. From top to bottom: two cycles of a ECG signal; output of the low-pass filter; output of high-pass filter; output of the derivative-based operator; output of the squared signal; and the result of the final integrator.

2.3 MIT-BIH Arrhythmia Database

Assessing the quality of different QRS detection algorithms is often difficult due to the lack of an ECG data set with known annotations, which label the characteristics of the actual heart beats.

2.3.1 Introduction

The *MIT-BIH Arrhythmia Database* is a collection of holter recordings obtained by the *Beth Israel Hospital Arrhythmia Laboratory* between 1975 and 1979. The patient records are listed in Table 2-2. A sample plot from the database is shown in Figure 2.4. The recordings were taken from 48 patients, who were 25 men (aged 32 to 89 years) and 23 women (aged 23 to 89 years). Each recording is 30 minutes long with a sampling rate of 360 Hz and 11-bit resolution over a 10 mV range. The MIT-BIH Database is frequently used for evaluating the performance of QRS complex detection and beat classification algorithms. We used this database because it is widely used (more than 500 citations) and easier to compare the results with other works.

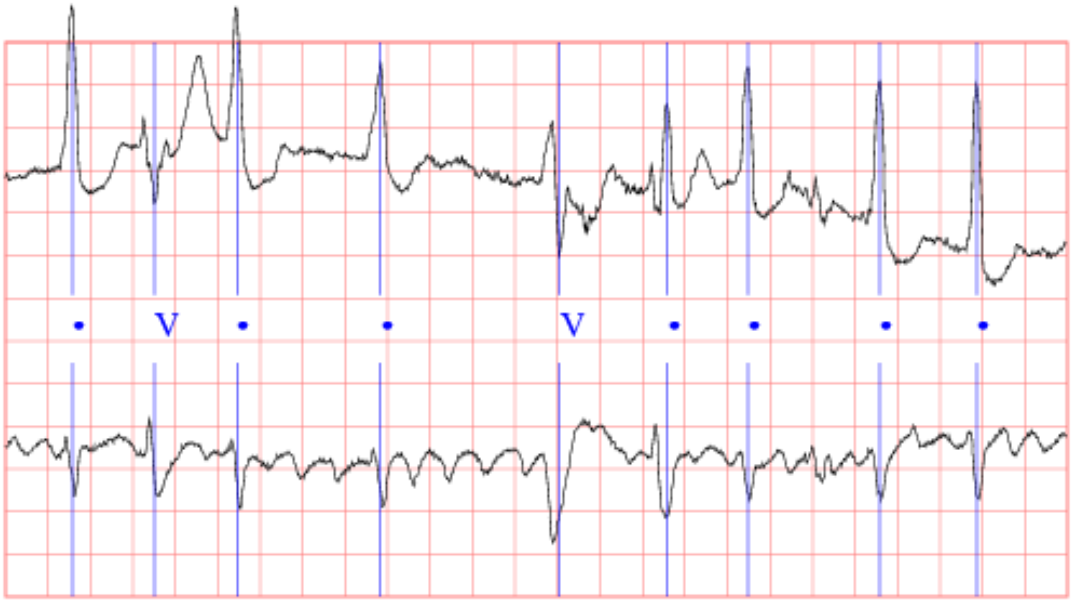

Figure 2-4. Sample ECG plot in *MIT-BIH Arrhythmia Database*.

Table 2-2. Patient records in the *MIT-BIH Arrhythmia Database*. (*) indicates Paced Beats; (**) indicates Left Bundle Branch Block; (***) indicates Right Bundle Branch Block.

Record	Record Patient	Normal / Paced / BBB	Special (PVC ..etc)	Record	Record Patient	Normal / Paced / BBB	Special (PVC ..etc)
100	Male, age 69	2239	34	200	Male, age 64	1743	861
101	Female, age 75	1860	5	201	Male, age 68	1625	375
102	Female, age 84	2028(*)	4	202	Male, age 68	2061	75
103	Male, age N/A	2082	2	203	Male, age 43	2529	451
104	Female, age 66	1380(*)	20	205	Male, age 59	2571	85
105	Female, age 73	2526	46	207	Female, age 89	1543(**)	789
106	Female, age 24	1507	520	208	Female, age 23	1586	1369
107	Male, age 63	2078(*)	59	209	Male, age 62	2621	384
108	Female, age 87	1740	35	210	Male, age 89	2423	227
109	Male, age 64	2492(**)	40	212	Female, age 32	2748(***)	0
111	Female, age 47	2123(**)	1	213	Male, age 61	2641	610
112	Male, age 54	2537	2	214	Male, age 53	2003(**)	259
113	Female, age 24	1789	6	215	Male, age 81	3195	168
114	Female, age 72	1820	59	217	Male, age 65	1786(*)	422
115	Female, age 39	1953	0	219	Male, age N/A	2082	205
116	Male, age 68	2302	110	220	Female, age 87	1954	94
117	Male, age 69	1534	1	221	Male, age 83	2031	396
118	Male, age 69	2166(***)	122	222	Female, age 84	2062	421
119	Female, age 51	1543	444	223	Male, age 73	2029	576
121	Female, age 83	1861	2	228	Female, age 80	1688	365
122	Male, age 51	2476	0	230	Male, age 32	2255	1
123	Female, age 63	1515	3	231	Female, age 72	1568(***)	5
124	Male, age 77	1531(***)	88	232	Female, age 76	397(***)	1383
				233	Male, age 57	2230	849
				234	Female, age 56	2700	53

2.3.2 Annotations

For each record, annotations were recorded by two cardiologists working independently. They noted detector missed beats, rhythm labels, signal quality labels, abnormal beats and comments. The types of annotation are listed in Table 2.3.

2.4 Matlab Simulations Results

2.4.1 Simulation Setup

First, a program reads in the selected ECG data sets and their attributes from the *MIT-BIH Arrhythmia Database* to Matlab workspace. Then, the data is re-sampled from 320 Hz to 250Hz,

and Matlab functions implemented for the *Thresholding* and *Pan-Tompkins* algorithms are executed. Finally, the QRS detection results are compared against the ground truth (annotations) to evaluate the performance.

Table 2-3. Heart beat annotations appearing in the *MIT-BIH Arrhythmia Database*.

Index	Beat Types	Index	Beat Types
1	Normal Beat	22	Comment annotation
2	Left bundle branch block beat	23	Measurement annotation
3	Right bundle branch block beat	24	P-wave peak
4	Aberrated atrial premature beat	25	Left or right bundle branch block
5	Premature ventricular contraction	26	Non-conducted pacer spike
6	Fusion of ventricular and normal beat	27	T-wave peak
7	Nodal (junctional) premature beat	28	Rhythm change
8	Atrial premature contraction	29	U-wave peak
9	Premature or ectopic supraventricular beat	30	Learning
10	Ventricular escape beat	31	Ventricular flutter wave
11	Nodal (junctional) escape beat	32	Start of ventricular flutter/fibrillation
12	Paced beat	33	End of ventricular flutter/fibrillation
13	Unclassifiable beat	34	Atrial escape beat
14	Signal quality change	35	Supraventricular escape beat
15	Not specified	36	Not specified
16	Isolated QRS-like artifact	37	Non-conducted P-wave (blocked APB)
17	Not specified	38	Fusion of paced and normal beat
18	ST change	39	Waveform onset
19	T-wave change	40	Waveform end
20	Systole	41	R-on-T premature ventricular contraction
21	Diastole		

2.4.2 Detection Accuracy

Essentially, we are interested in how well the algorithm performs in discriminating normal beats from abnormal beats and recognizing different types of abnormal beats. There are several

terms defined for serving this purpose. *TP* (true positives) is the number of correct detections. *FP* (false positives), sometimes called *false alarms*, is the number of incorrect detection. *FN* (false negatives), sometimes called *misses*, is incorrect miss-detection. For each beat type, the performance is measured using the following parameters:

$$\text{Sensitivity} = \frac{TP}{TP + FN}$$

$$\text{Positive Predictivity} = \frac{TP}{TP + FP}$$

Sensitivity is defined as the amount of correctly detected beats for each annotated beat. Positive Predictivity is the probability that a positive detection is correct. Note that the total number of annotated beats is the sum of *TP* and *FN*, and the total number of detected beats is the sum of *TP* and *FP*.

2.4.3 Discussions

Tables 2-4 and 2-5 list the simulation results for *Pan-Tompkins* and *Thresholding* algorithms using record #100 to #124 in *MIT-BIH Arrhythmia Database*. For some records, the detection accuracy is too low due to a misalignment of the positions sequence calculated by the algorithm in comparison to the annotation files. To correct these errors, human visual inspection and manual annotation position change is required, which is a time consuming task. Therefore, we eliminated these records in the subsequent performance comparisons.

Figure 2-5(a) shows the sensitivity comparison between these two algorithms. Among 14 records, *Pan-Tompkins* algorithm outperforms the *Thresholding* algorithm in 9 records. This is because there are more missed R-peaks using *Thresholding*, causing large FN number. In *Pan-Tompkins* algorithm, the search-back logic using lower second threshold reduces the number of missed R-peaks.

Table 2-4. QRS detection results using the Pan-Tompkins algorithm (Records #100 - #124).

Record	Annotated Beats	Detected Beats	TP	FP	FN	Sensitivity TP/(TP+FN)	Predictivity TP/(TP+FP)
100	2273	2252	2028	224	245	89.22%	90.05%
101	1874	1834	1747	87	127	93.22%	95.26%
102	2191	2248	1767	481	424	80.60%	78.60%
103	2090	2154	2052	102	38	98.18%	95.26%
104	2310	1736	1571	165	739	68.01%	90.50%
105	2691	2553	868	1685	1823	32.23%	34.00%
106	2098	1982	1306	676	792	62.25%	65.89%
107	2140	2315	2023	292	117	94.53%	87.39%
108	1824	2374	1459	915	365	79.99%	61.46%
109	2534	2652	1496	1156	1038	59.04%	56.41%
111	2133	2025	1978	47	155	92.73%	97.68%
112	2549	2704	1458	1246	1091	57.20%	53.92%
113	1795	2059	1752	307	43	97.60%	85.09%
114	1890	1222	1047	175	843	55.40%	85.68%
115	1961	2178	1922	256	39	98.01%	88.25%
116	2420	2650	1565	1085	855	64.67%	59.06%
117	1538	1526	1235	291	303	80.30%	80.93%
118	2301	2139	1734	405	567	75.36%	81.07%
119	2094	1910	1140	770	954	54.44%	59.69%
121	1875	2012	1826	186	49	97.39%	90.76%
122	2478	2439	1114	1325	1364	44.96%	45.67%
123	1519	1924	774	1150	745	50.95%	40.23%
124	1633	1624	1405	219	228	86.04%	86.51%

Table 2-5. QRS detection results using Thresholding method (Records #100 - #124).

Record	Annotated Beats	Detected Beats	TP	FP	FN	Sensitivity TP/(TP+FN)	Predictivity TP/(TP+FP)
100	2273	2270	1888	382	385	83.06%	83.17%
101	1874	1863	1853	10	21	98.88%	99.46%
102	2191	1820	1787	33	404	81.56%	98.19%
103	2090	2075	2025	50	65	96.89%	97.59%
104	2310	1051	967	84	1343	41.86%	92.01%
105	2691	2517	215	2302	2476	7.99%	8.54%
106	2098	1735	1258	477	840	59.96%	72.51%
107	2140	1966	1951	15	189	91.17%	99.24%
108	1824	1255	1208	47	616	66.23%	96.26%
109	2534	2372	134	2238	2400	5.29%	5.65%
111	2133	1854	1841	13	292	86.31%	99.30%
112	2549	2536	25	2511	2524	0.98%	0.99%
113	1795	1792	1761	31	34	98.11%	98.27%
114	1890	608	569	39	1321	30.11%	93.59%
115	1961	1948	1921	27	40	97.96%	98.61%
116	2420	1927	730	1197	1690	30.17%	37.88%
117	1538	1532	1527	5	11	99.28%	99.67%
118	2301	2220	1592	628	709	69.19%	71.71%
119	2094	1984	1158	826	936	55.30%	58.37%
121	1875	1858	1808	50	67	96.43%	97.31%
122	2478	2472	487	1985	1991	19.65%	19.70%
123	1519	1516	1000	516	519	65.83%	65.96%
124	1633	1571	1524	47	109	93.33%	97.01%

Figure 2-5(b) shows the predictivity comparison. Among 14 records, *Thresholding* algorithm outperforms *Pan-Tompkins* algorithm in 12 records. This is because Pan-Tompkins produces more FPs due to T-waves and noise that are mistaken as QRS complexes. However, as stated before, the *Thresholding* algorithm has lower hardware complexity. Further studies on the tradeoff between performance and hardware implementation cost will be forthcoming.

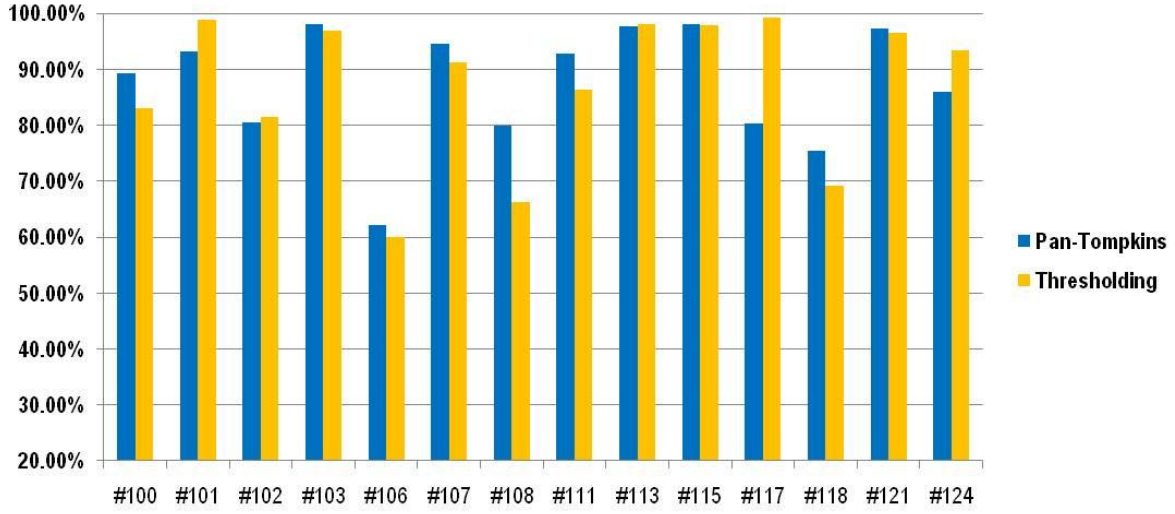

a

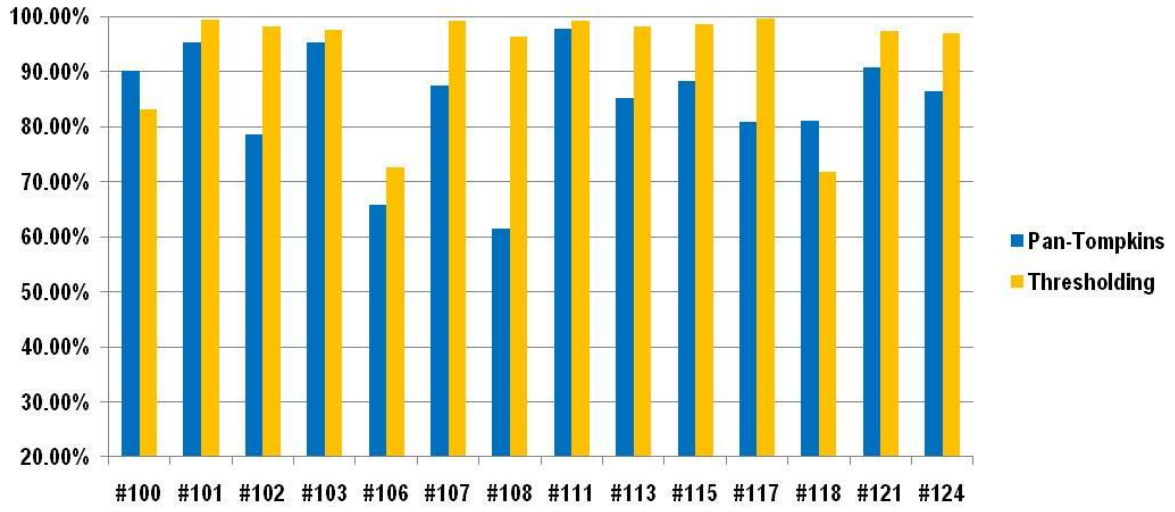

b

Figure 2-5. Performance comparison using *MIT-BIH Arrhythmia Database*. (a) sensitivity; (b) positive predictivity.

CHAPTER 3
BEAT CLASSIFICATION

Heart beat classification is an essential part of ECG signal processing. When a QRS complex is detected, its morphology change can be analyzed and associated with cardiac problems. The classification techniques fall into three main categories – time domain, frequency domain, and time-frequency domain. For the time domain, the shape-correlation is a frequently used approach. For frequency domain, the Fast Fourier Transform (FFT) is the most popular method to obtain the frequency components of the ECG record [68]. For the time-frequency domain, a widely used beat classification technique is wavelets decomposition [11].

As stated in Chapter 1, a low cost, automatic real-time approach to classify heart beats is desired. Here we propose and evaluate a time-domain method that correlates each detected beat with a previously stored template beat. The difference from the template beat is calculated and then used to cluster similar beats together. Normally, heart beats from a healthy ECG have similar shapes and thus only one cluster is formed. However, when abnormal beats or noises are present, more different clusters will be formed. The formation of additional clusters indicates potential heart problems, and thus a need to generate appropriate warnings to notify patients and remote healthcare centers.

3.1 Types of Arrhythmia

An arrhythmia is an irregular heartbeat - the heart may beat too fast (tachycardia), too slow (bradycardia), too early (premature contraction) or too irregularly (fibrillation). Arrhythmias are heart rhythm problems -- they occur when the electrical impulses to the heart that coordinate heartbeats are not working properly, making the heart beat too fast, too slow or inconsistently.

The occurrence of abnormal beats is useful in diagnosing arrhythmia. Annotated beats that frequently appear in the *MIT-BIH Arrhythmia Database* are Normal Beat (#1), PVC (Premature

Ventricular Contraction, #5), APB (Atrial Premature Beat, #8), RBBB (Right Bundle Branch Block Beat, #3), LBBB (Left Bundle Branch Block Beat, #2), Paced Beat and Fusion (Fusion of Ventricular and Normal Beat, #6). Table 3-1 categorizes the characteristics of these annotated beats and their medical indication.

Snapshots of each annotated beat are shown in Figures 3-1 and 3-2. The waveforms are acquired, overlapped, and plotted in Matlab using the *MIT-BIH Arrhythmia Database*. In each plot, the unit on the x-axis represents the number of samples of the detected waveforms (sampled at 250Hz). The y-axis is set to display a scaled version of the original voltage amplitude sensed by the recording devices. The amplitude swing in each waveform is from -2 to 2.

Table 3-1. Overview of annotated beat types.

Beat Types	# of Records	Characteristics	Medical Indication
Normal Beat	40	Normal QRS	Healthy human heart
Premature Ventricular Contraction (PVC)	37	Widened QRS, Bizarre shape	Three or more PVCs occur in a row indicate ventricular Tachycardia
Atrial Premature Beat (APB)	26	Early P-wave	When occurring frequently, treatment is necessary.
Right Bundle Branch Block (RBBB)	6	Widened S-wave	Warning sign of other, more serious heart conditions.
Left Bundle Branch Block (LBBB)	4	Broad R-wave Longer QRS	Same with RBBB
Paced Beat	4	Pacing spike followed by a wide QRS	Pacemaker in use
Fusion (Paced & Normal)	2	Flat P-, Q- and S-waves	Pacemaker in use

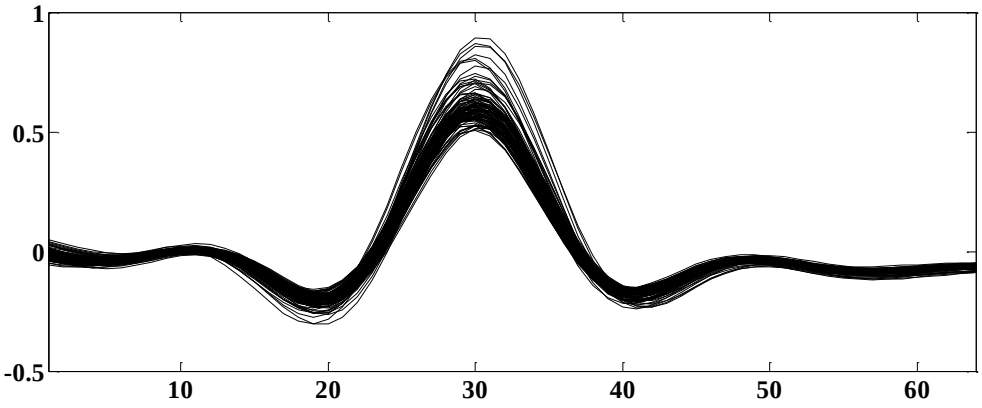

Normal Beat (*MIT-BIH* #100)

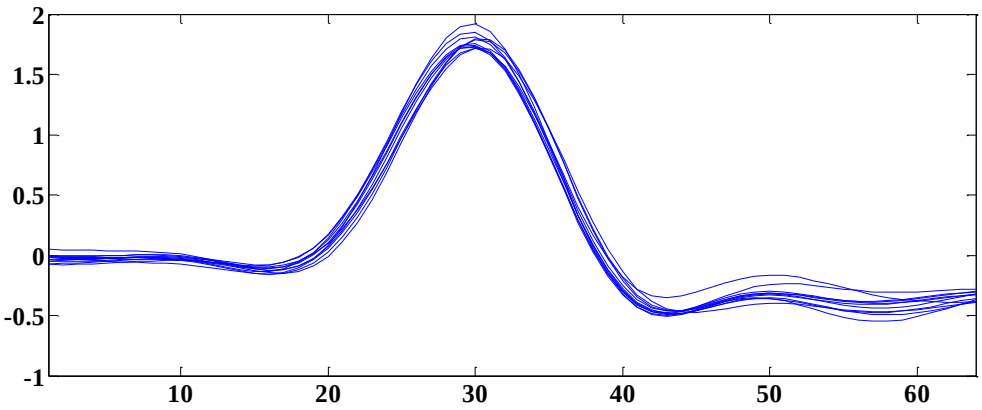

Premature Ventricular Contraction (*MIT-BIH* #105)

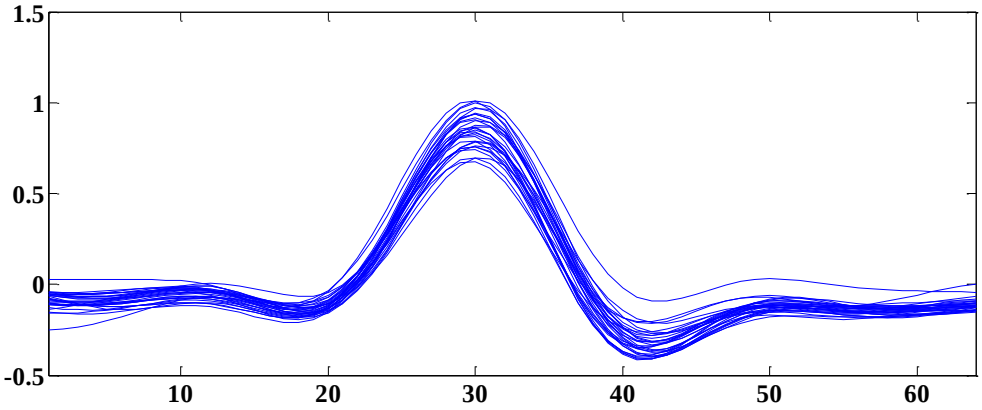

Atrial Premature Beat (*MIT-BIH* #200)

Figure 3-1. Normal beat, PVC, and APB.

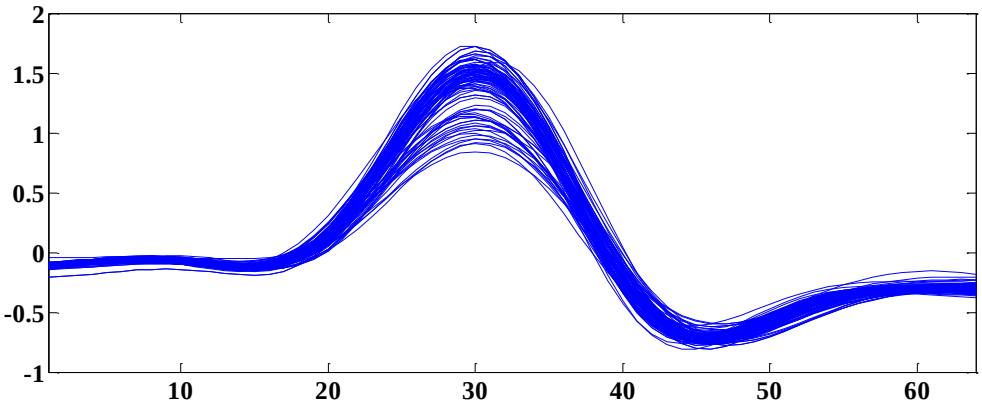

Left Bundle Branch Block Beat (*MIT-BIH* #109)

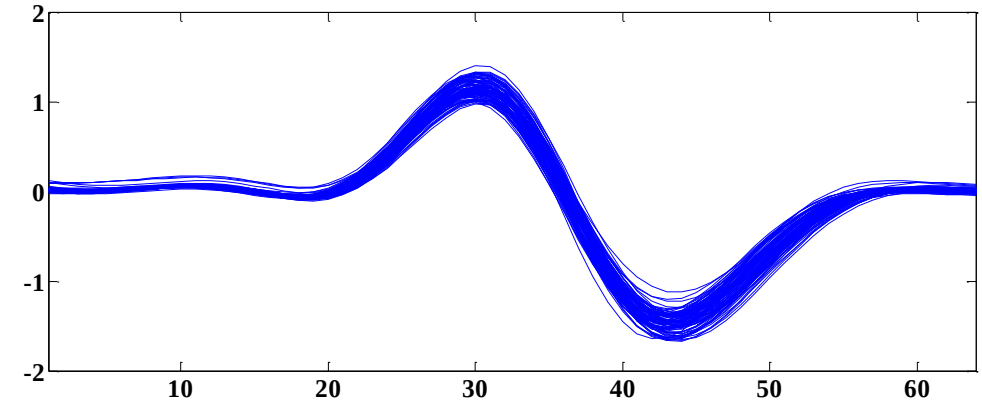

Right Bundle Branch Block Beat (*MIT-BIH* #118)

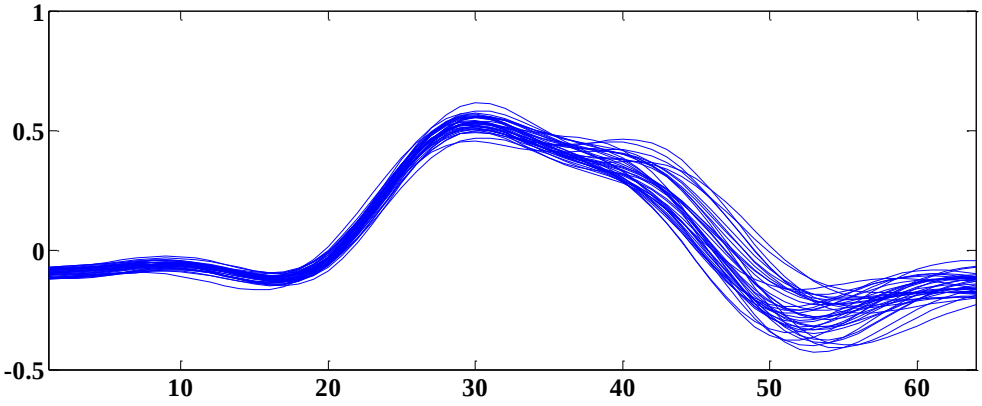

Paced Beat (*MIT-BIH* #102)

Figure 3-2. LBBB, RBBB, and Paced Beat.

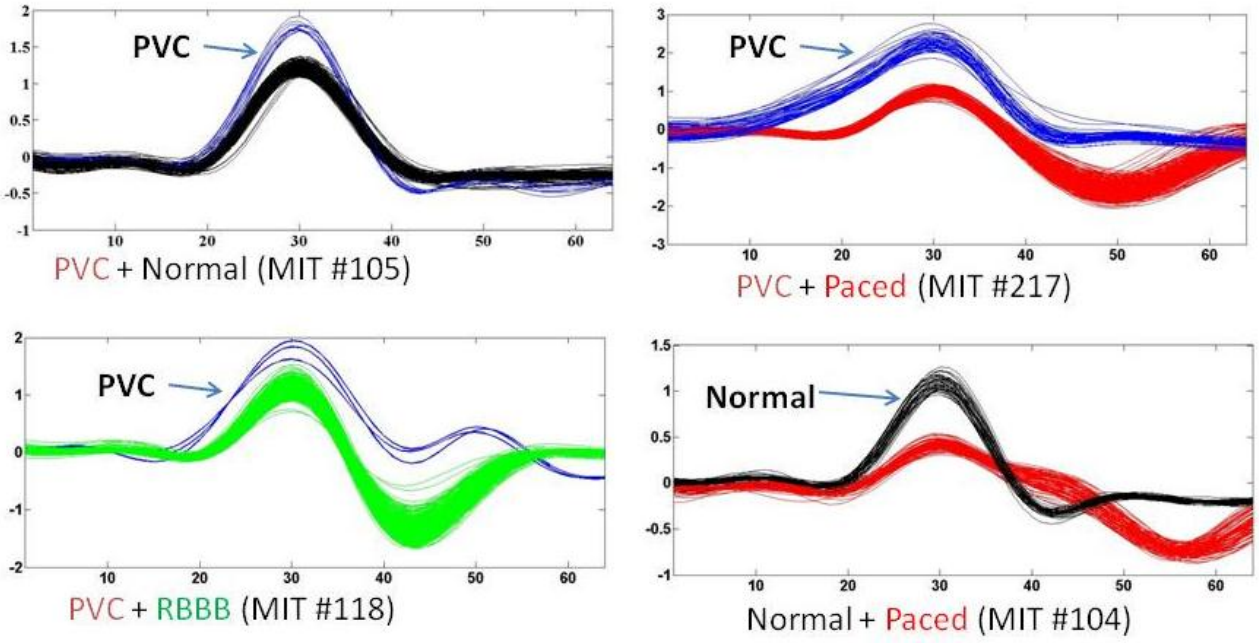

Figure 3-3. Snapshots of abnormal beats using the *MIT-BIH Arrhythmia Database*.

Figure 3-3 shows snapshots of different beat types that are in the same record. For example, in record 105 there are PVC and normal beats presented. Also, from the plots we can observe that PVCs usually have wider shapes. It is clear that the shapes are different for different beat types, suggesting the shape-correlation method that will be discussed in the next chapter.

3.2 Clustering Analysis

3.2.1 Distance Distribution

Euclidean distance is a frequently used approach in image of video analysis to measure the similarity of two vectors. In [67], the Euclidean distance method was used for ECG beat detection. Here we proposed to use this method for the heart beat classification.

The Euclidean distance *d* between two shapes $P = (p_1, p_2, \dots, p_n)$ and $Q = (q_1, q_2, \dots, q_n)$ is defined as followed,

$$d(P,Q) = \sqrt{(p_1 - q_1)^2 + (p_2 - q_2)^2 + \cdots + (p_n - q_n)^2} = \sqrt{\sum_{i=1}^{n} (p_i - q_i)^2}$$

We determine the similarity between heart beat shapes be calculating their Euclidean distance to a common template beat. To evaluate the beats clustering using the Euclidean distance method, we performed simulations using the *MIT-BIH Arrhythmia Database* and Matlab. The template beats were arbitrarily chosen from those beats within the majority beat types. For each patient's record, only the main beat types (Normal Beat, PVC, LBBB, RBBB, and Paced) were simulated. The Euclidean distances of all the beats with the template beats were computed and recorded, and then the histograms of the distance distribution were plotted.

In Figures 3-4 and 3-5, a total of 48 plots illustrate the beat clustering for each record in the database. In each plot, the scale on the x-axis represents the results of Euclidean distance calculation between the two beat shapes that have amplitude swings of 4. On the y-axis is the number of beats that belong to the predefined distance ranges.

From the plots, we can clearly see the distance distribution of different beat types that are in the records. Some distances are closely clustered within a relatively small range, indicating that the majority of the beats in the clusters have very similar shapes. On the other hand, the presence of wide clusters indicates that the beats within these clusters have large shape variations.

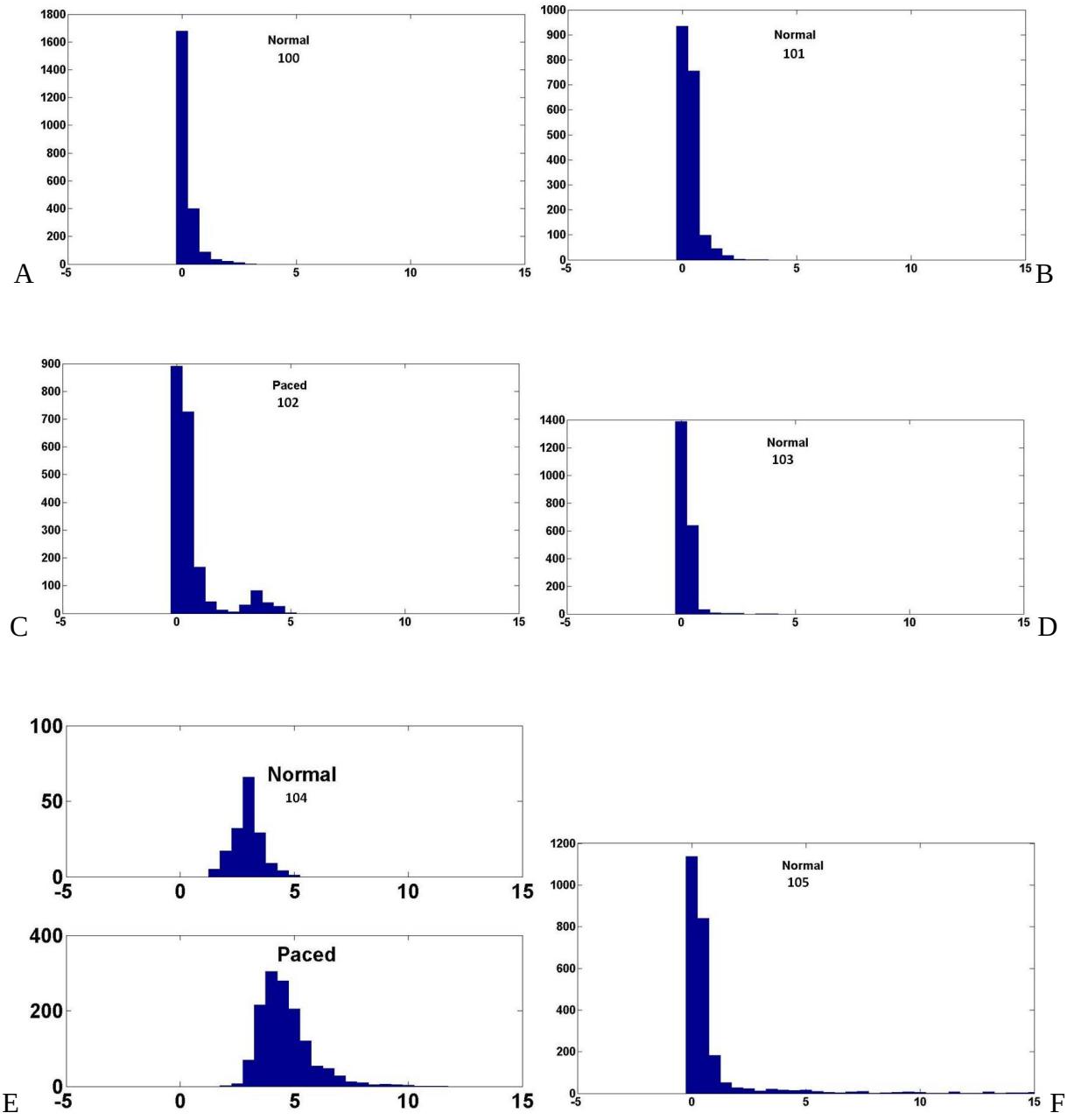

Figure 3-4. The distance distribution plots simulated using records #100 to #124 in the *MIT-BIH Arrhythmia Database*. A) Record #100. B) Record #101. C) Record #102. D) Record #103. E) Record #104. F) Record #105. G) Record #106. H) Record #107. I) Record #108. J) Record #109. K) Record #111. L) Record #112. M) Record #113. N) Record #114. O) Record #115. P) Record #116. Q) Record #117. R) Record #118. S) Record #119. T) Record #121. U) Record #122. V) Record #123. W) Record #124.

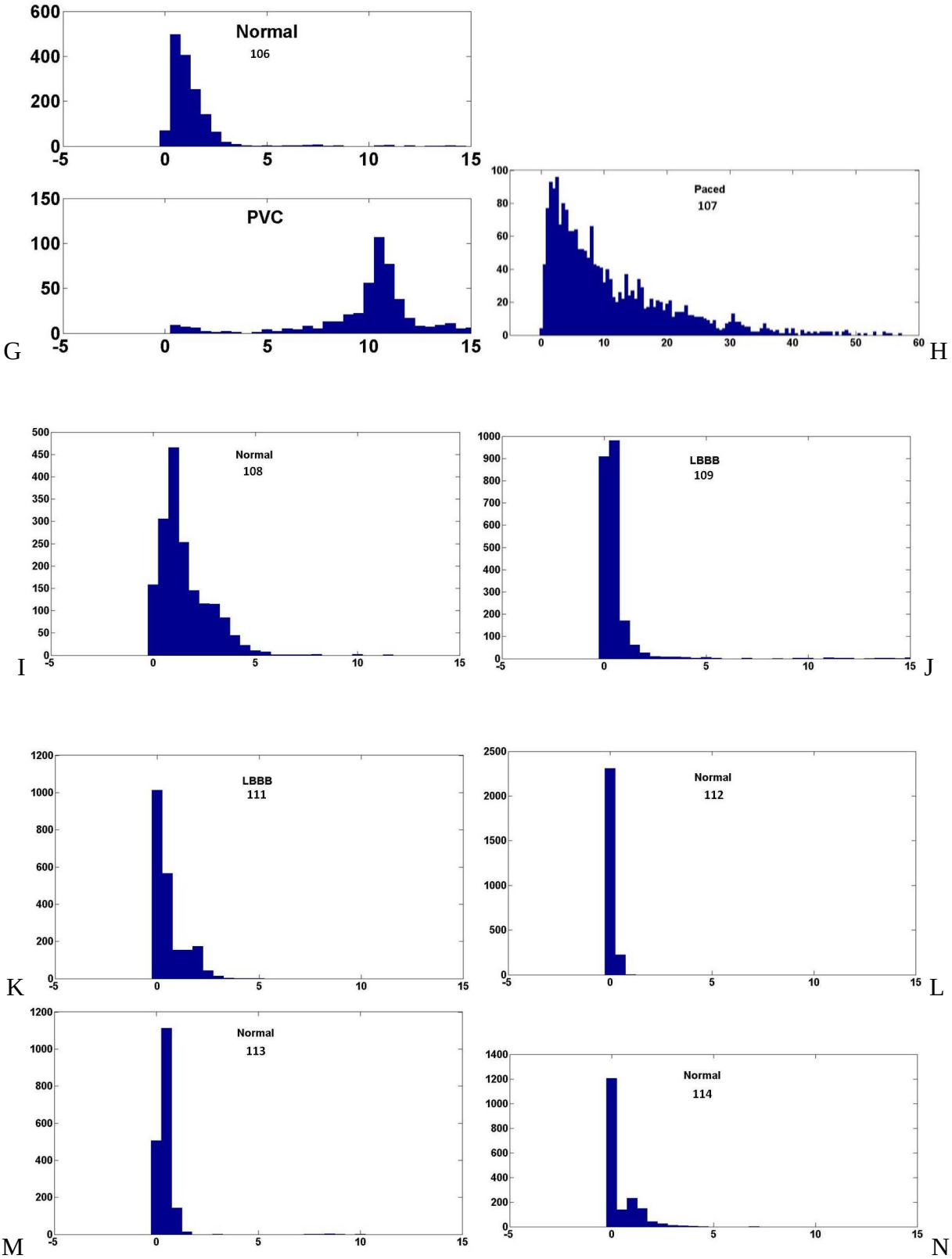

Figure 3-4. Continued

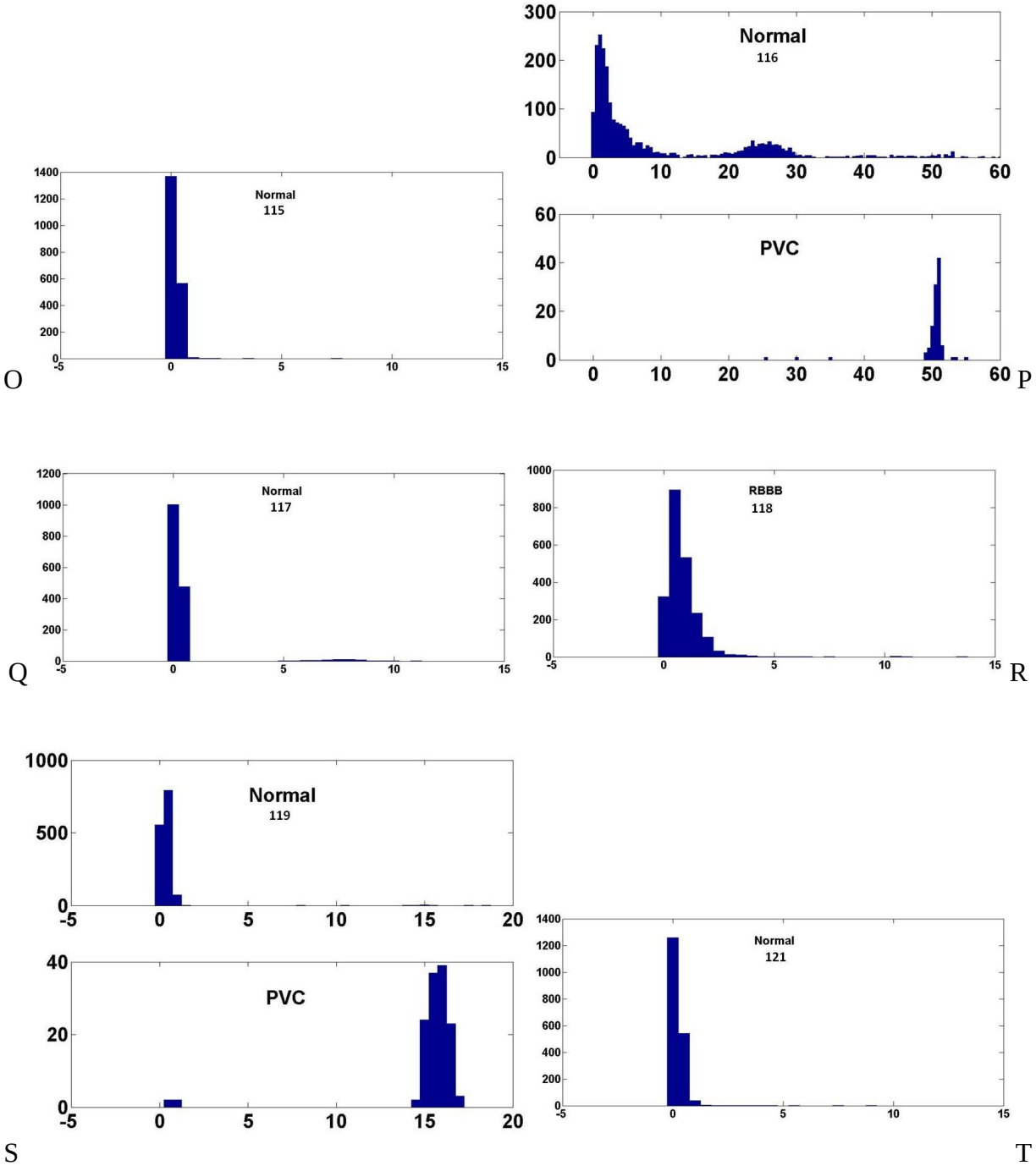

Figure 3-4. Continued

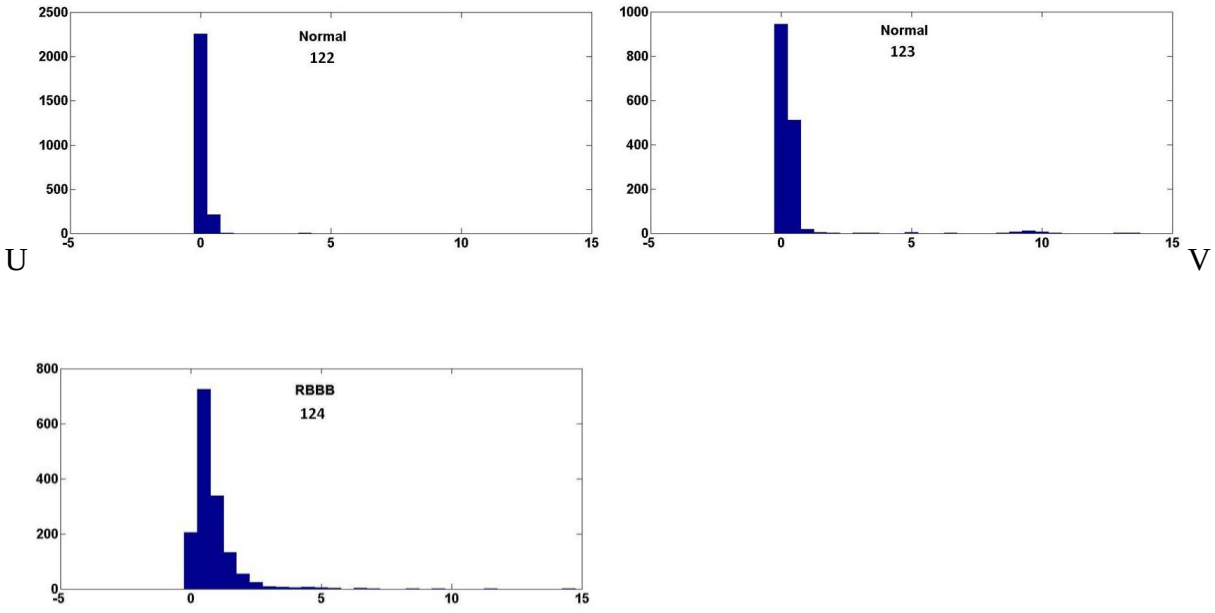

U V W

Figure 3-4. Continued

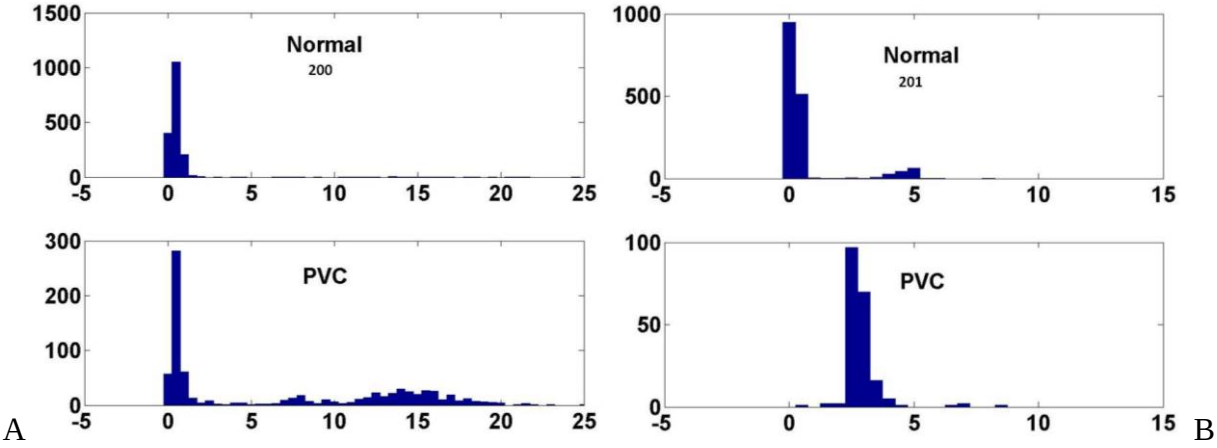

A B

Figure 3-5. The distance distribution plots simulated using records #200 to #234 in the *MIT-BIH Arrhythmia Database*. A) Record #200. B) Record #201. C) Record #202. D) Record #203. E) Record #205. F) Record #207. G) Record #208. H) Record #209. I) Record #210. J) Record #212. K) Record #213. L) Record #214. M) Record #215. N) Record #217. O) Record #219. P) Record #220. Q) Record #221. R) Record #222. S) Record #223. T) Record #228. U) Record #230. V) Record #231. W) Record #232. X) Record #233. Y) Record #234.

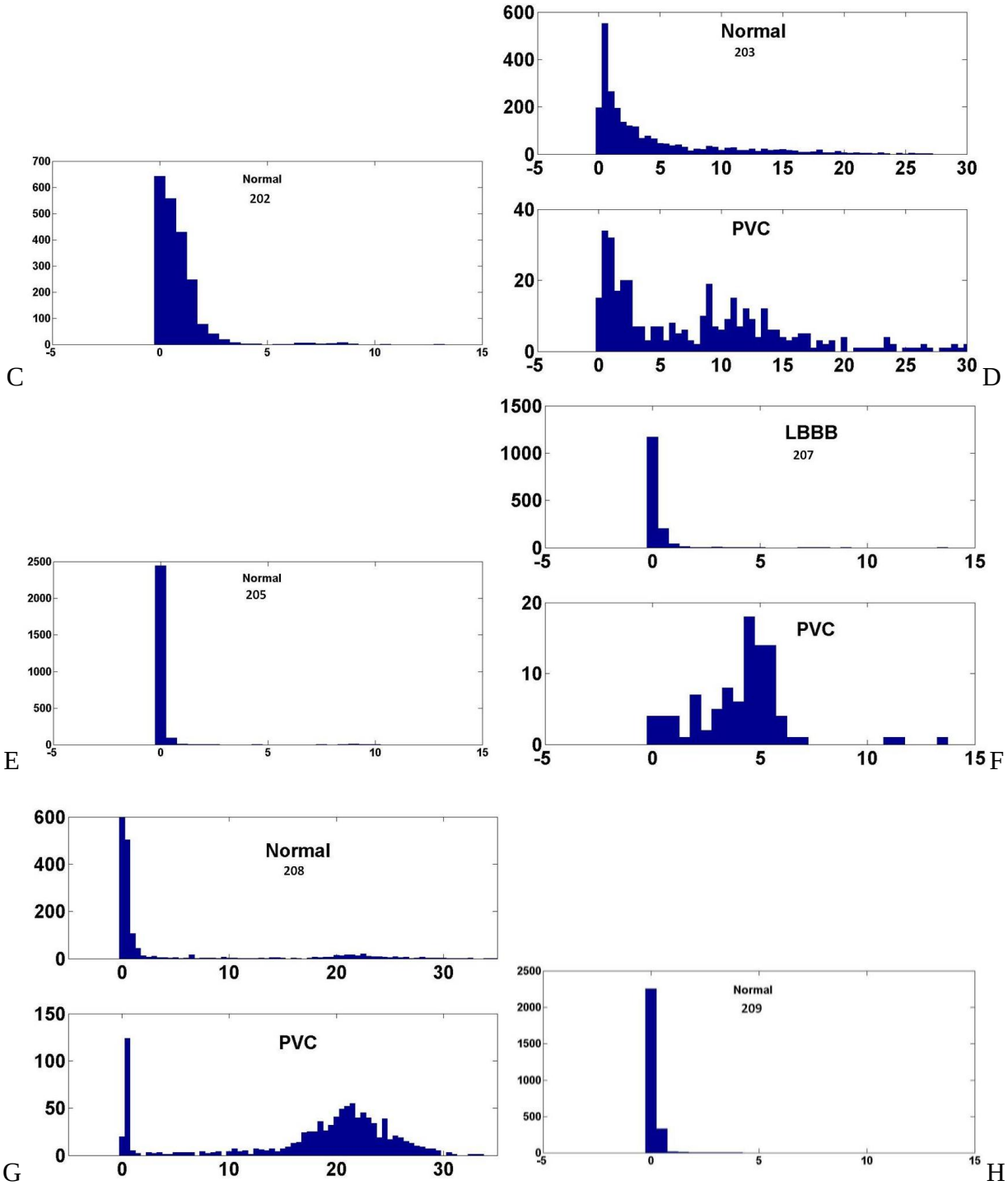

Figure 3-5. Continued.

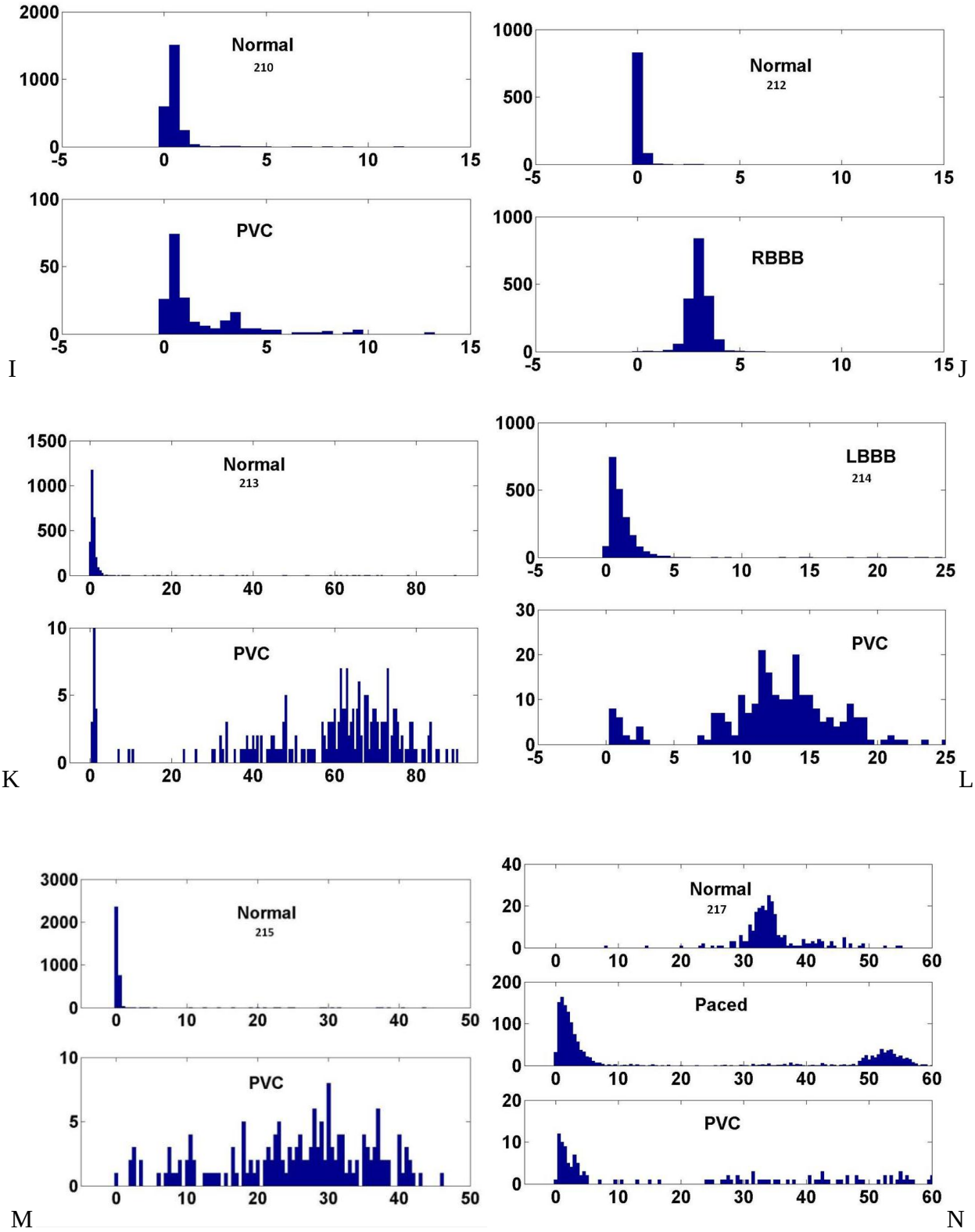

Figure 3-5. Continued.

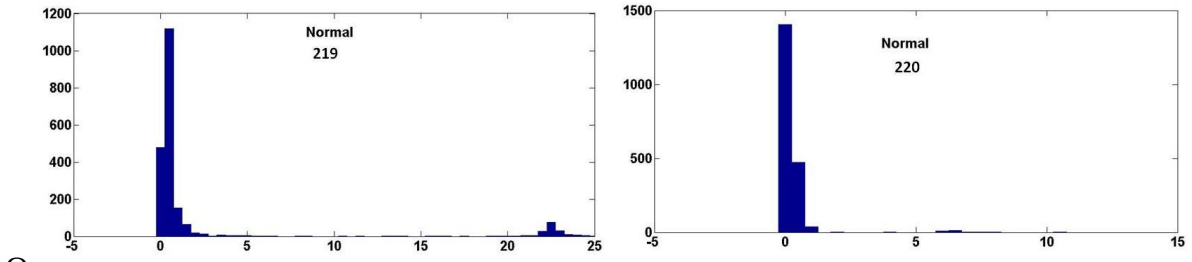

O P

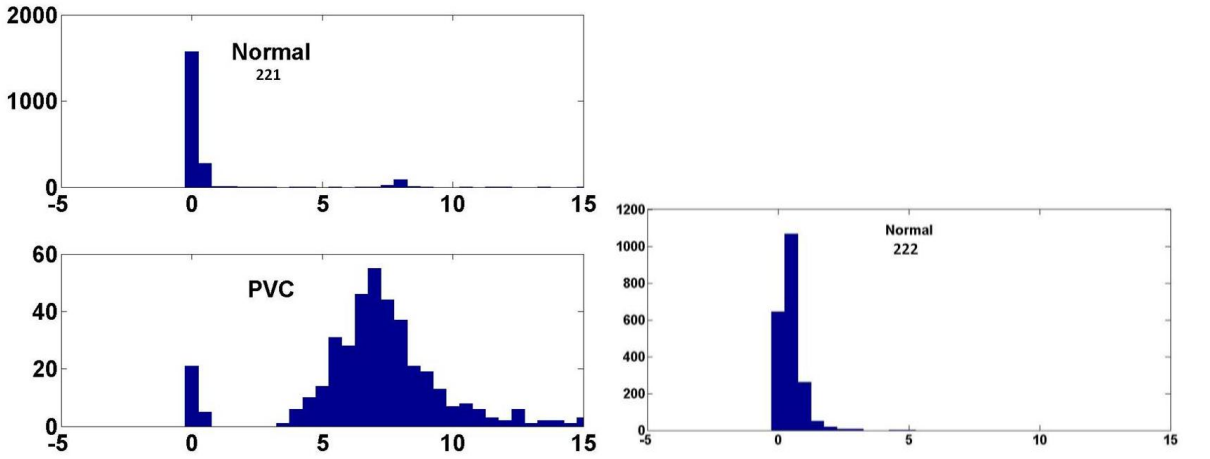

Q R

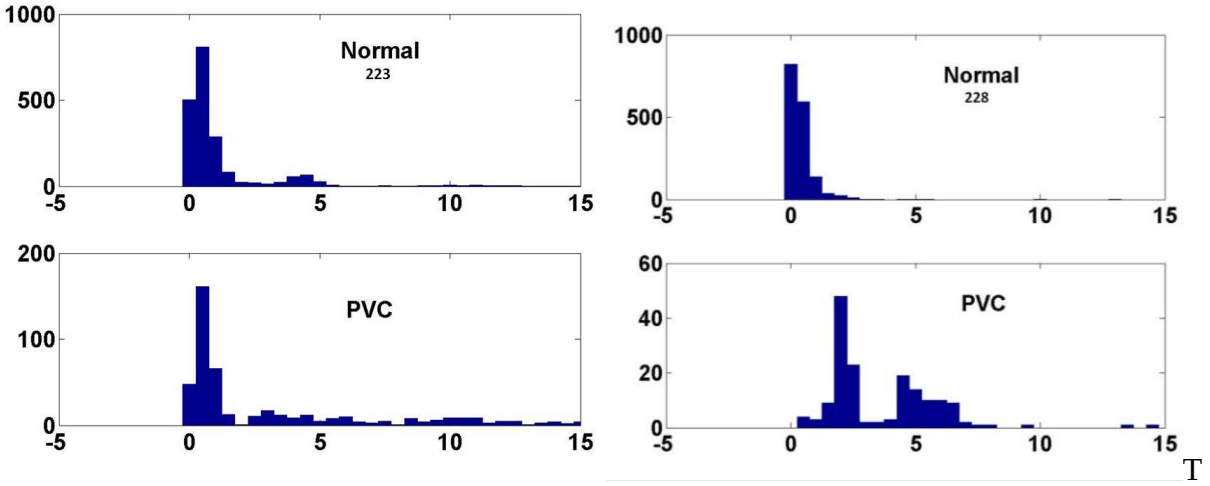

S T

Figure 3-5. Continued.

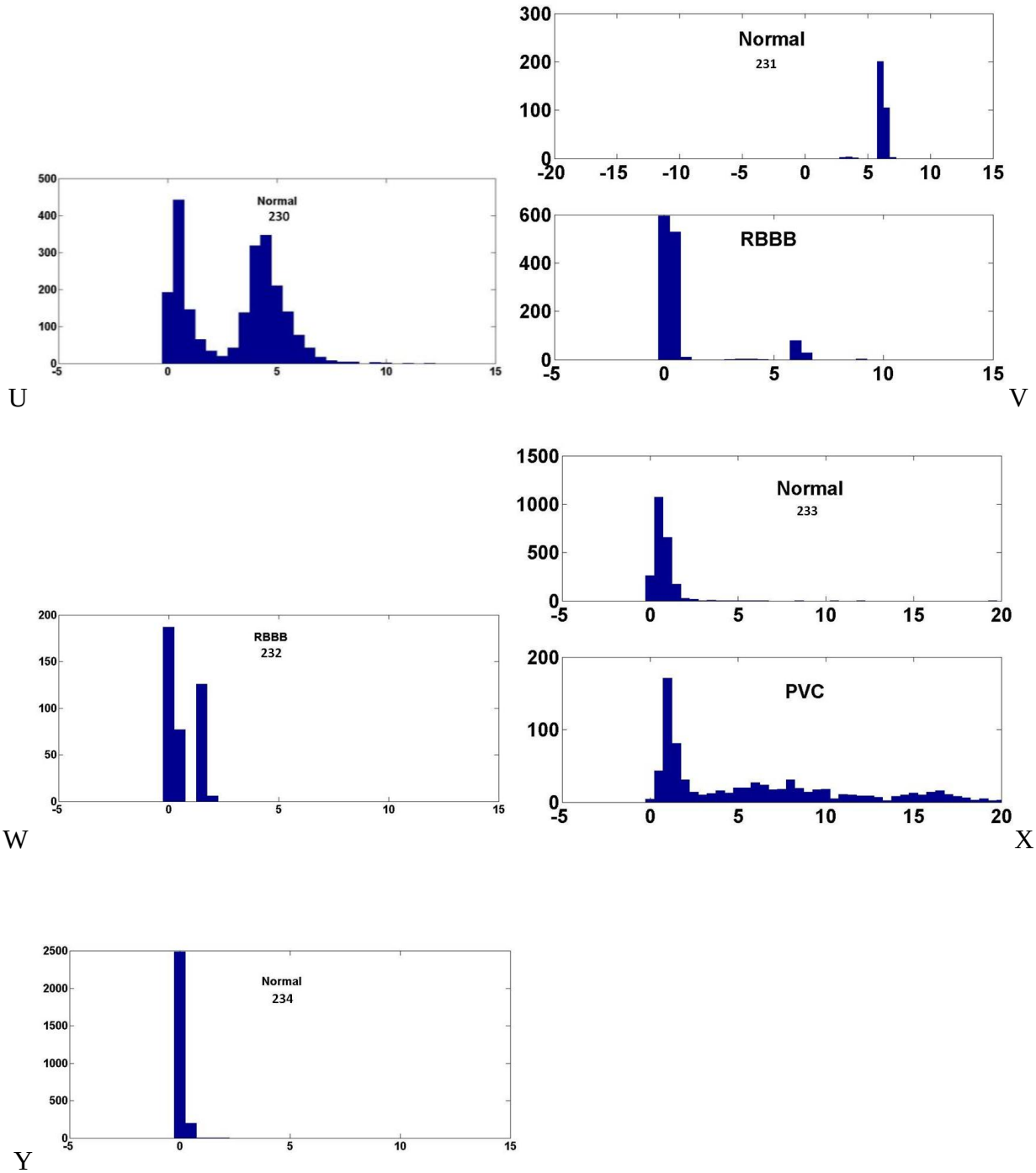

Figure 3-5. Continued.

3.2.2 Principal Component Analysis

Principal component analysis (PCA) transforms a number of correlated variables into a smaller number of uncorrelated variables (principal components) [66]. For ECG signals, most of

the variability is preserved even after reducing the dimensionality of heart beat signal datasets. Previous studies have shown that heart beat classification is a common application using PCA in which a subset of the principal components serves as features which are used to distinguish between normal sinus beats and abnormal waveforms. [63].

PCA consists of the following steps: store the original data, subtract the mean from each of the data dimensions, calculate the covariance matrix, calculate the eigenvectors and eigenvalues of the covariance matrix, and choose components and forming a feature vector. Applying PCA to a set of pre-recorded heart beats, the associated pattern of principal components reflects the degree of morphologic beat-to-beat variability. When the eigenvalue associated with the first principal component is much larger than those associated with other components, the set exhibits a low morphologic variability, whereas a slow fall-off of the principal component values indicates a large variability [63].

PCA was performed on the 48 data sets in the *MIT-BIH Arrhythmia Database* using Matlab. The resulting 48 plots are shown in Figures 3-6 and 3-7. The beats belong to the same beat type is plotted in the same color. Thus, for each cluster in the graph we can read off the compactness of each cluster and the distances between clusters.

From the PCA plots, we made the first observation: for data sets with only one major beat type, the clusters are clearly compact. For example, there are 21 records that include only the normal beat type: 100, 101, 103, 105, 108, 112, 113, 114, 115, 117, 121, 122, 123, 202, 205, 209, 219, 220, 222, 230, and 234. All the records show compact clustering except the 230, in which there are two different shapes presented.

The second observation is that the redundancies are revealed in some of the records that have only normal beats. The redundancy indicates the degree of correlation between PCs, and is

reflected in the shapes of the clusters. For example, there are several records show long stripe-shaped clusters including 100, 101, 103, 115, 121 and 200. These types of shapes are the results of high degree of correlation between two of their PCs.

Finally, for data sets with two or more major beat types, the results vary. For example, PVCs in the database have larger beat shape variation, resulting in PVC clusters which are diffuse and inseparable from the normal beat clusters in several cases. On the other hand, clusters of RBBBs and LBBBs show clear distinction from the normal beat clusters, as shown in record 207, 212, and 231.

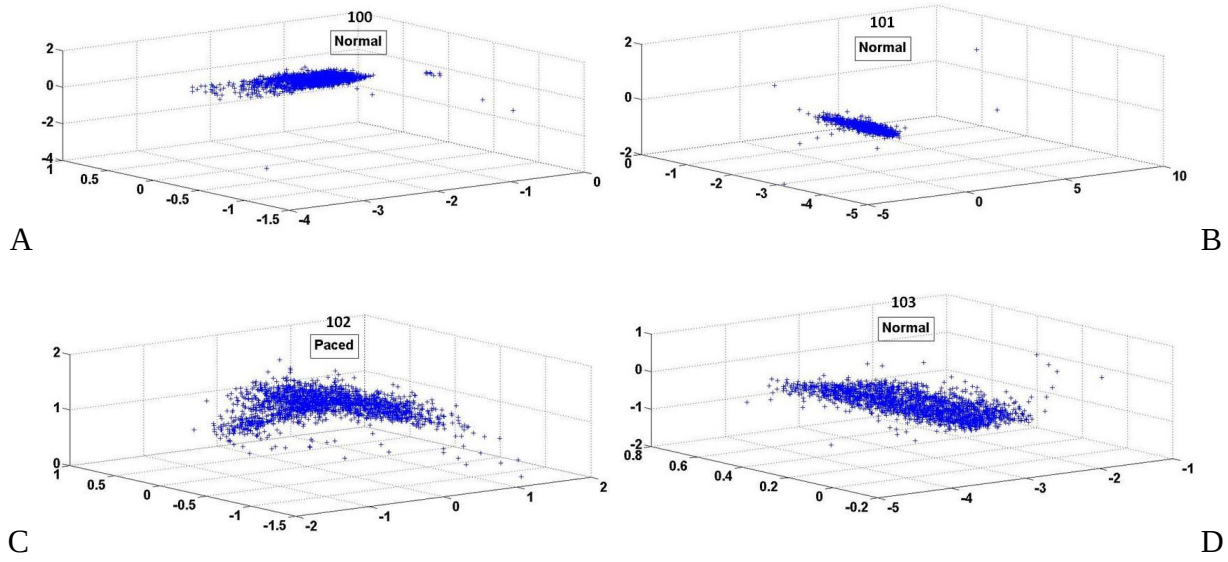

Figure 3-6. The PCA plots for records from #100 to #124 in the *MIT-BIH Arrhythmia Database*. A) Record #100. B) Record #101. C) Record #102. D) Record #103. E) Record #104. F) Record #105. G) Record #106. H) Record #107. I) Record #108. J) Record #109. K) Record #111. L) Record #112. M) Record #113. N) Record #114. O) Record #115. P) Record #116. Q) Record #117. R) Record #118. S) Record #119. T) Record #121. U) Record #122. V) Record #123. W) Record #124.

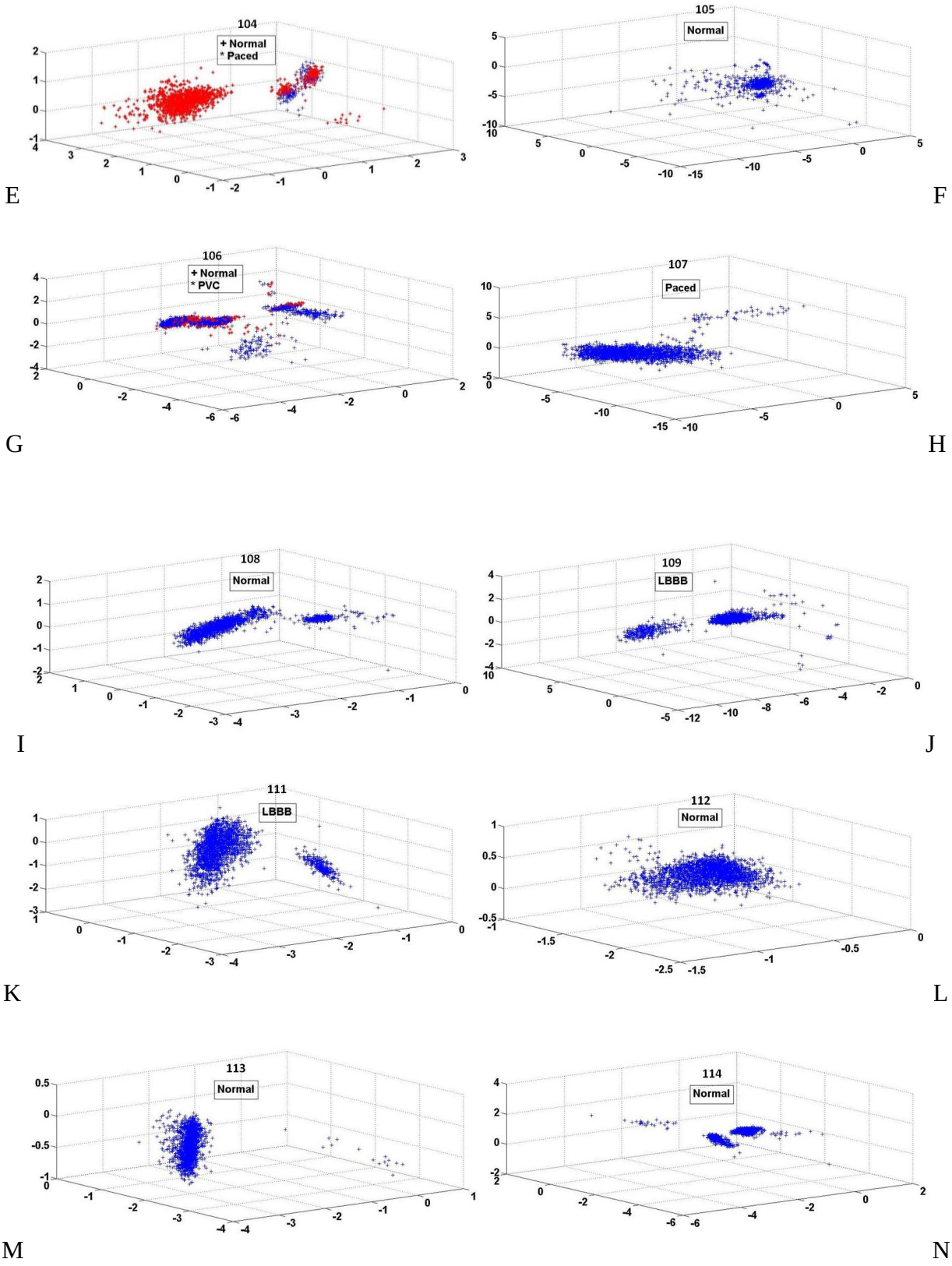

Figure 3-6. Continued.

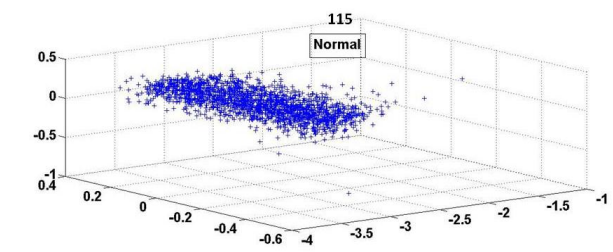

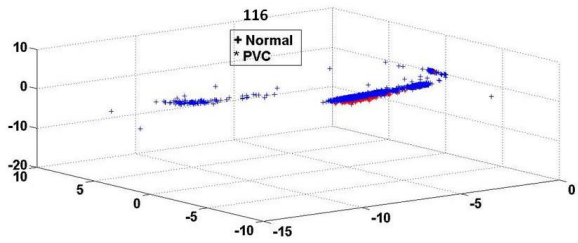

O P

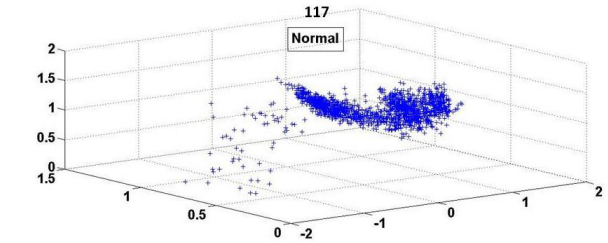

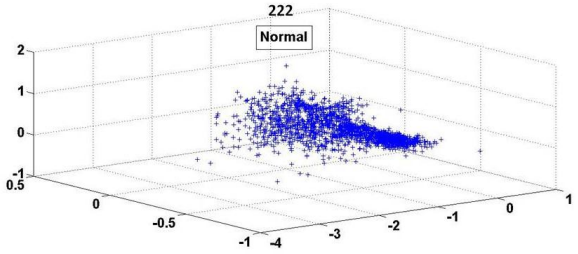

Q R

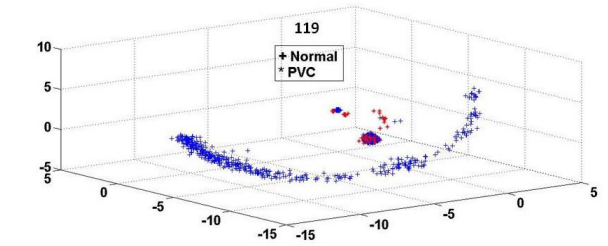

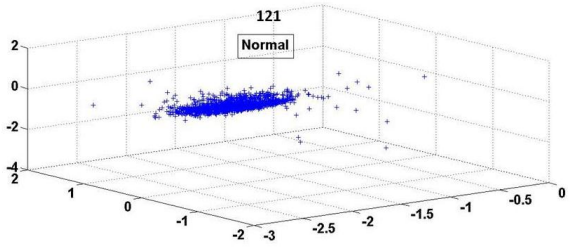

S T

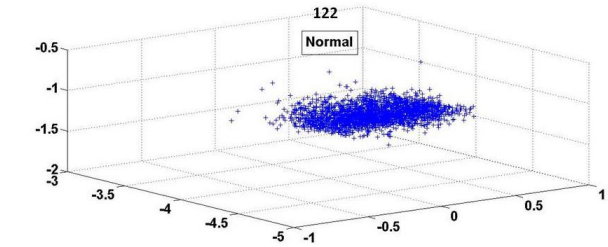

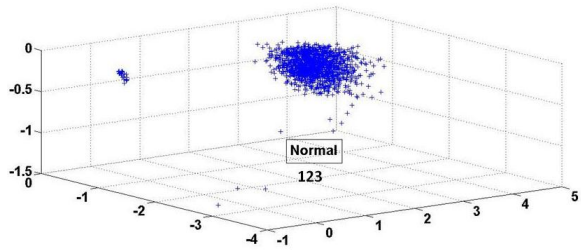

U V

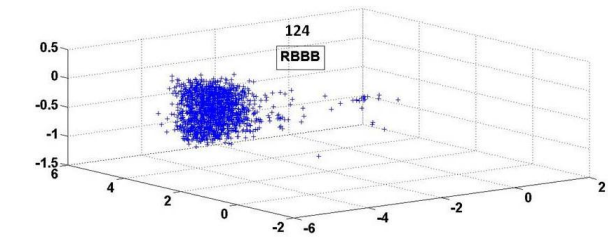

W

Figure 3-6. Continued

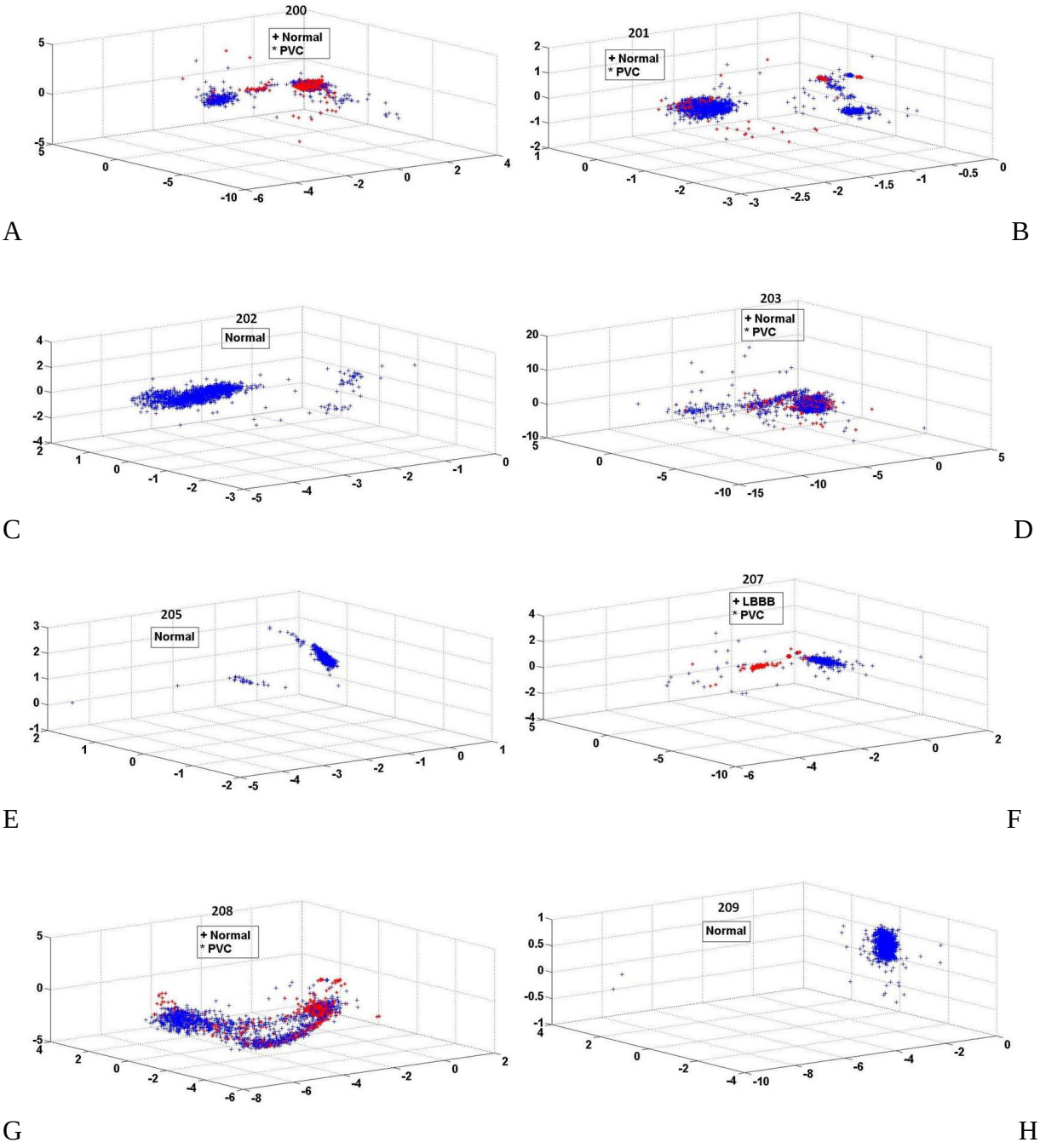

Figure 3-7. The PCA plots for records from #200 to #234 in the *MIT-BIH Arrhythmia Database*. A) Record #200. B) Record #201. C) Record #202. D) Record #203. E) Record #205. F) Record #207. G) Record #208. H) Record #209. I) Record #210. J) Record #212. K) Record #213. L) Record #214. M) Record #215. N) Record #217. O) Record #219. P) Record #220. Q) Record #221. R) Record #222. S) Record #223. T) Record #228. U) Record #230. V) Record #231. W) Record #232. X) Record #233. Y) Record #234.

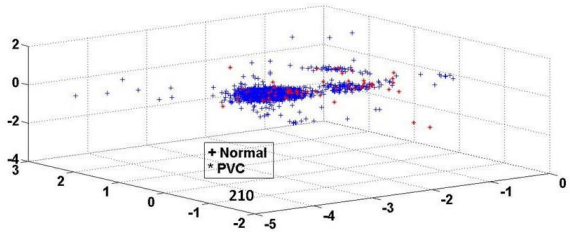

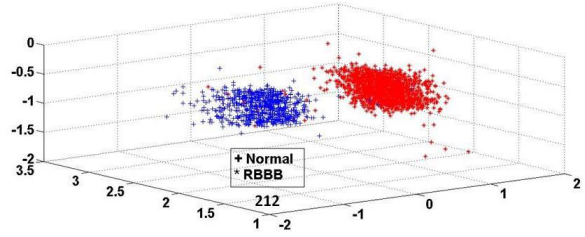

I J

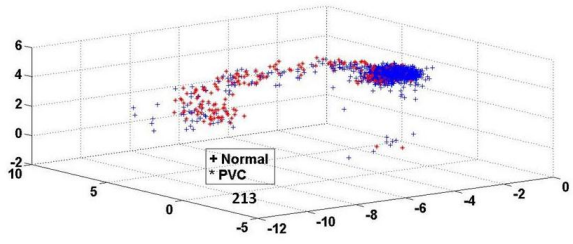

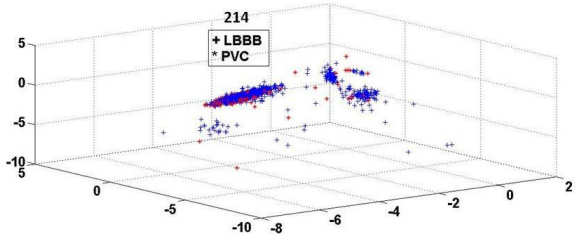

K L

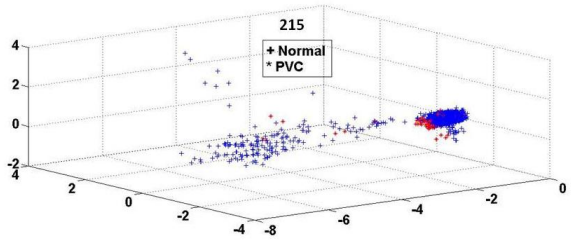

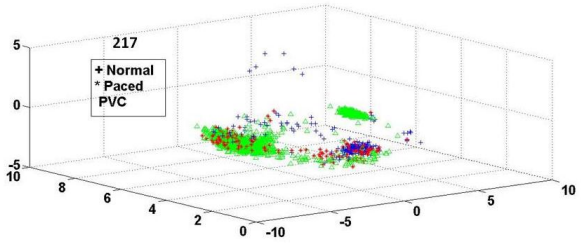

M N

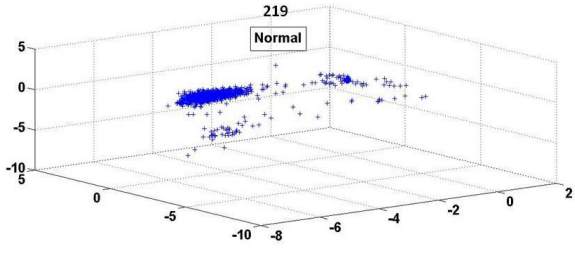

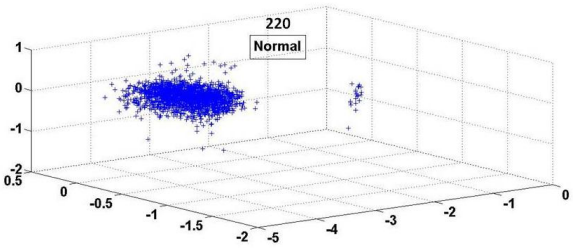

O P

Figure 3-7. Continued.

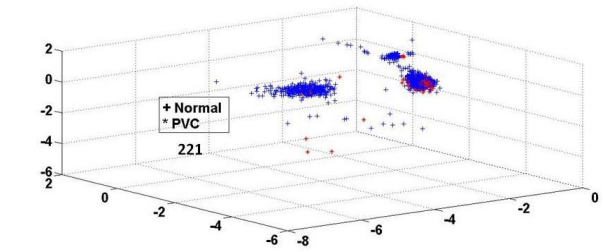

Q

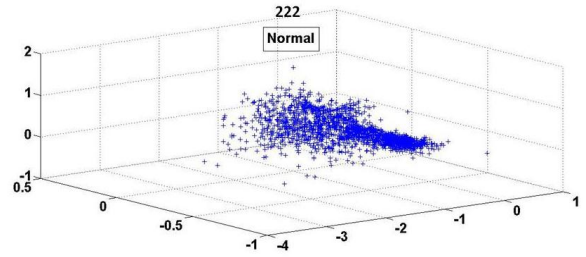

R

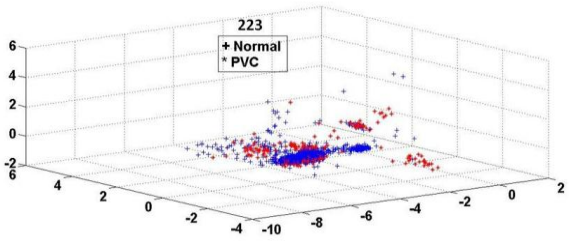

S

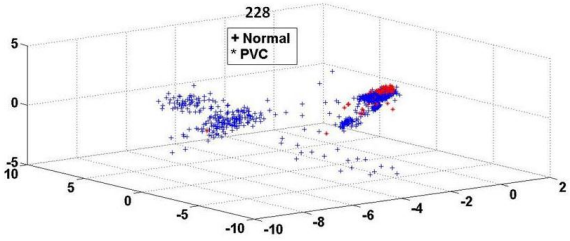

T

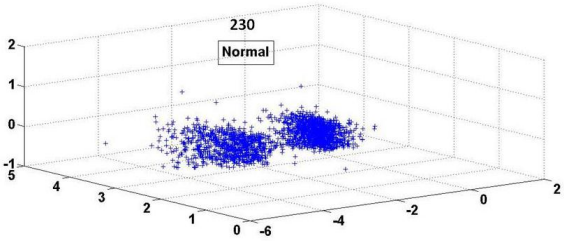

U

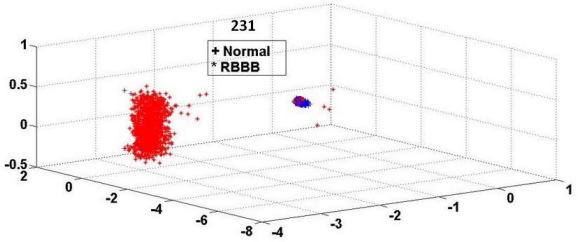

V

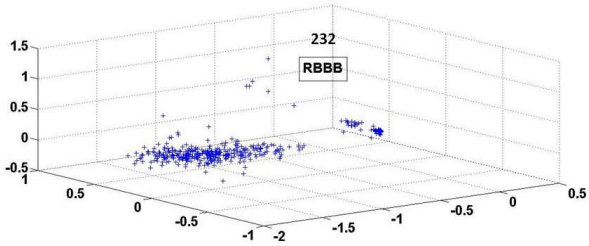

W

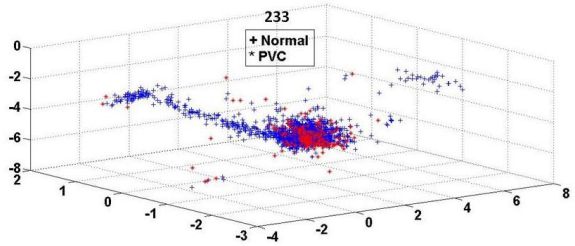

X

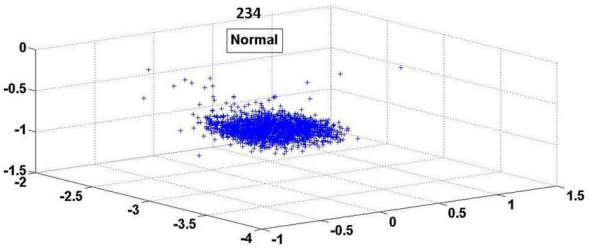

Y

Figure 3-7. Continued.

3.3 Morphological Variation

ECG signals have non-stationary and easily disturbed features. Even for a single person, the amplitude and shape of detected heart beats can change over time due to changes in the propagation medium between heart and sensor, measurement variability in ECG recordings affecting the amplitude levels, implanted devices drift, and mental status changes.

Consider the stress test plot in Figure 3-8, computed for sequential thirty second intervals during a 28 minute interval, as an example. The plot shows representative beats (i.e., average beats) during the stress test [65]. Clearly changes in mental status can cause the heart beat shapes to change drastically.

The solution to the morphological variation is dynamically adapting to the shape changes. Whenever shape changes occur, new clusters needs to be created immediately and given sufficient time and space to grow. The clusters with old beat shapes need to be gradually flushed out of the system to free up the space for future clusters.

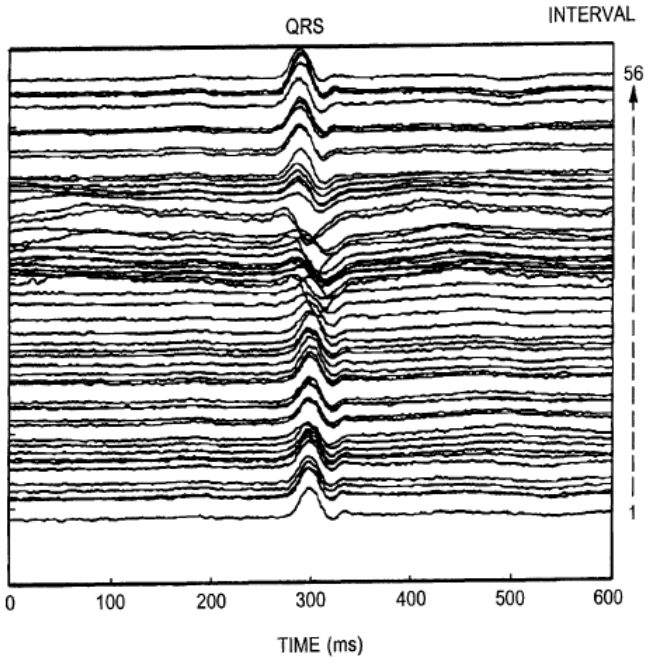

Figure 3-8. Representative beats during a stress test

CHAPTER 4
ARCHITECTURE

4.1 Computational Model

In response to the growing demand for the need to transmit ECG data wirelessly, heart beat classification can be performed onsite and online in a hardware solution, instead of in software as traditionally performed. Previous studies show that online digital beat classification is feasible on the FPGA platform [2]. To design efficient hardware architecture for heart beat classification, we need to first develop an underlying computational model based on a fundamental understanding of the nature of ECG signals.

ECG, along with neural spikes and respiration signals, are recurrent biomedical signals. Figure 4-1 illustrates a top-down flowchart for the classification process of these recurrent biomedical signals. First, the detection stage captures the occurrences of the recurrent signal. Second, the feature extraction stage converts the original signal into a set of features. The features, extracted by arithmetic logic units, can then be weighted by different coefficients depending on the classification algorithms. These weighted features can be considered as identifications for the signals. Third, the system searches the prior knowledge, recorded in the form of memory, to determine if the identifications satisfy the criteria for different clusters. If there are any recorded criteria met in the memory, they will be updated to reflect the changes caused by newly detected signals. If there are no satisfied criteria, a set of newly created features will be merged into the existing knowledge. Finally, the system resets to the initial state and is ready for the next signal. Based on this model, the use of memory elements in the system is inevitable, whether for storing coefficients or the classification criteria set. The size of the memory needed is determined by the complexity of the classification algorithms.

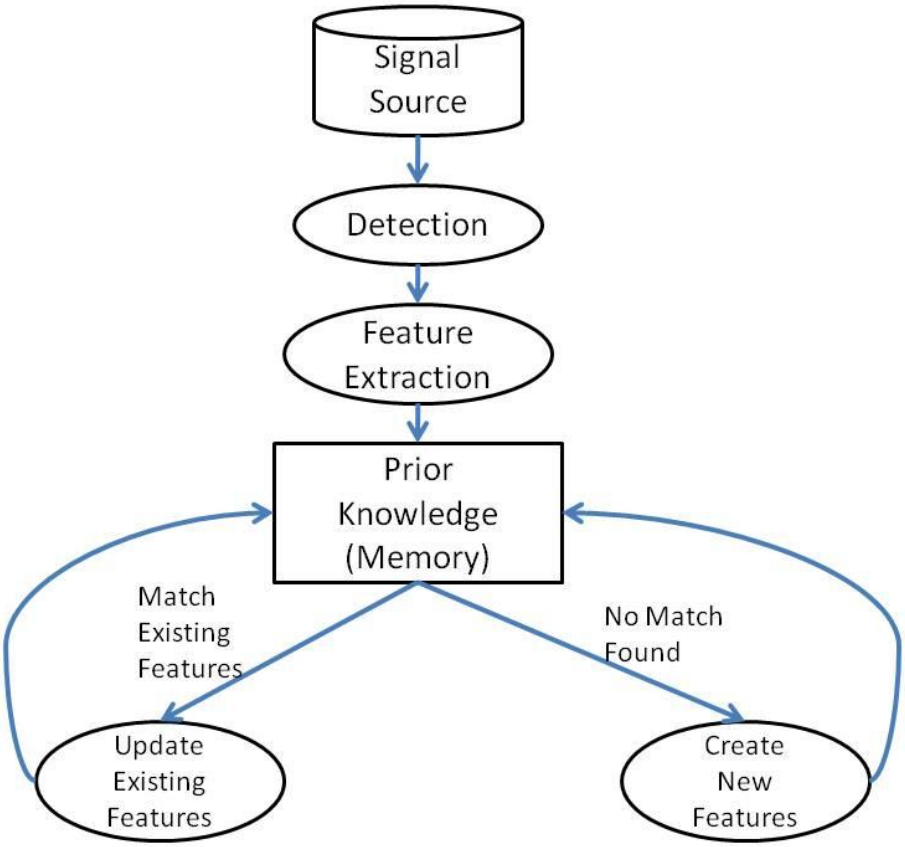

Figure 4-1. A generalized computational model for the biomedical signals classification.

4.2 Clustering Architecture

4.2.1 Cache

In Sections 3.2.1 and 3.2.2, we observed the clustering properties of heart beats through analytical tools such as Euclidean distance distribution and PCA. In Section 3.2.3, we demonstrated the temporal properties of the heart beat shape changes. Combining the generalized computational model described in Section 4.1 with the requirements of ultra low-power consumption and small memory space for implantable medical devices, we propose a hardware solution that benefits from the cache concept in Computer Architecture.

Cache holds a crucial role in Computer Architecture and has a history spanning several decades. Caches are used as a temporary storage area to reduce the effective latency between the

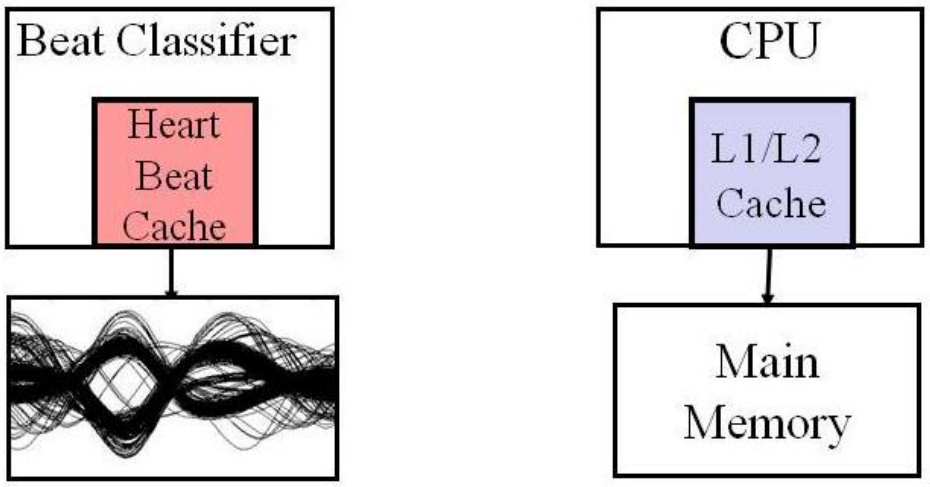

Figure 4-2. Analogy between normal cache and Heart Beat Cache.

processor and main memory by providing rapid access to recently used or frequently needed data. Furthermore, the small on-chip cache reduces the overall system hardware cost.

Before directly applying the cache concept to the heart beat classification problem, we review some important underlying principles. The most fundamental is the *principle of locality*, which considers both temporal locality and spatial locality. Temporal locality (locality in time) states that a data block that is referenced will tend to be referenced again soon. Spatial locality (locality in space) states that if a data block is referenced, data blocks whose addresses are close will tend to be referenced soon [62].

There is thus a need to find the locality properties within the heart beat clustering process. In beat classification applications, only those detected real beats are stored for faster classification of future beats. Multiple detected beats of the same types are used to form a cluster. Instead of storing the entire set of heart beat waveforms in one cluster, only the extracted information such as distance range, beat occurrence frequency, and number of beats are stored in a cache entry. Temporal locality is exploited so that frequently occurring beat types are maintained in the cache with high priority. Spatial l locality is different from the traditional

definition in the cache concept, where the data accessing behavior causes the nearby cache blocks to be fetched from the main memory to the cache. Here, those beats with Euclidean distance similar to the template beat are clustered together in the cache. Nonetheless, the similarity lies in the fact that the spatially close data are grouped together in the cache.

We proposed the use of cache in the application of beat classification, which is extremely memory-optimized compared to previous proposed architecture [30], in which a larger memory size is used for adopting the neural network algorithms.

4.2.2 Reuse Distance of Detected Heart Beats

To gain further insight in the applicability of recording recent heart beats for heart beats classification, we study the reuse behavior using real ECG databases. Caches take advantage of data reuse. Reuse distance, measured as the number of unique addresses accessed since the last reference to the requested data, is a useful metric of cache behavior [64]. Figure 4-3 is an illustration of the reuse distance.

Reuse distance is directly related to the origin of cache misses. The cache hit/miss ratio, the number of cache hits divided by number of cache misses, is a main performance characteristic of a cache. Cache misses are categorized by their three causes - compulsory misses, conflict misses, and capacity misses. A compulsory miss is caused by the first access to a block that has never been in the cache. Capacity misses are those due to insufficient cache capacity (i.e., the reuse distance is too large). Conflict misses are those misses in a direct-mapped or set-associative cache that are eliminated in a fully associative cache of the same size [62].

A fully associative cache with the Least Recently Used (LRU) policy indicates that a reference is a cache hit if its reuse distance is smaller than the number of cache lines. If the reuse distance is larger than the number of cache lines, it results in a miss. Heart Beat Cache (HBC)

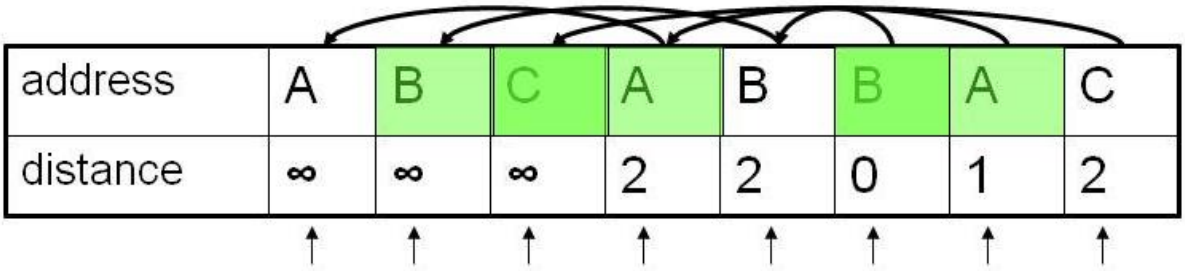

Figure 4-3. An illustration of the definition of reuse distance in cache behavior.

can be considered as a special kind of fully associative cache such that a data block (heart beats clusters) can be stored in any cache line, while the mapping is determined by Euclidean distance ranges instead of data addresses. In HBC, the hit/miss ratio reflects the ability to identify and retain the real heart beats. Moreover, this ration reflects the accuracy of the classification process.

Similarly, the reuse distance can be used to characterize the behavior of HBC. For each record in the *MIT-BIH Arrhythmia Database*, we performed the following procedure to evaluate the reuse distance distribution. First, the entire distance span is divided equally into 50 segments. The number 50 was determined based on the close examination of the distance distribution for all 48 records. Most of the clusters can be covered completely in the range of 1, which is exactly the length of one segment. Second, each detected heart beat is assigned an ID which is the segment index where its distance (with the template) falls into. Third, the reuse distance of each detected heart beat is calculated by counting the number of beats between the current beat and the previous beat with the same ID. Finally, all of the reuse distances are sorted into bins for analysis.

Figure 4-4 shows the reuse distance distribution for the 48 records in the *MIT-BIH Arrhythmia Database*. From Figure 4-4, we made the following observations. (1) The records

that consist of normal beats without the presence of other abnormal beats have the densest concentrations in short reuse distances. This is because of the strong recurrence and similar-shape properties of normal beats. (2) The abnormal beats with larger shape variations (such as PVCs) occupy more Euclidean distance segments and therefore cause the distribution curve to expand into the region of long reuse distance. (3) For almost all records, the majority of the beats are found within the reuse distance of 1. This is a strong indication of the spatial and temporal locality in the proposed classification architecture.

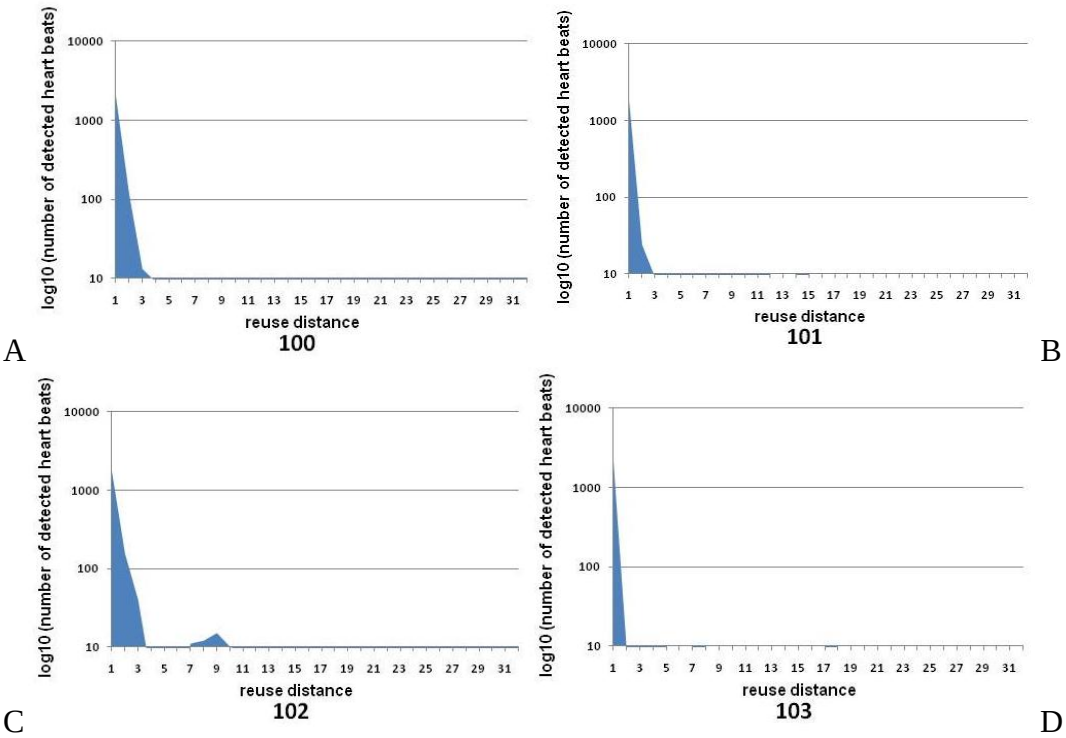

Figure 4-4. The reuse distance plots from record #100 to #124 in the *MIT-BIH Arrhythmia Database*. A) Record #100. B) Record #101. C) Record #102. D) Record #103. E) Record #104. F) Record #105. G) Record #106. H) Record #107. I) Record #108. J) Record #109. K) Record #111. L) Record #112. M) Record #113. N) Record #114. O) Record #115. P) Record #116. Q) Record #117. R) Record #118. S) Record #119. T) Record #121. U) Record #122. V) Record #123. W) Record #124.

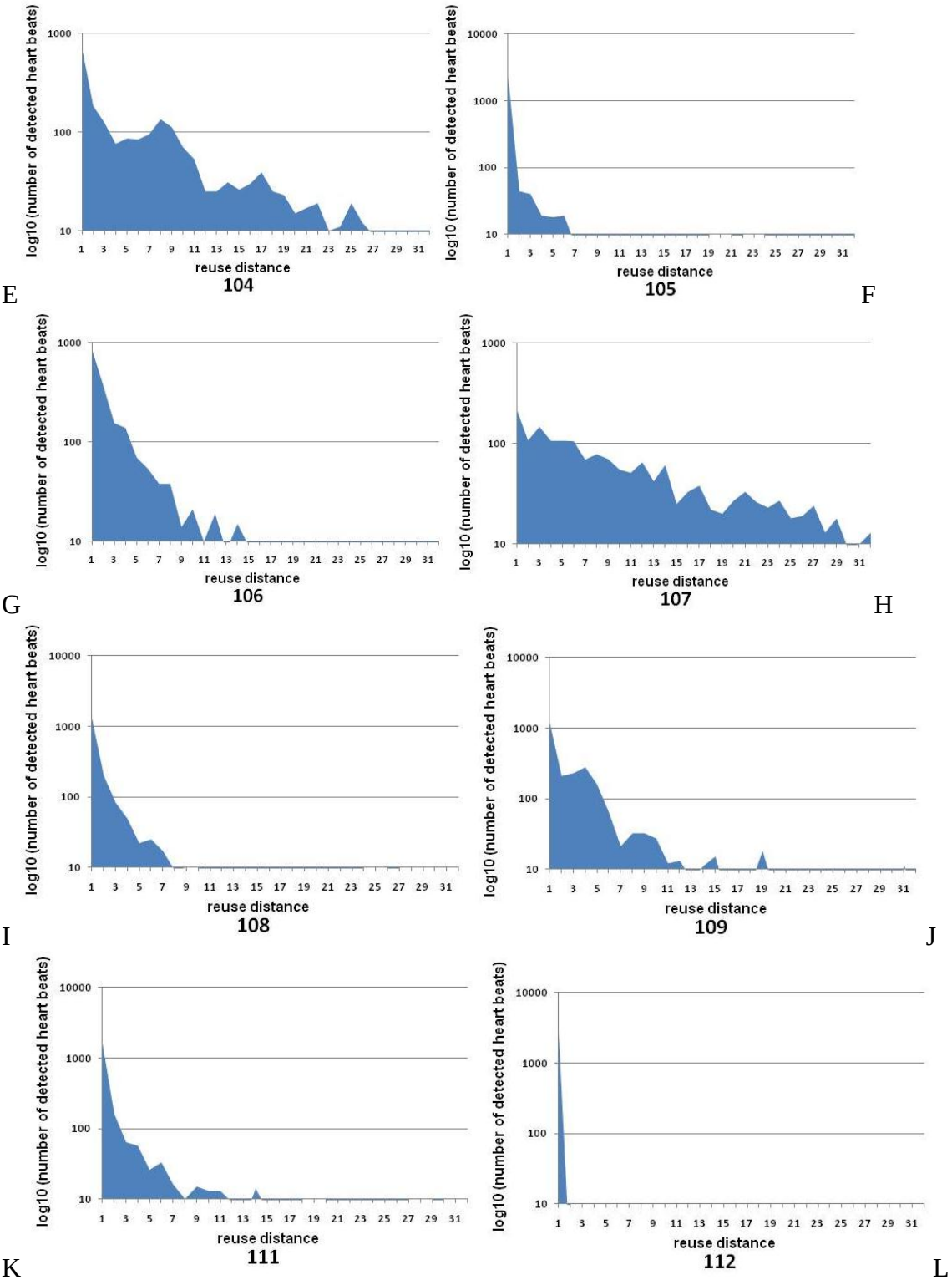

E F G H I J K L

Figure 4-4. Continued.

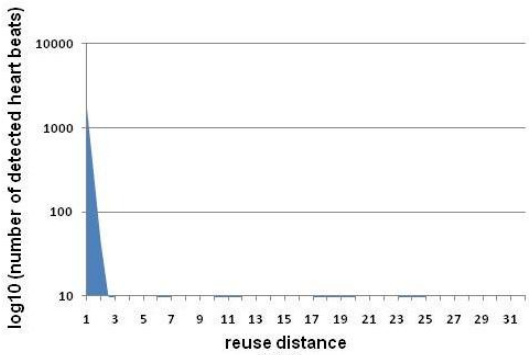

M **113**

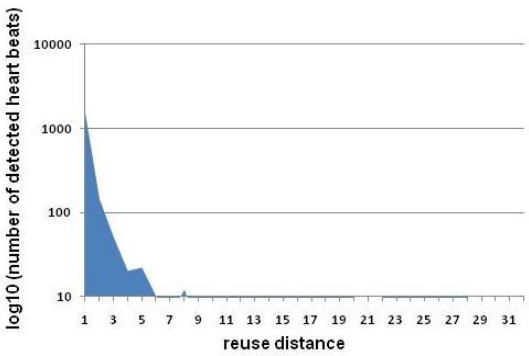

114 N

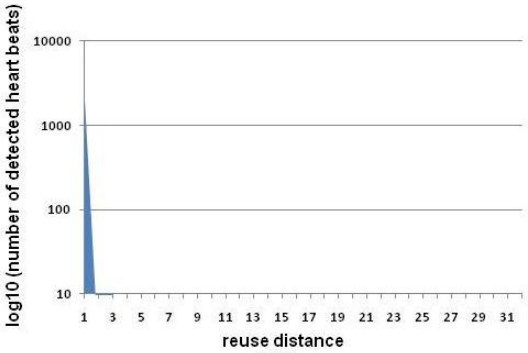

O **115**

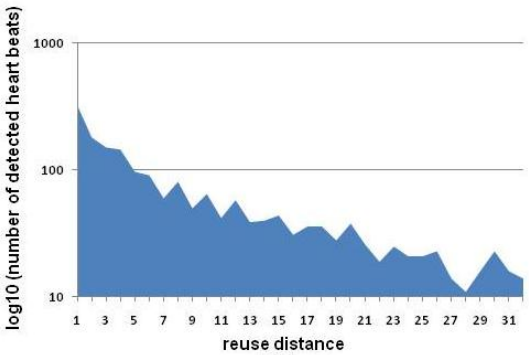

116 P

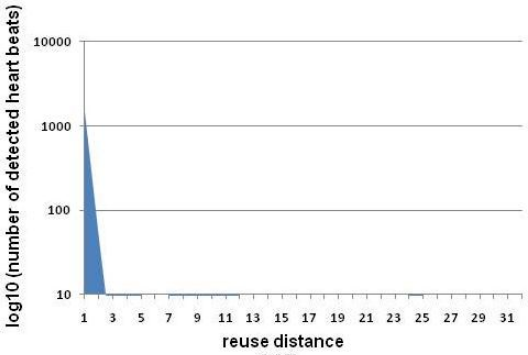

Q **117**

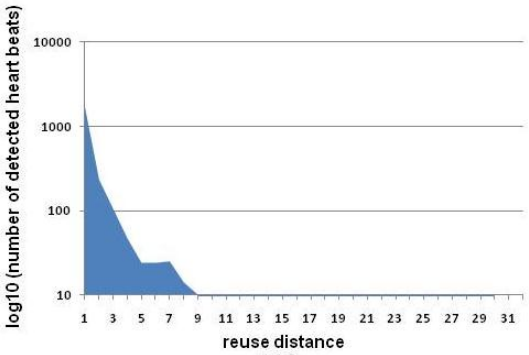

118 R

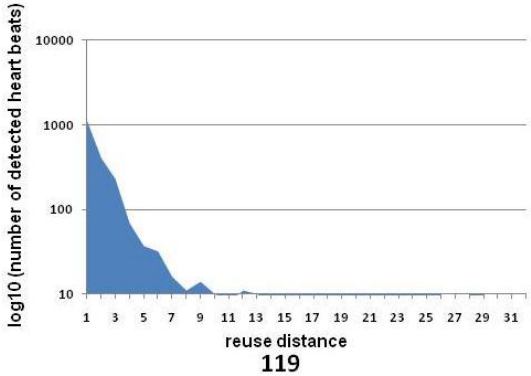

S **119**

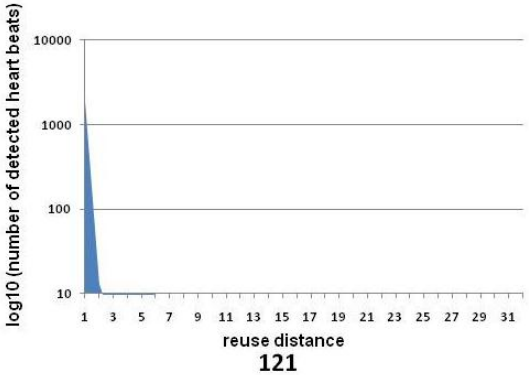

121 T

Figure 4-4. Continued.

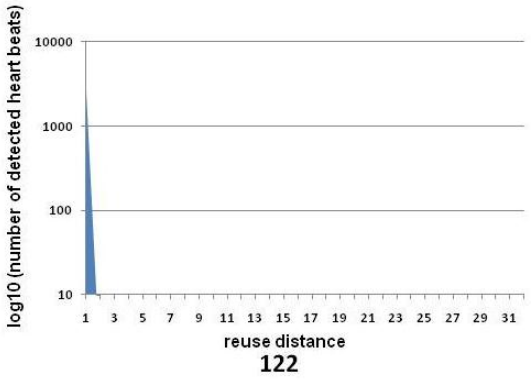

122

U

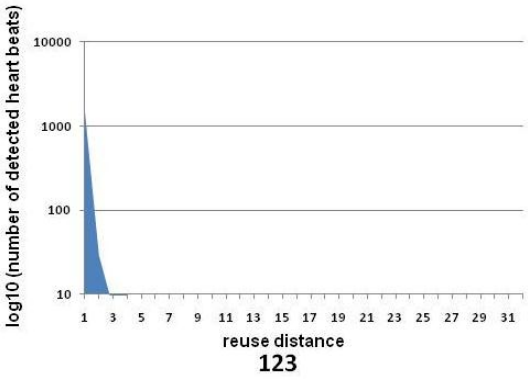

123

V

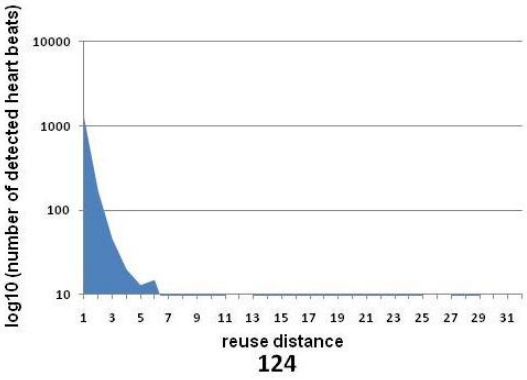

124

W

Figure 4-4. Continued.

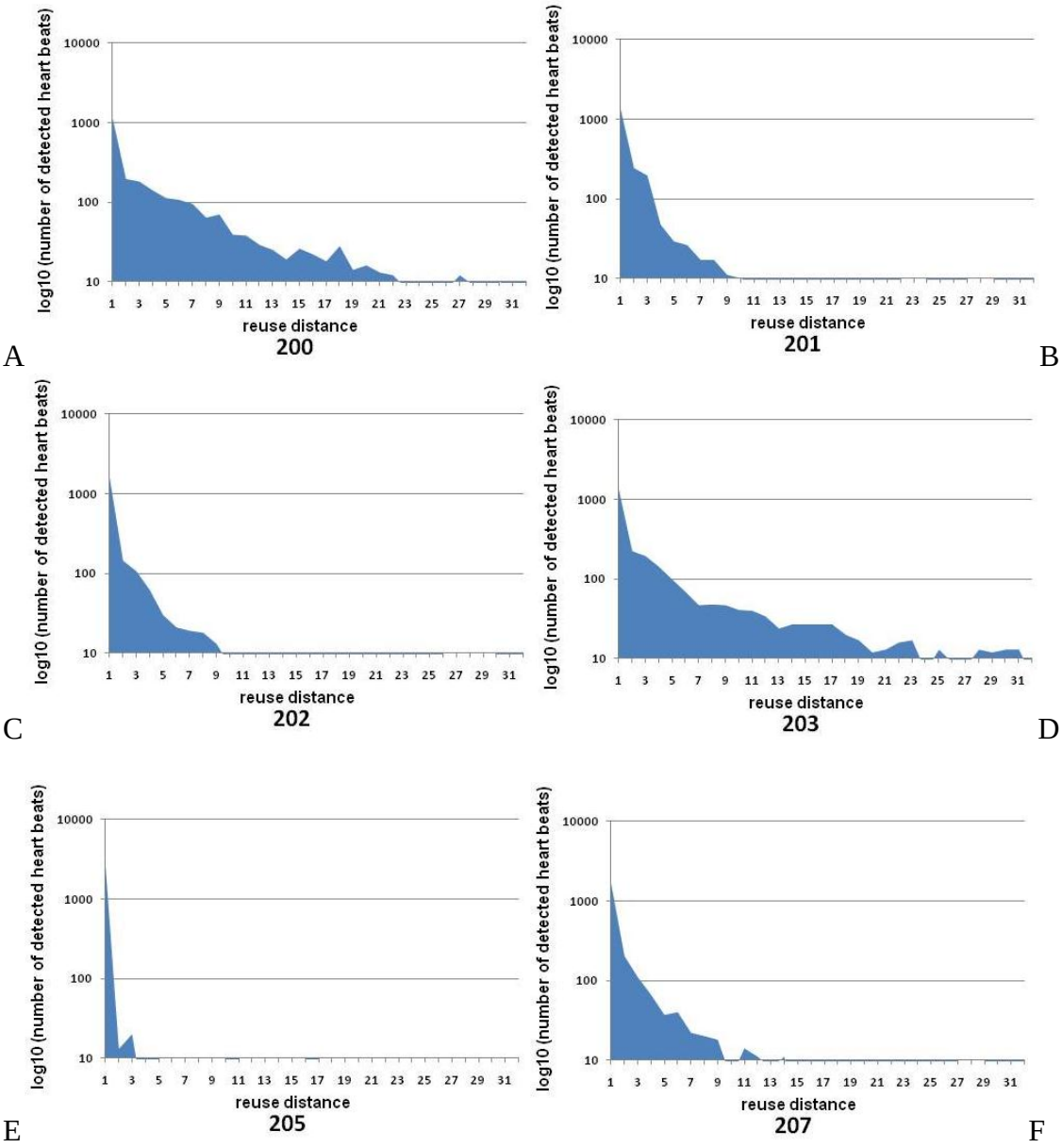

Figure 4-5. The reuse distance plots simulated using records #200 to #234 in the *MIT-BIH Arrhythmia Database*. A) Record #200. B) Record #201. C) Record #202. D) Record #203. E) Record #205. F) Record #207. G) Record #208. H) Record #209. I) Record #210. J) Record #212. K) Record #213. L) Record #214. M) Record #215. N) Record #217. O) Record #219. P) Record #220. Q) Record #221. R) Record #222. S) Record #223. T) Record #228. U) Record #230. V) Record #231. W) Record #232. X) Record #233. Y) Record #234.

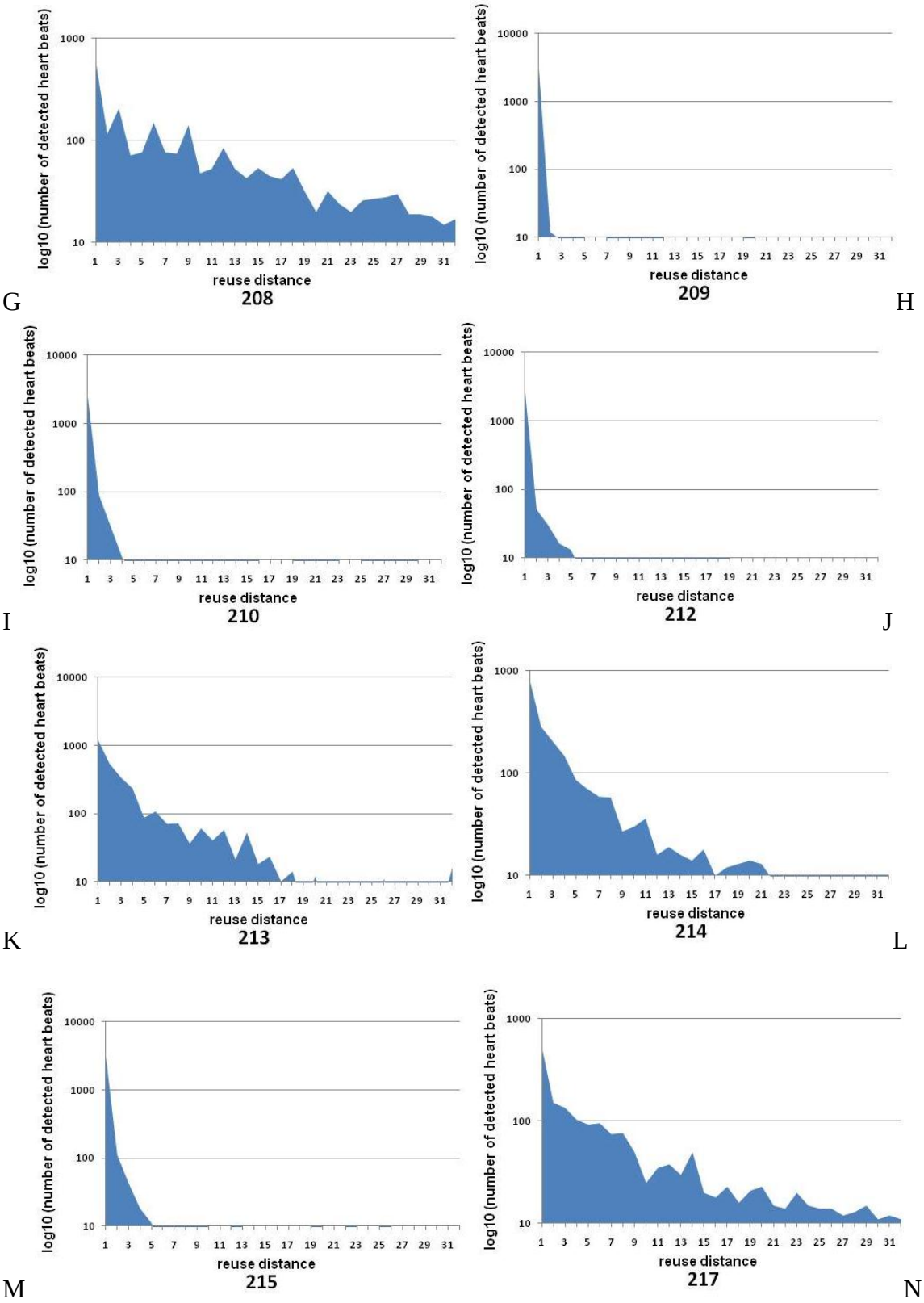

Figure 4-5. Continued.

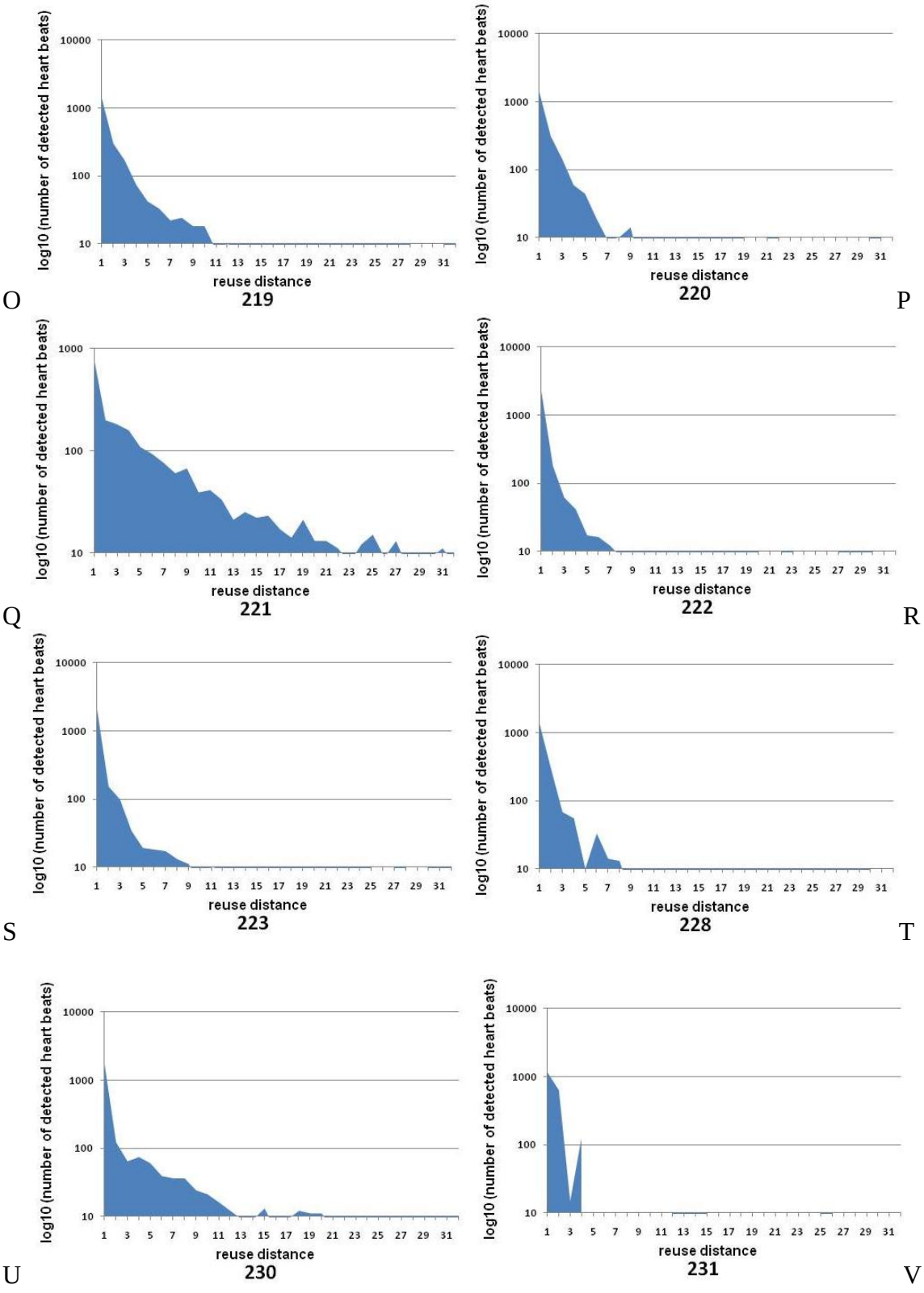

Figure 4-5. Continued.

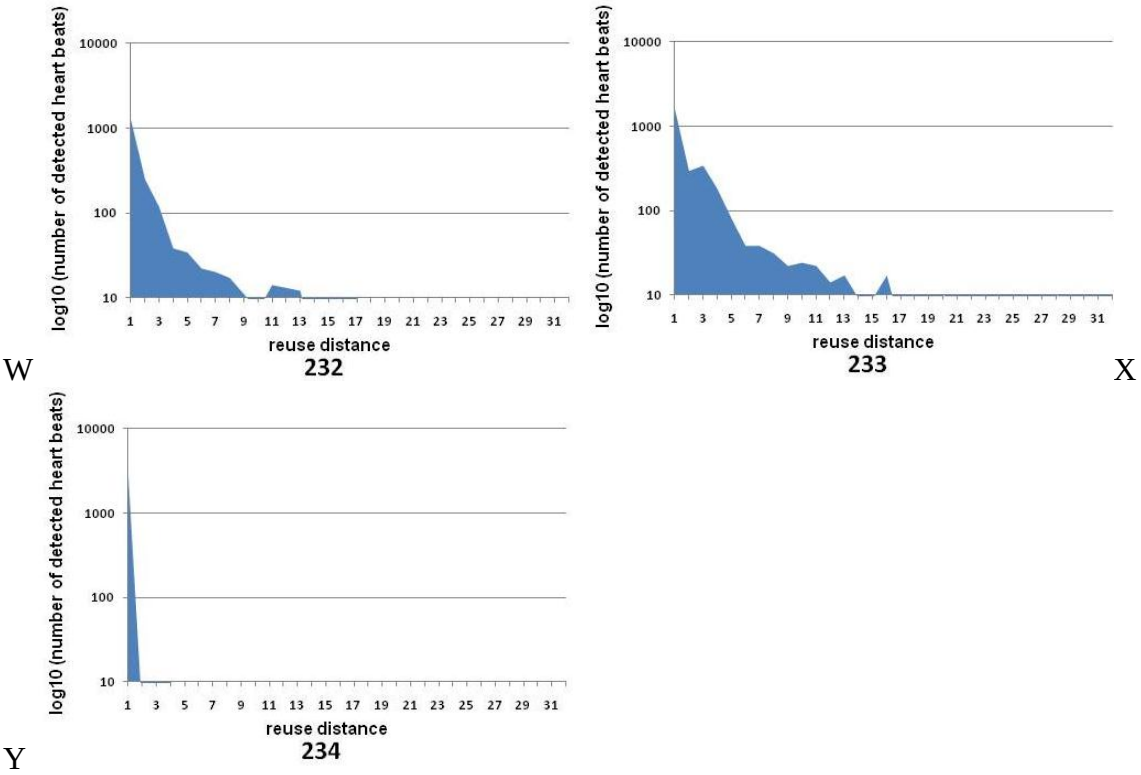

W X Y

Figure 4-5. Continued.

After comparing the 48 reuse distance plots against the simulated used cache entries in Table 4-7, we found that most of the reuse distance plots project the simulated number of used cache entries quite accurately, except for record #208, record #221, and record #228. To understand the underlying causes of the behaviors of these three records, we further investigated their reuse distance distribution by changing the bin sizes. Rather than using the original bin size that is calculated by dividing the entire distance span equally into 50 bins, we in turn divided the distance span into 40, 30, 20, and 10 segments. The simulations were performed for all of these configurations.

Figure 4-6 shows the reuse distance plots with all the different configurations and the distance distribution plot for the record #208. Clearly the plots show that the wider the bin size (fewer segments for the entire distance span), the narrower the reuse distances distribution. It is

because the PVC beat types in record #208 have larger shape variations compared to the distance range we normally defined for other beat types. Therefore, more than one bin was needed to cover the entire distance range, resulting in the longer reuse distance for PVC beats.

Figure 4-7 conveys similar information as Figure 4-6. In Figure 4-8, the large reuse distance distribution is caused by the PVCs that constitute with two major ranges.

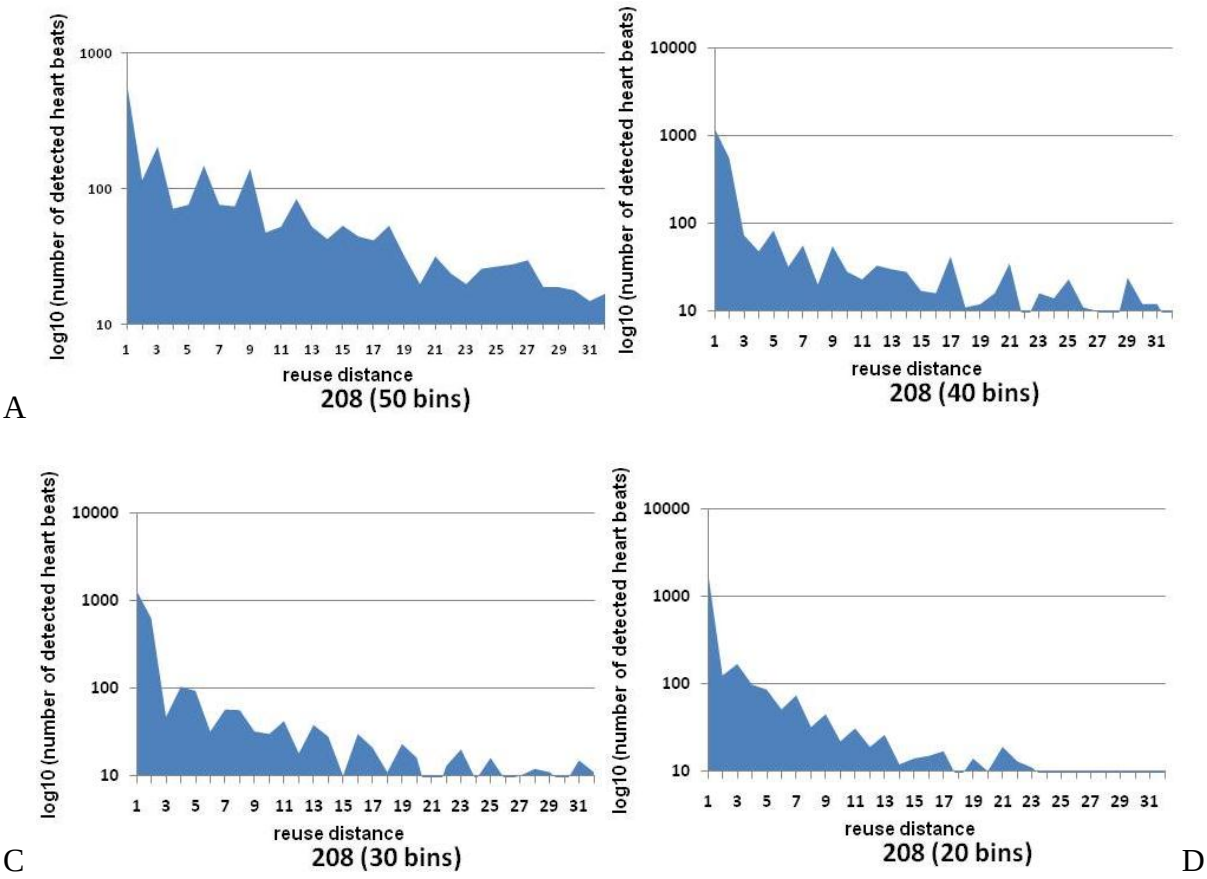

Figure 4-6. The reuse distance plots simulated using record #208 in the *MIT-BIH Arrhythmia Database*. A) 50 bins. B) 40 bins. C) 30 bins. D) 20 bins. E) 10 bins. F) Distance distribution.

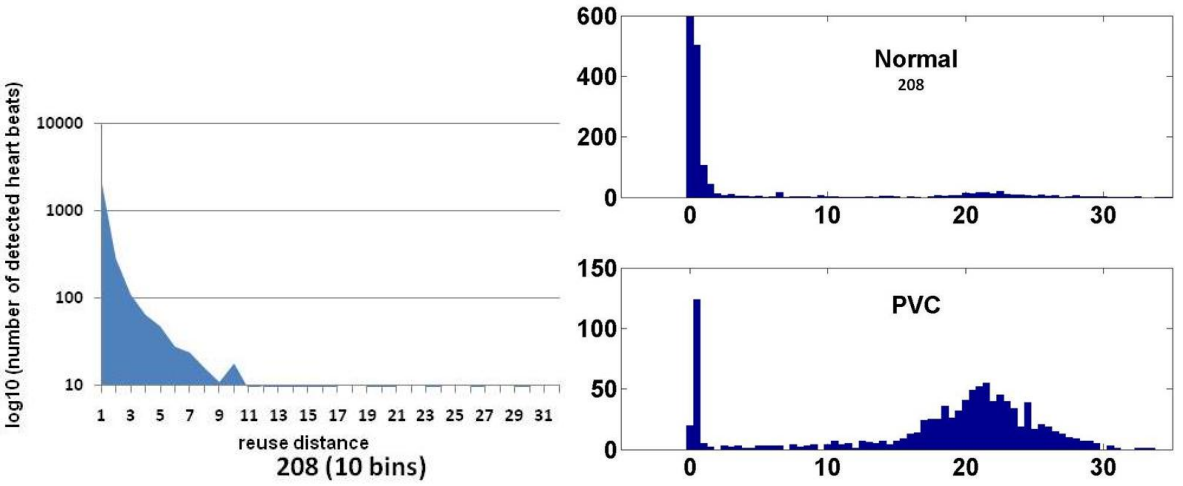

E F

Figure 4-6. Continued

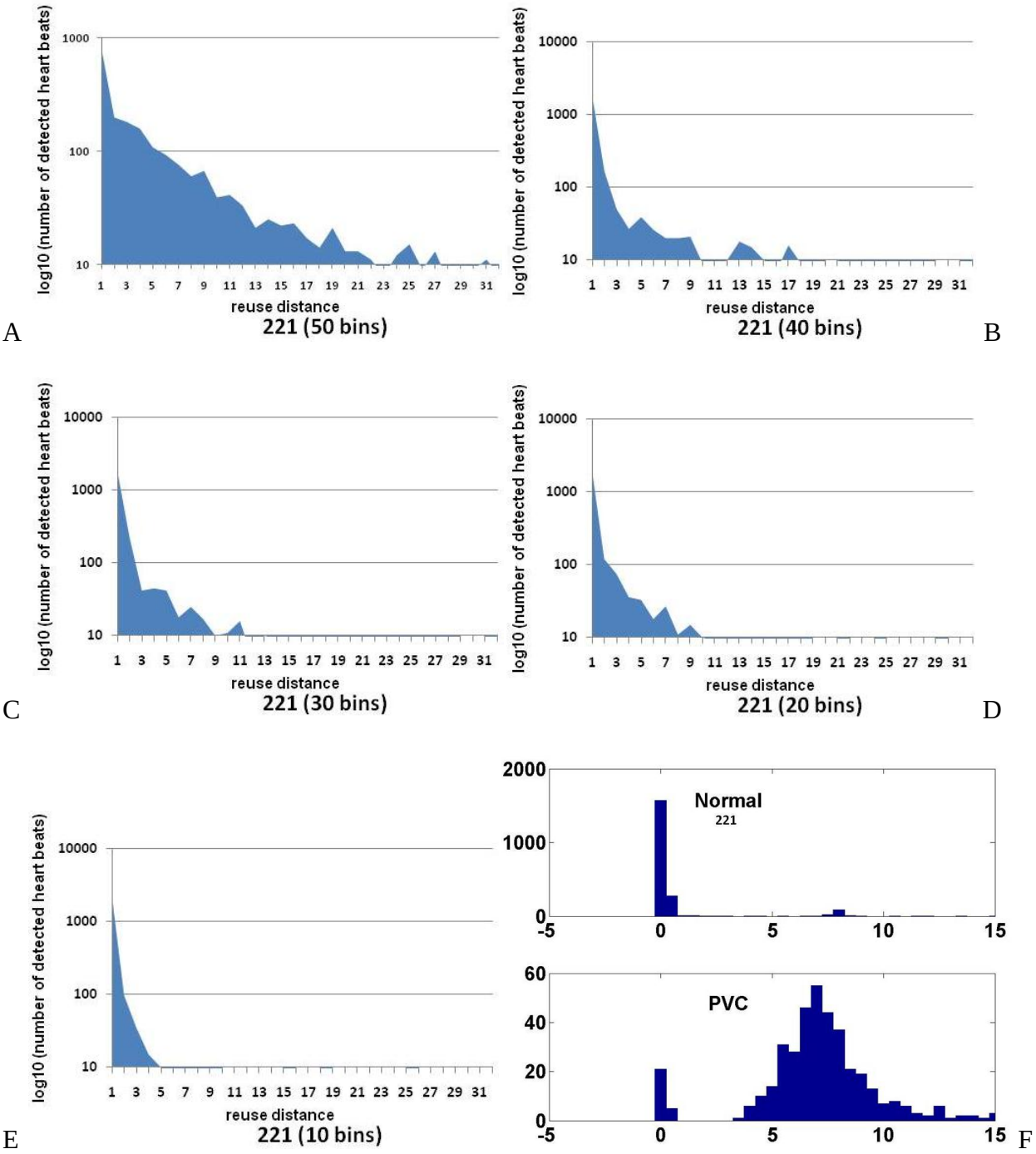

Figure 4-7. The reuse distance plots simulated using record #221 in the *MIT-BIH Arrhythmia Database*. A) 50 bins. B) 40 bins. C) 30 bins. D) 20 bins. E) 10 bins. F) Distance distribution.

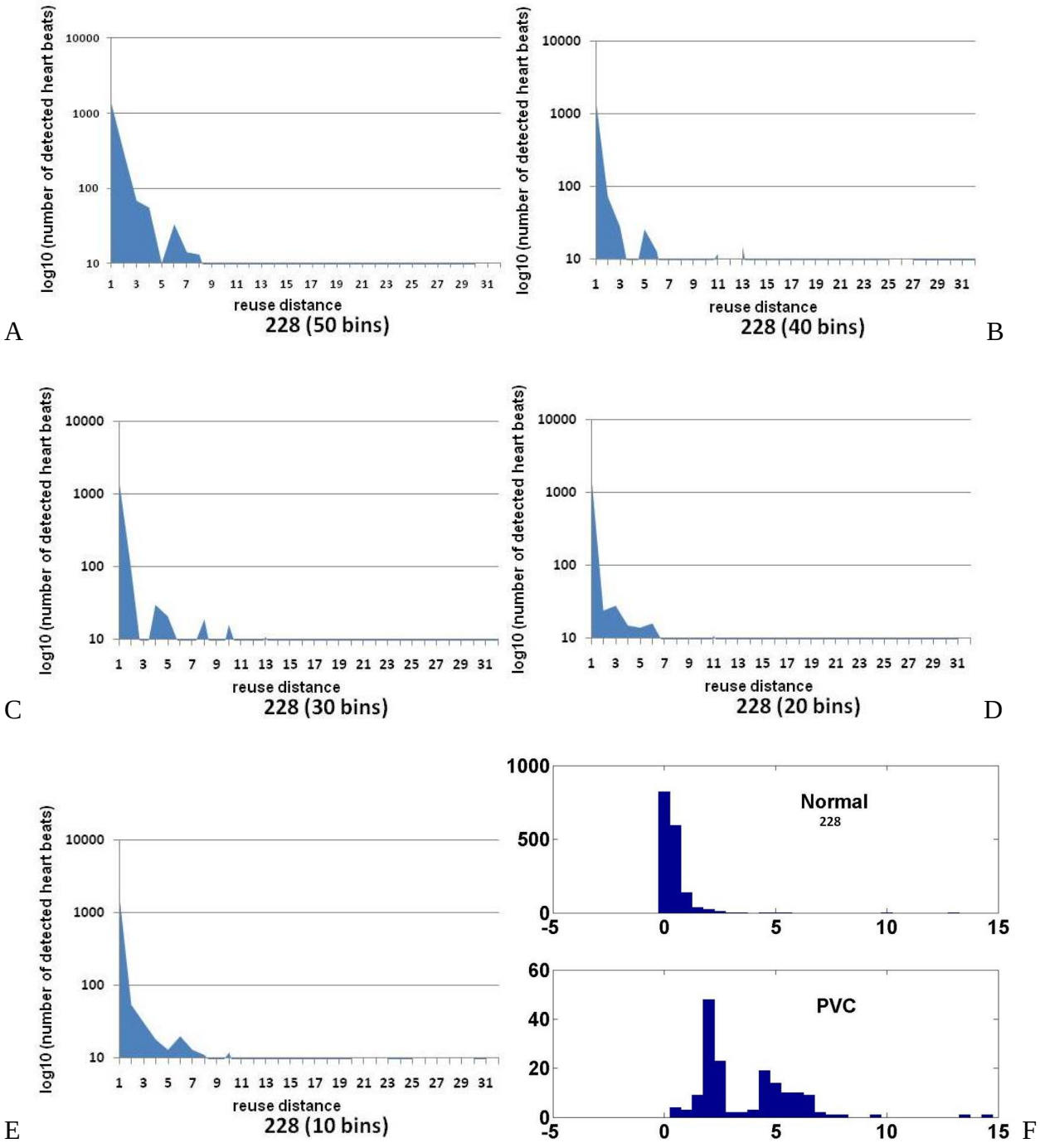

Figure 4-8. The reuse distance plots simulated using record #228 in the *MIT-BIH Arrhythmia Database*. A) 50 bins. B) 40 bins. C) 30 bins. D) 20 bins. E) 10 bins. F) Distance distribution.

Figure 4-9 shows a summed reuse distance distribution of all the records in the *MIT-BIH Arrhythmia Database*. The x-axis represents the reuse distance and the y-axis represents the number of beats expressed in log scale. Clearly most similarly shape heart beats occur at short reuse distance, and the number of heart beats decreases strongly with the increase of reuse distance: there is an approximately 100-times reduction at a distance of 8, and 1000-times reduction at a distance of 32.

Alternatively, Figure 4-9 can be viewed as the probability of hitting the cache at a certain reuse distance. As an example, we can specify the number of beats that can be stored in cache and use the distribution curve to find the corresponding reuse distance. This chosen reuse distance, considered to be equivalent to the number of cache lines under ideal SNR, is then padded with a number of extra lines for storing the noise clusters.

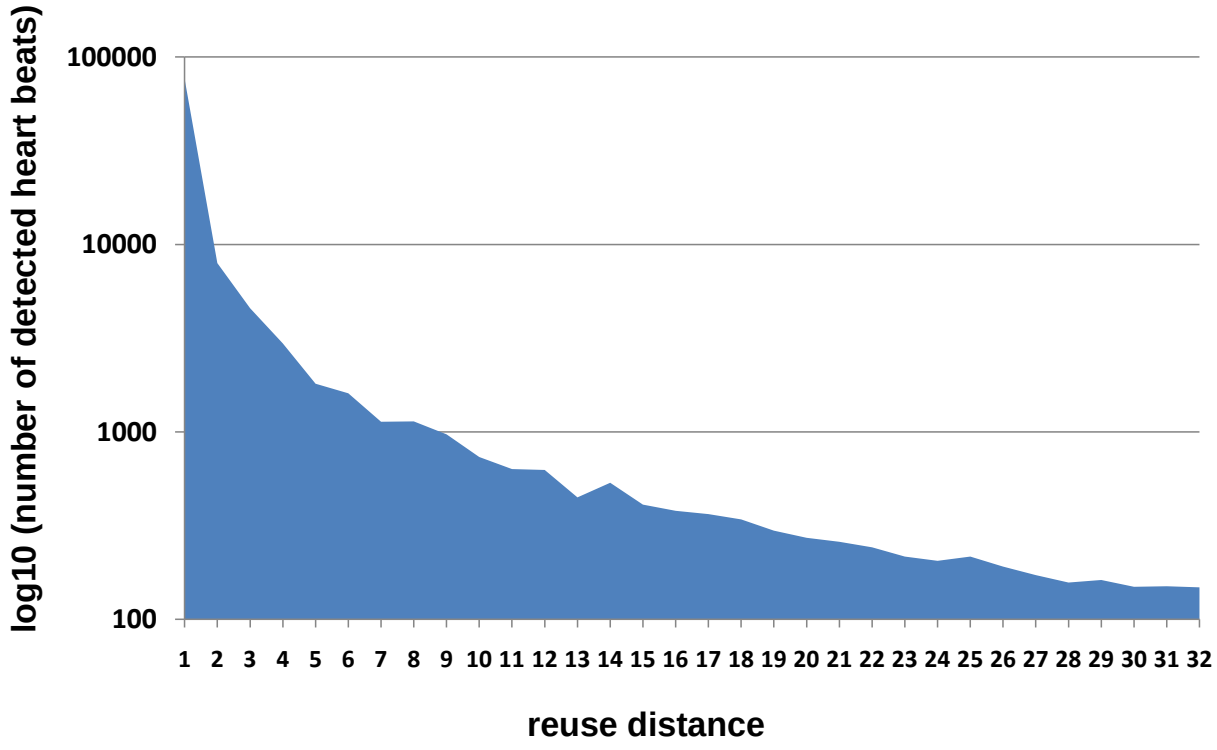

Figure 4-9. The distribution of the summed reuse distance for all the detected heart beats in the *MIT-BIH Arrhythmia Database*.

4.3 Heart Beat Cache

4.3.1 Cache Organization

The heart beat classification architecture presented in this study is the Heart Beat Cache, a term inspired by the Computer Architecture field. The online beat classification system is illustrated in Figure 4-10 and consists of a custom designed static random access memory (SRAM), a memory controller, and a Euclidean distance calculator. The key idea is to maintain a small table which provides the necessary information to determine the cluster attributes. On the right bottom side of Figure 4-10 is the Euclidean distance distribution of these three beat types that appear in record #207. Figure 4-11 shows the overlapped beat waveforms of these three beat types.

The cache consists of six columns as described below,

- Valid: if the bit is set to '1', the cluster is active. Otherwise, the entry will be shut down to save power.
- Mean [7:0]: the mean distance value of all the beats belonging to this cluster.
- Max [7:0]: the upper bound value of the cluster.
- Min [7:0]: the lower bound value of the cluster.
- Age [5:0]: the total number of beats detected after the last beat assigned to this cluster. In other words, it represents how often this cluster is updated.
- Count [5:0]: the total number of beats that belong to this cluster, with the maximum value being 63.

4.3.2 Cache Operations

Cache operations begin by storing a newly detected beat in a first-in, first-out (FIFO) in the QRS complex detector. The first detected beat is stored as a temporary template inside the Heart Beat Cache. All the subsequent beats are compared using their Euclidean distance against the template. Those beats whose Euclidean distance falls within a specified range belong to the same

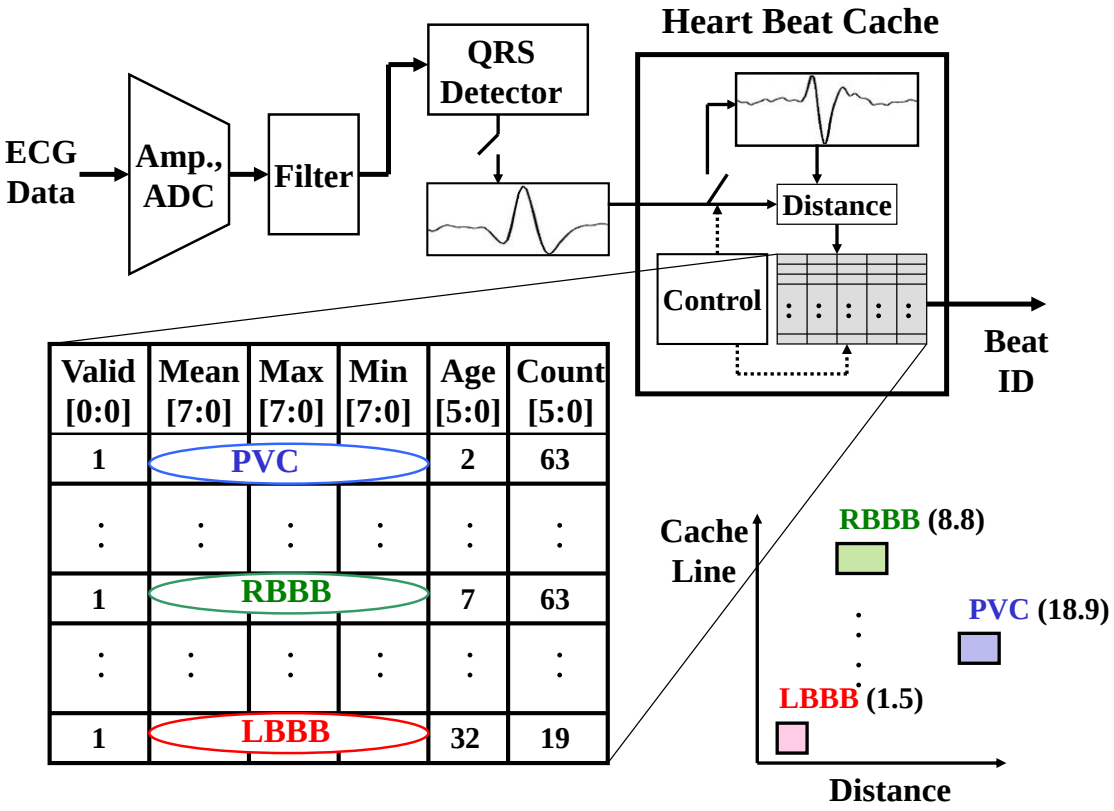

Figure 4-10. System block diagram and detailed Heart Beat Cache organization.

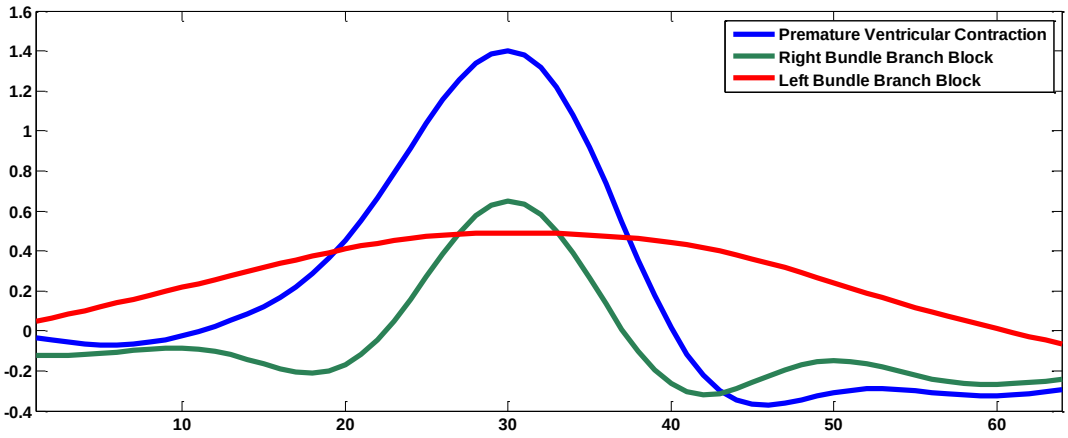

Figure 4-11. Heart beats samples taken from record #207 in *MIT-BIH Arrhythmia Database*.

cluster. The extracted cluster attributes are stored in one entry of the Heart Beat Cache and the counter value for that entry is updated whenever a new beat gets added to the cluster. When the counter reaches the chosen maximum value, a valid beat type cluster is identified in the cache. The next beat that belongs to this cluster is then chosen as the new template and replaces the current template. Afterwards, for each new incoming beat, the Heart Beat Cache only needs to perform the following three routine operations:

1) Insertion: For each newly detected beat, the Euclidean distance from the template beat is computed. The memory controller then searches the cache for a valid cluster that this new beat belongs to. If there is no valid cluster found, the first available free entry will be turned on and filled in.

2) Merge: A newly detected beat is compared against all the clusters. If a beat can be classified as belonging to more than one of the clusters, these clusters are merged into one. The merging process involves a recalculation of the cluster attributes and a gradual expansion of the upper and lower cluster boundaries.

3) Deletion: When the 'Age' value for a cluster reaches the specified maximum value, the cluster is deleted. The deletion of 'old' clusters can prevent overlapped beats and noise beats from forming a valid beat type cluster. It also frees the cache space for future beat clustering.

4.3.3 Power Management

The leakage power becomes increasingly significant in deep sub-micron technologies. For ECG processing applications, the operating frequency is typically low, and thus the dynamic power is not as important as the leakage power. The best way to control leakage is to turn off power to the memory with power gating. Simulation results reveal that 14 entries are sufficient to store the cluster information at all times.

4.4 Matlab Simulation Results

4.4.1 Simulation Setup

First, a program reads in the selected ECG data sets and their attributes from *MIT-BIH Arrhythmia Database* to the Matlab workspace. The data is then re-sampled from 320 Hz to

250Hz and band-pass filtered. A Matlab function implemented for the *Heart Beat Cache* algorithm is then executed. Finally, the performance evaluation for the classification results is calculated by comparing against the ground truth (annotations). The illustration of the simulation

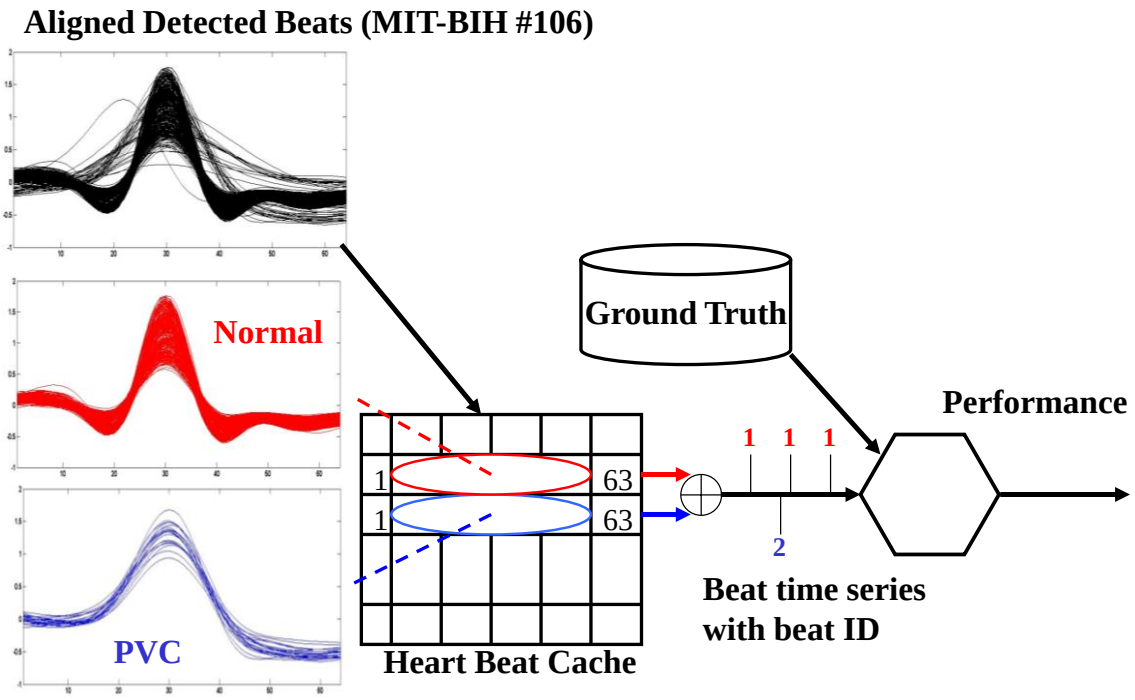

Figure 4-12. Simulation setup illustration using the record #106 from *MIT-BIH Arrhythmia Database*.

setup is shown in Figure 4-12. In this example, the *MIT-BIH* #106 data set is used, and two dominant beat types (Normal and PVC) are successfully clustered into different cache entries.

4.4.2 Evaluation of Classification Performance

We are essentially interested in how well the algorithm performs in terms of discriminating normal beats from abnormal beats, and also in recognizing different abnormal beats. Here we define several terms to serve this purpose. *TP* (true positives) refers to the correct classification, i.e., the beats with one annotation being clustered into one cache entry. *FP* (false positives), sometimes called *false alarms*, is an incorrect classification which means the beats with other annotated types fall into a cache entry occupied by beats that belong to a specific annotated type.

FN (false negatives), sometimes called *misses*, is an incorrect misclassification which means the annotated beats fall out of their designated cache entry. For each beat type, the performance is measured by the following parameters:

$$\text{Sensitivity} = \frac{\text{TP}}{\text{TP} + \text{FN}}$$

$$\text{Positive Predictivity} = \frac{\text{TP}}{\text{TP} + \text{FP}}$$

Sensitivity is defined as the amount of correctly clustered beats for each annotated type. Positive Predictivity is defined as the amount of correctly clustered beats for all the detected beats for each annotated type. Note that the total number of annotated beats is the sum of *TP* and *FN*, and the total number of detected beats is the sum of *TP* and *FP*.

4.4.3 Normal Beats

Normal beats account for the majority of the detected beats in the database. Since we choose the template from the majority of the beats, the Euclidean distance between the detected normal beats and the template is small. The majority of the beats occupy cache entries with high beat counts and high occurrence frequency, as shown in the 'Count' and 'Age' columns in the cache. The simulated clustering result for normal beats for the 48 records in database is summarized in Table 4-1 and Figure 4-13.

4.4.4 Premature Ventricular Contraction

Table 4-2 and Figure 4-14 show the clustering results for PVC. PVCs yield more inconsistent results due to their larger shape variation and the possibility of PVCs in some records containing more than one shape type.

4.4.5 Other Abnormal Beats

Tables 4-3, 4-4, 4-5, and 4-6 show the clustering results for other abnormal beat types. Other abnormal beat types have better performance than PVCs.

4.4.6 Cache Size Usage

Table 4-7 records the number of cache entries used during the simulation. Figure 4-10 shows the number of records versus the number of used entries. The number of cache entries is strongly dependent on the number of detected beat types, the SNR of the signals, and the frequency of the beat shapes' changes. When a beat with a new shape is detected, such that it doesn't match any of the pre-existent entries, more cache entries may need to be inserted to accommodate these newly formed clusters, which are spread out to begin with. Later these spread-out clusters can get merged, the more unqualified clusters can get deleted and finally the number of valid entries decreases and comes back to a stable value. The simulation shows that, the maximum cache size is 14 entries for the worst case, while on an average, 6 entries are used.

4.5 Discussions

Based on the results in Table 4-2, the classification of normal beats shows consistent performance throughout 48 data sets, with good average sensitivity (95.83%) and predictivity (89.92%). This consistency is due to less shape variation among normal beats and results in better clustering.

PVCs yield more inconsistent results due to their larger shape variation and the possibility of PVCs in some records containing more than one shape type. Several records had poor performance caused by a larger *FP* or *FN*. *FP* is large when the specified range for an initial cluster is too large, causing beats that do not belong to get assigned to that cluster. On the other hand, *FN* is large when the initial range for a cluster is too small, causing beats to miss the range. Further studies to improve the classification performance for PVCs are needed.

Table 4-8 and Figure 4-11 summarize the performance comparison between [2] and *Heart Beat Cache*. Armato's work outperforms the *Heart Beat Cache* on Paced, LBBB and Fusion, but not on RBBB. However, the *Heart Beat Cache* requires much less hardware complexity.

Table 4-1. Clustering results for Normal beats.

Record	Record Patient	# QRS	TP	FP	FN	Sensitivity	Predictivity
100	Male, age 69	2238	2232	33	6	99.73%	98.54%
101	Female, age 75	1860	1853	7	7	99.62%	99.62%
102	Female, age 84	99	99	36	0	100.00%	73.33%
103	Male, age N/A	2081	2077	8	4	99.81%	99.62%
104	Female, age 66	163	114	584	49	69.94%	16.33%
105	Female, age 73	2526	2382	128	144	94.30%	94.90%
106	Female, age 24	1507	1475	93	32	97.88%	94.07%
108	Female, age 87	1739	1733	84	6	99.65%	95.38%
112	Male, age 54	2536	2532	12	4	99.84%	99.52%
113	Female, age 24	1788	1775	0	13	99.27%	100.00%
114	Female, age 72	1820	1815	43	5	99.73%	97.69%
115	Female, age 39	1952	1947	8	5	99.74%	99.59%
116	Male, age 68	2301	1687	15	614	73.32%	99.12%
117	Male, age 69	1533	1476	2	57	96.28%	99.86%
119	Female, age 51	1543	1424	54	119	92.29%	96.35%
121	Female, age 83	1860	1852	13	8	99.57%	99.30%
122	Male, age 51	2475	2470	2	5	99.80%	99.92%
123	Female, age 63	1515	1481	3	34	97.76%	99.80%
200	Male, age 64	1742	1693	604	49	97.19%	73.70%
201	Male, age 68	1624	1468	58	156	90.39%	96.20%
202	Male, age 68	2060	2034	70	26	98.74%	96.67%
203	Male, age 43	2529	2280	411	249	90.15%	84.73%
205	Male, age 59	2570	2551	30	19	99.26%	98.84%
208	Female, age 23	1585	1304	377	281	82.27%	77.57%
209	Male, age 62	2620	2615	428	5	99.81%	85.93%
210	Male, age 89	2422	2401	236	21	99.13%	91.05%
212	Female, age 32	922	909	23	13	98.59%	97.53%
213	Male, age 61	2640	2604	411	36	98.64%	86.37%
215	Male, age 81	3194	3165	42	29	99.09%	98.69%
217	Male, age 65	244	197	134	47	80.74%	59.52%
219	Male, age N/A	2082	2052	244	30	98.56%	89.37%
220	Female, age 87	1953	1941	114	12	99.39%	94.45%
221	Male, age 83	2030	1873	41	157	92.27%	97.86%
222	Female, age 84	2061	2053	571	8	99.61%	78.24%
223	Male, age 73	2028	1995	468	33	98.37%	81.00%
228	Female, age 80	1688	1636	176	52	96.92%	90.29%
230	Male, age 32	2254	2247	210	7	99.69%	91.45%
231	Female, age 72	314	311	7	3	99.04%	97.80%
233	Male, age 57	2229	2223	683	6	99.73%	76.50%
234	Female, age 56	2700	2697	62	3	99.89%	97.75%

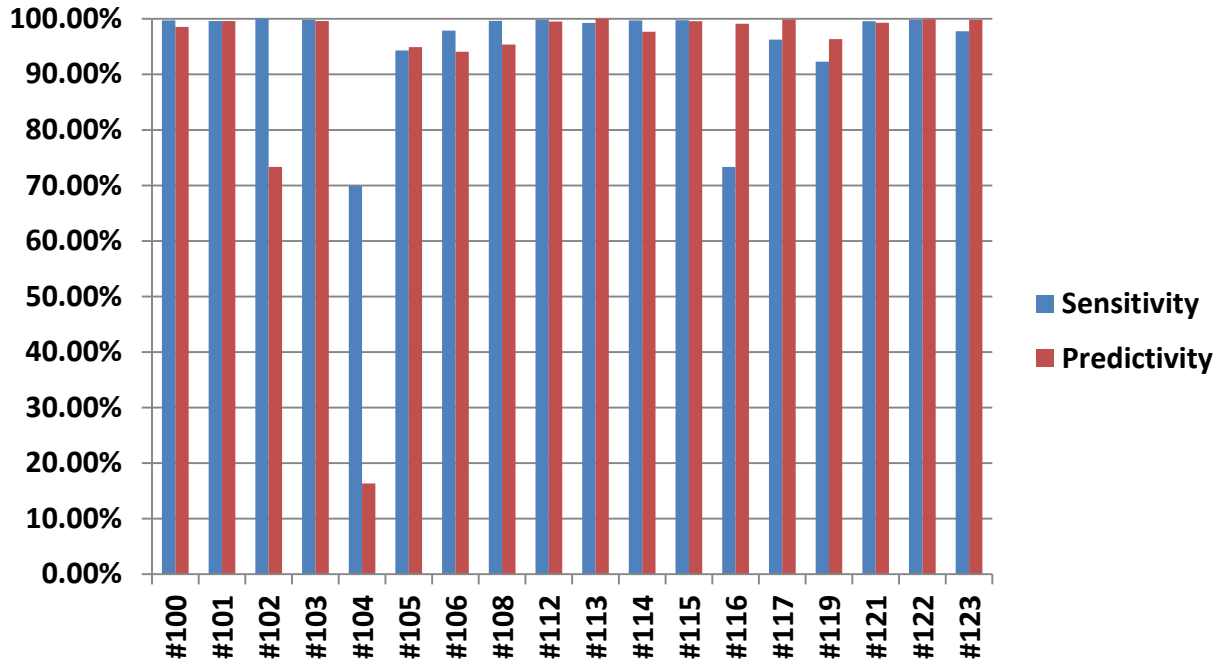

A

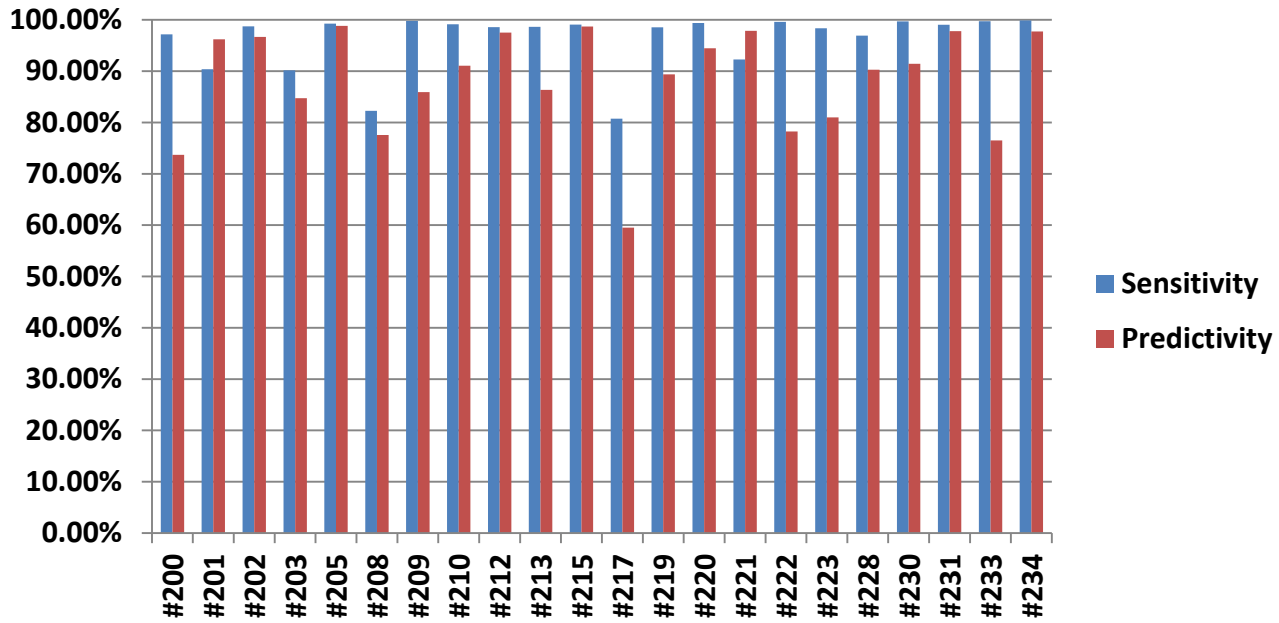

B

Figure 4-13. Clustering performance results for normal beats. A) Records #100 to #123. B) Records #200 to #234.

Table 4-2. Clustering results for Premature Ventricular Contraction (PVC) beats.

Record	Record Patient	# QRS	TP	FP	FN	Sensitivity	Predictivity
100	Male, age 69	1	1	0	0	100.00%	100.00%
102	Female, age 84	4	0	0	4	--	--
104	Female, age 66	2	1	0	1	50.00%	100.00%
105	Female, age 73	41	24	103	17	58.54%	18.90%
106	Female, age 24	520	446	45	74	85.77%	90.84%
107	Male, age 63	59	8	121	51	13.56%	6.20%
108	Female, age 87	17	0	0	17	--	--
109	Male, age 64	38	12	1	26	31.58%	92.31%
111	Female, age 47	1	1	0	1	100.00%	100.00%
114	Female, age 72	43	21	4	22	48.84%	84.00%
116	Male, age 68	109	103	25	6	94.50%	80.47%
118	Male, age 69	16	9	19	7	56.25%	32.14%
119	Female, age 51	444	436	163	8	98.20%	72.79%
121	Female, age 83	1	0	0	1	--	--
123	Female, age 63	3	0	0	3	--	--
124	Male, age 77	47	40	15	7	11.26%	72.73%
200	Male, age 64	826	365	98	461	44.19%	78.83%
201	Male, age 68	198	196	313	2	98.99%	38.51%
202	Male, age 68	19	19	17	0	100.00%	52.78%
203	Male, age 43	444	50	32	394	11.26%	60.98%
205	Male, age 59	71	48	21	23	67.61%	69.57%
207	Female, age 89	105	50	39	55	47.62%	56.18%
208	Female, age 23	992	720	304	272	72.58%	70.31%
209	Male, age 62	1	1	1	0	100.00%	100.00%
210	Male, age 89	194	18	22	176	9.28%	45.00%
213	Male, age 61	220	82	22	138	37.27%	78.85%
214	Male, age 53	256	204	36	52	79.69%	85.00%
215	Male, age 81	164	156	31	8	95.12%	83.42%
217	Male, age 65	162	72	812	90	44.44%	8.14%
219	Male, age N/A	64	22	194	34	34.38%	10.19%
221	Male, age 83	396	365	163	31	66.92%	69.13%
223	Male, age 73	473	127	44	346	26.85%	74.27%
228	Female, age 80	362	178	50	184	49.17%	78.07%
230	Male, age 32	1	0	0	1	--	--
231	Female, age 72	2	1	1	1	50.00%	50.00%
233	Male, age 57	831	177	8	654	21.30%	95.68%
234	Female, age 56	3	0	0	3	--	--

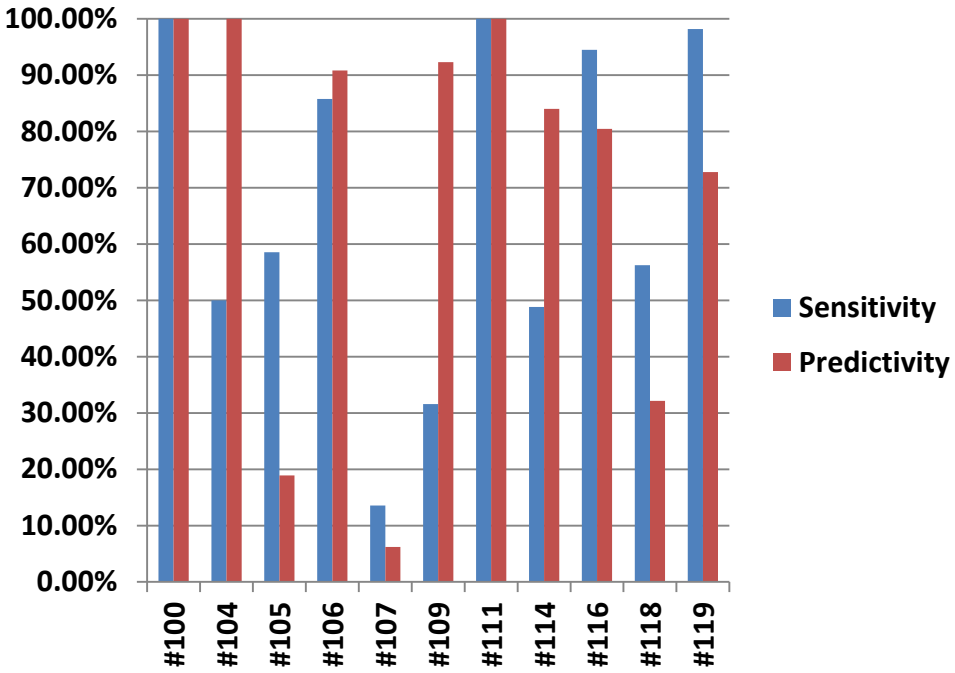

A

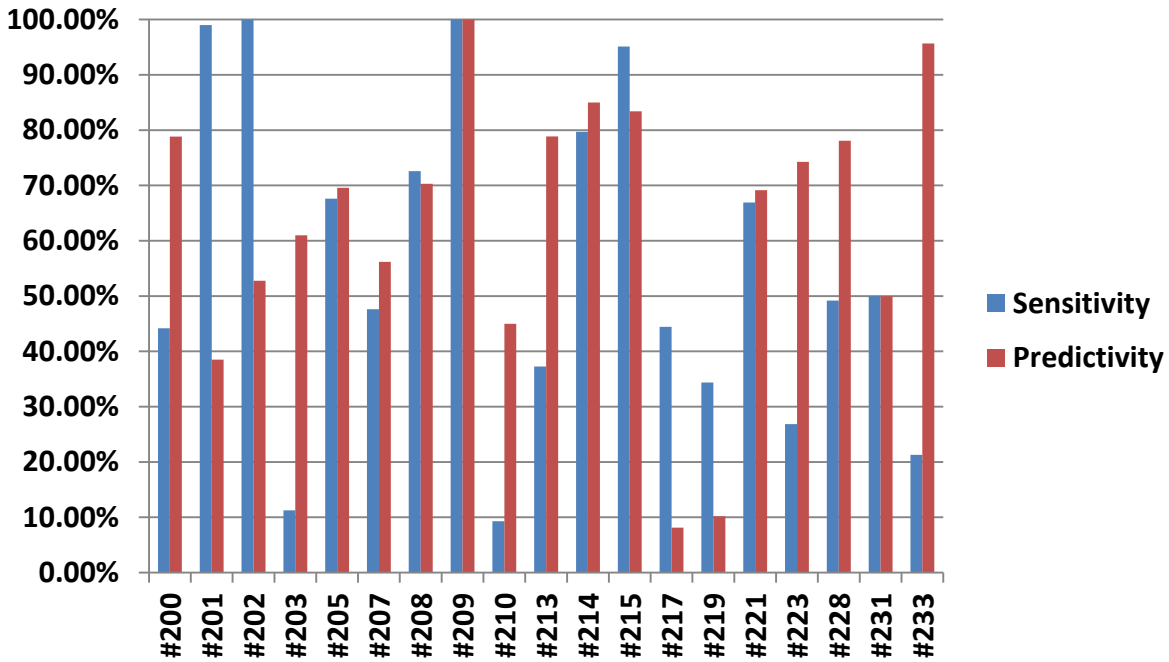

B

Figure 4-14. Clustering performance results for PVCs. A) Records #100 to #119. B) Records #200 to #233.

Table 4-3. Clustering results for Paced beats.

Record	Record Patient	# QRS	TP	FP	FN	Sensitivity	Predictivity
102	Female, age 84	2027	2024	163	3	99.85%	92.55%
104	Female, age 66	1379	1360	145	19	98.62%	90.37%
107	Male, age 63	2078	1864	18	214	89.70%	99.04%
217	Male, age 65	1542	1021	160	521	78.60%	86.45%

Table 4-4. Clustering results for Left Bundle Branch Block (LBBB) beats.

Record	Record Patient	# QRS	TP	FP	FN	Sensitivity	Predictivity
109	Male, age 64	2492	2143	13	49	86.00%	99.40%
111	Female, age 47	2123	2119	8	4	99.81%	99.62%
207	Female, age 89	1457	1444	315	9	99.11%	82.09%
214	Male, age 53	2002	1970	43	32	98.40%	97.86%

Table 4-5. Clustering results for Right Bundle Branch Block (RBBB) beats.

Record	Record Patient	# QRS	TP	FP	FN	Sensitivity	Predictivity
118	Male, age 69	2166	2156	100	10	99.54%	95.57%
124	Male, age 77	1530	1515	43	15	99.02%	97.24%
207	Female, age 89	86	23	24	63	26.74%	48.94%
212	Female, age 32	1825	1808	11	17	99.07%	99.40%
231	Female, age 72	1253	1250	9	3	99.76%	99.29%
232	Female, age 76	397	318	29	79	80.10%	91.64%

Table 4-6. Clustering results for fusion of Paced and Normal beats.

Record	Record Patient	# QRS	TP	FP	FN	Sensitivity	Predictivity
104	Female, age 66	1379	1360	145	19	98.62%	90.37%
217	Male, age 65	1542	1021	160	521	66.21%	86.45%

Table 4-7. Number of cache entries used during the simulation.

Record	Patient	Number of Used Entries	Record	Patient	Number of Entries
100	Male, age 69	3	200	Male, age 64	11
101	Female, age 75	5	201	Male, age 68	5
102	Female, age 84	1	202	Male, age 68	5
103	Male, age N/A	1	203	Male, age 43	13
104	Female, age 66	4	205	Male, age 59	5
105	Female, age 73	14	207	Female, age 89	9
106	Female, age 24	6	208	Female, age 23	9
107	Male, age 63	13	209	Male, age 62	3
108	Female, age 87	2	210	Male, age 89	4
109	Male, age 64	4	212	Female, age 32	6
111	Female, age 47	2	213	Male, age 61	14
112	Male, age 54	1	214	Male, age 53	14
113	Female, age 24	2	215	Male, age 81	9
114	Female, age 72	6	217	Male, age 65	14
115	Female, age 39	2	219	Male, age N/A	13
116	Male, age 68	12	220	Female, age 87	3
117	Male, age 69	2	221	Male, age 83	7
118	Male, age 69	6	222	Female, age 84	3
119	Female, age 51	7	223	Male, age 73	9
121	Female, age 83	2	228	Female, age 80	14
122	Male, age 51	2	230	Male, age 32	5
123	Female, age 63	5	231	Female, age 72	4
124	Male, age 77	8	232	Female, age 76	7
			233	Male, age 57	12
			234	Female, age 56	2

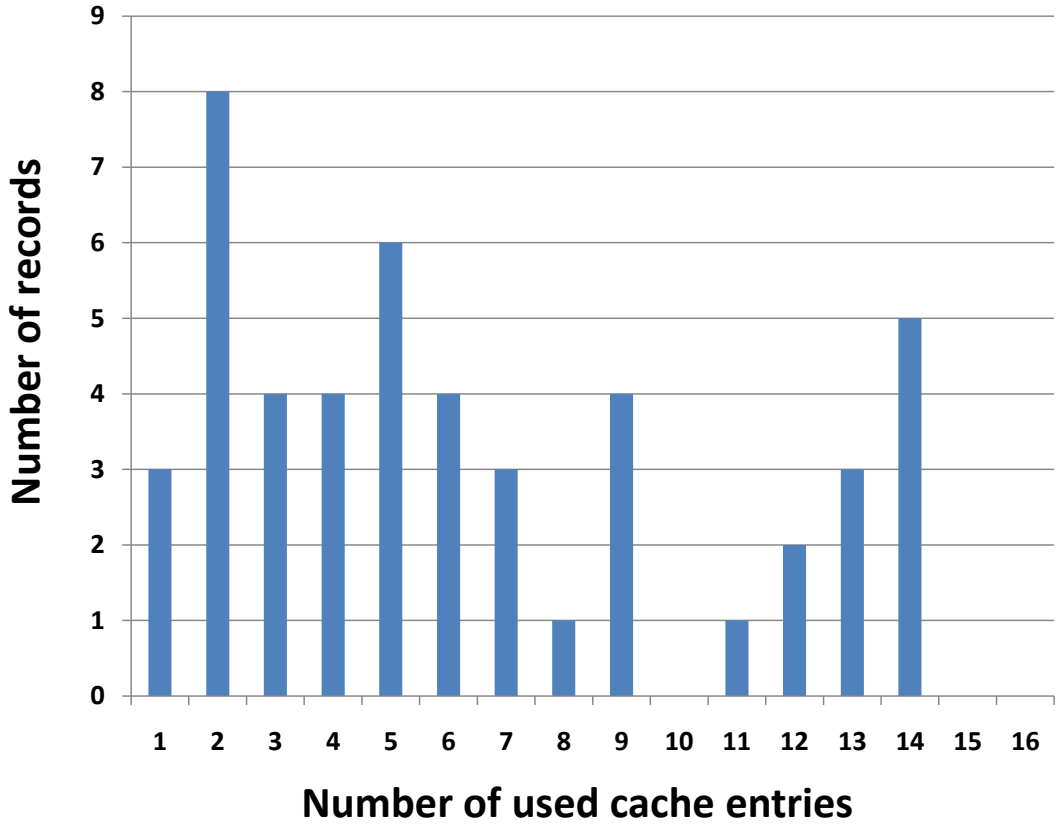

Figure 4-15. Number of used cache entries for 48 data sets.

Table 4-8. Performance comparison results for two beat classification algorithms.

Armato et al.				*Heart Beat Cache*		
Heartbeat	Record	Sensitivity	+P	Heartbeat	Sensitivity	+P
Normal	119, 200, 209, 212, 217, 221, 231, 233	--	--	Normal	95.83%	89.92%
PVC	119, 200, 214, 221, 233	94.10%	95.43%	PVC	55.75%	61.74%
Paced	107, 217	99.69%	92.17%	Paced	91.69%	92.10%
LBBB	109,111, 214	96.05%	94.74%	LBBB	95.83%	94.74%
RBBB	118,124, 212,231, 232	92.45%	95.16%	RBBB	95.50%	96.63%
Fusion	217	91.53%	22.71%	Fusion	82.42%	88.41%

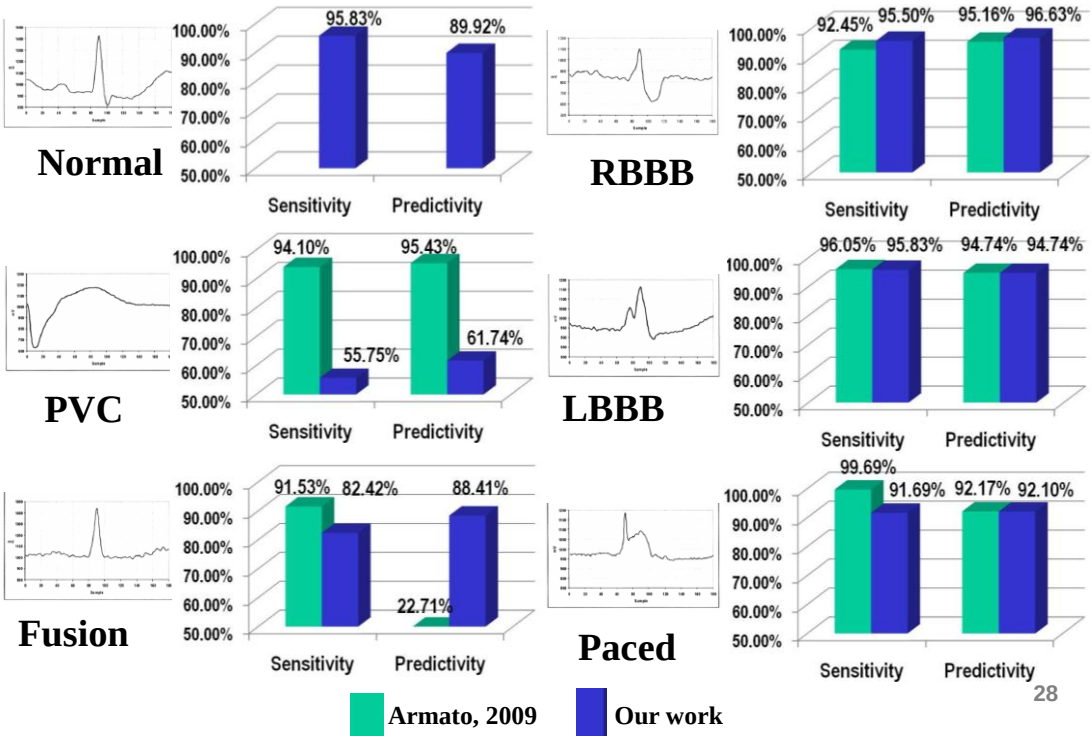

Figure 4-16. Performance comparison for two beat classification algorithms.

CHAPTER 5
HARDWARE IMPLEMENTATION

5.1 ECG System

ECG systems should ideally be able to operate in a continuous and autonomous fashion without human intervention. Several hardware characteristics needed to achieve a fully autonomous and self-contained system are:

(1) Autonomous beat template generation: The template-matching algorithm needs known beat waveforms before execution begins. In current practice, a template is often formed by averaging the manually selected beats from a set of test data. For autonomous template generation, our system generates beat templates by continuously learning from the detected beats without user input. Even with drastic extreme shape changes, a new template can be quickly regenerated.

(2) Real-time online beat classification: For a vital signs monitoring system, fast and autonomous beat classification is required for both bandwidth reduction and online diagnosis. Most current beat classification algorithms require a manual definition of each cluster before classification begins, and thus these algorithms cannot be initialized when a number of beat clusters and templates are unknown. To avoid this disadvantage, we propose a real-time online beat classification architecture that can dynamically determine the number of beat clusters and store the relevant characteristics.

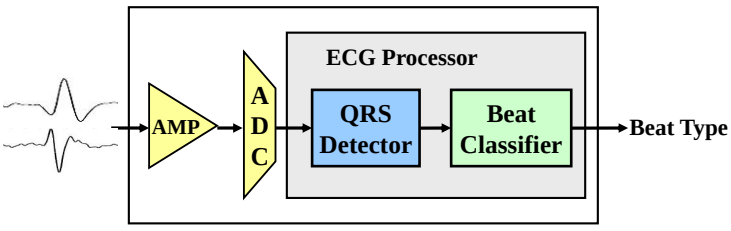

Figure 5-1. Single ECG processor block diagram.

5.2 RTL Implementation

In this chapter a hardware implementation for a self-contained ECG processing architecture is described in register transfer level (RTL). The datapath consists of application-specific functional units for arithmetic and conditional logic as well as the memory space for beat templates and the *Heart Beat Cache*. As shown in Figure 5-3, there are four stages in the

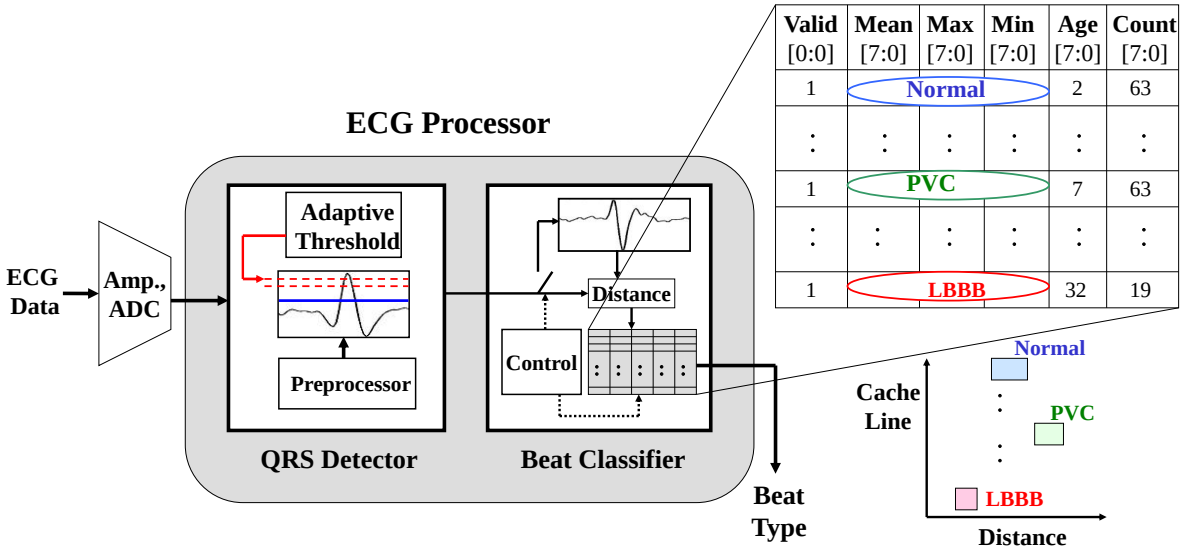

Figure 5-2. Detailed ECG processor block diagram.

datapath – the QRS detector, beat templates, Euclidean distance calculator, and the *Heart Beat Cache* with memory controller. An equal number of clock cycles is required for the execution of each stage offering the opportunity for a pipeline operation to accommodate beats from other leads in close temporal proximity.

5.2.1 QRS Detector

The QRS detector, which uses threshold-crossing method, has a FIFO which is 64-deep with an 8-bits in width. The QRS detection is performed by comparing the amplitude of the 38th sample in the FIFO with the threshold. If the amplitude crosses the threshold, a 64-cycle wide

pulse will be generated by the pulse generator. During which the entire beat waveform will be received by the beat classifier. At other times the beat classifier ignores the incoming samples.

5.2.2 Beat Classifier

Upon receiving notification from the QRS detector, one of the template memory locations will be filled with the complete detected beat waveform, while the other is kept fixed with a known beat shape as reference.

The Euclidean Distance calculator determines the Euclidean distance between two beat templates and is implemented using the arithmetic IPs in the Synopsys DesignWare Library.

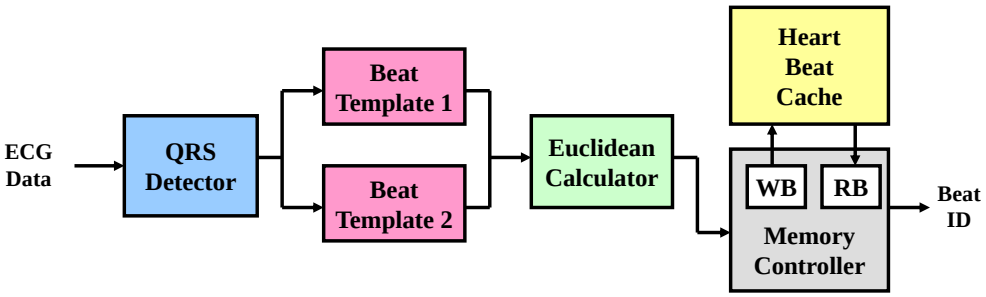

Figure 5-3. Single-channel processor datapath block diagram.

The memory controller oversees the cache read/write operations and beat classification algorithm executions. Upon notification from the Euclidean calculator that the newly calculated distance is ready, the controller scans the cache and compares the distance with the stored max-min distance range for each cluster entry. The appropriate actions to be taken depend on the cluster's metadata. The cycle-accurate timing diagram of the memory controller is given in Figure 5-5.

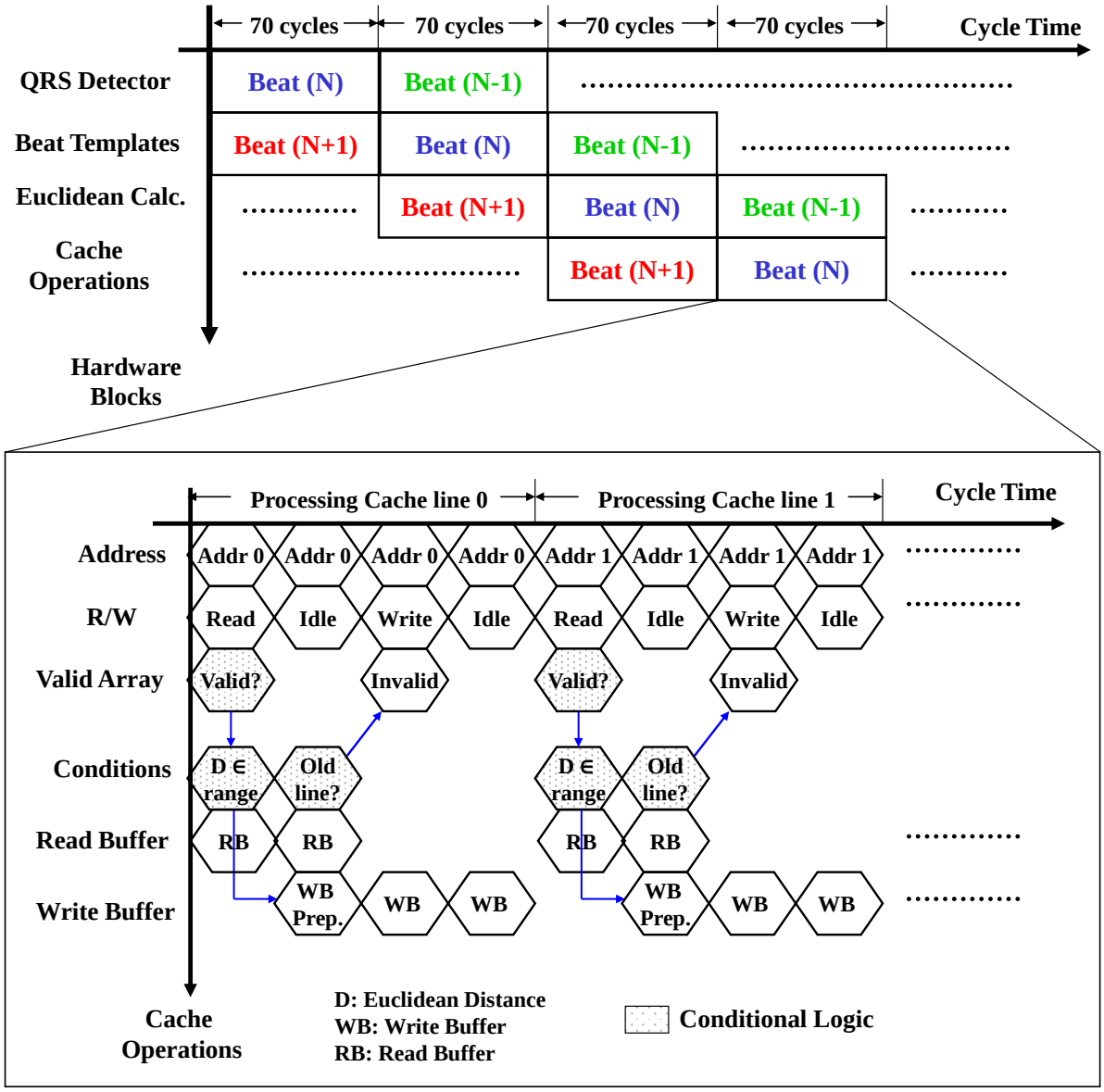

Figure 5-4. Timing diagram for the processor pipeline datapath and the detailed Heart Beat Cache read/write operations of the memory controller.

5.2.3 Functional Simulations

Functionality is verified using Cadence NCSim with previously generated ECG data sets. The data set is first converted from the Matlab file format to the NCSim-compatible binary format, and then the cycle-based simulation results are closely examined to ensure that the fixed-point RTL design is functionally equivalent to the floating-point algorithms in Matlab.

Screenshots, from the NCSim program using MIT-BIH ECG data are given in Figure 5-6 and 5-7. Figure 5-6 shows the function simulation waveforms for the QRS detector, and Figure 5-7 shows the waveforms for beat classifier.

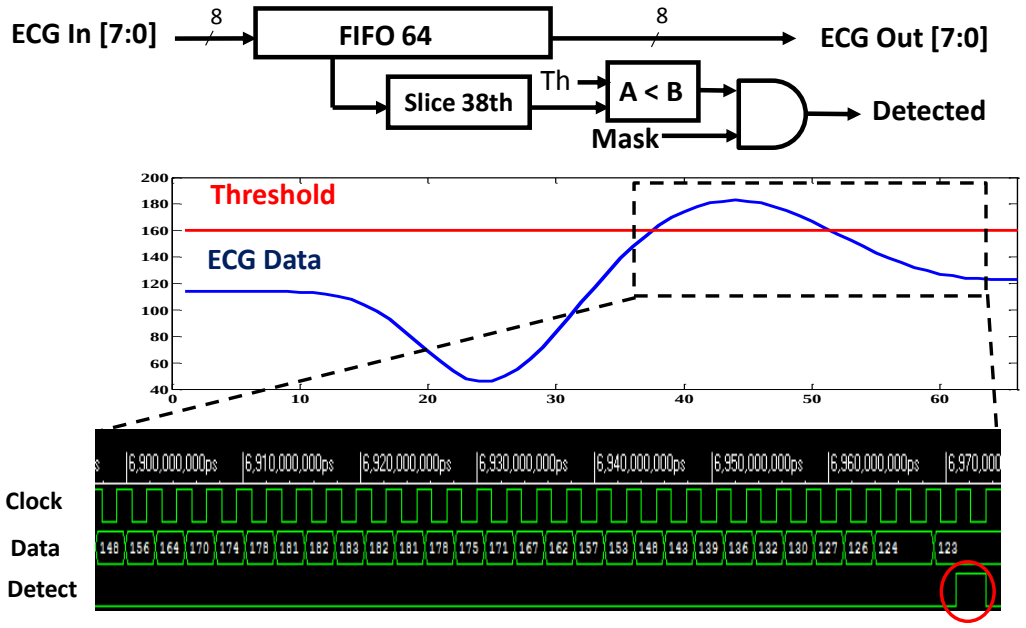

Figure 5-5. Function simulation waveforms for QRS detector in NCSim.

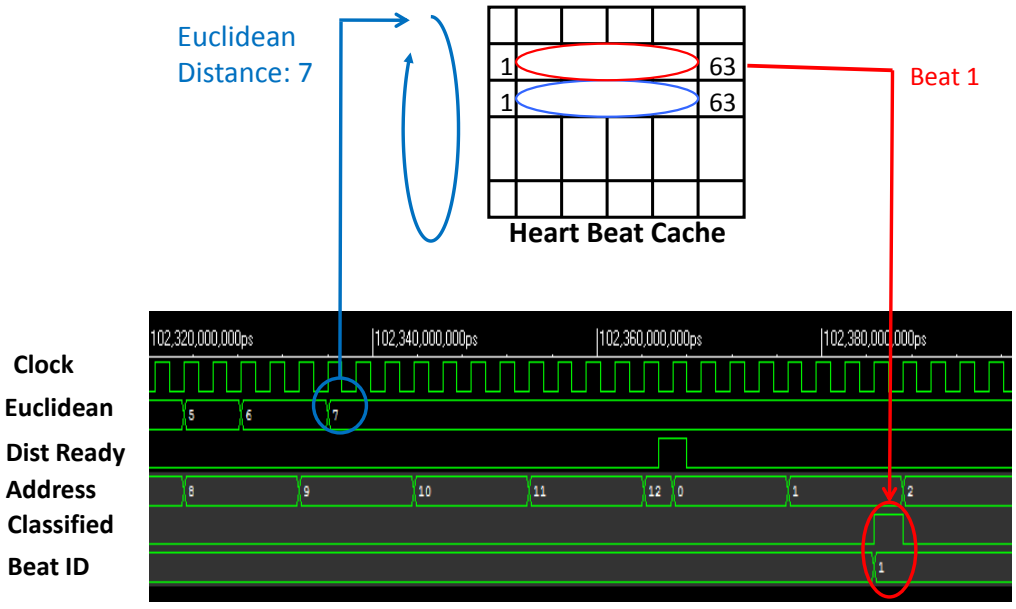

Figure 5-6. Function simulation waveforms for beat classifier in NCSim.

5.3 FPGA Implementation

5.3.1 Synthesis

The implementation was synthesized using Xilinx ISE 10.1 and mapped onto the Virtex-IV (4VSX35FF668-10) FPGA chip. The synthesis results are listed in Table 5-1.

Table 5-1. FPGA synthesis report.

Function Block	Slices	4-input LUTs	Flip-Flops
QRS Detector	254 (69.8%)	550 (88.0%)	158 (52.1%)
Euclidean Calculator	57 (15.7%)	44 (7.0%)	72 (23.8%)
Cache Controller	53 (14.6%)	31 (5.0%)	73 (24.1%)
Total	364	625	303
4VSX35FF668-10	15360	30720	30720

5.3.2 Memory

Two ZBT SRAMs are placed on the FPGA board and used to store the beat templates (128 bytes) and the *Heart Beat Cache* (80 bytes).

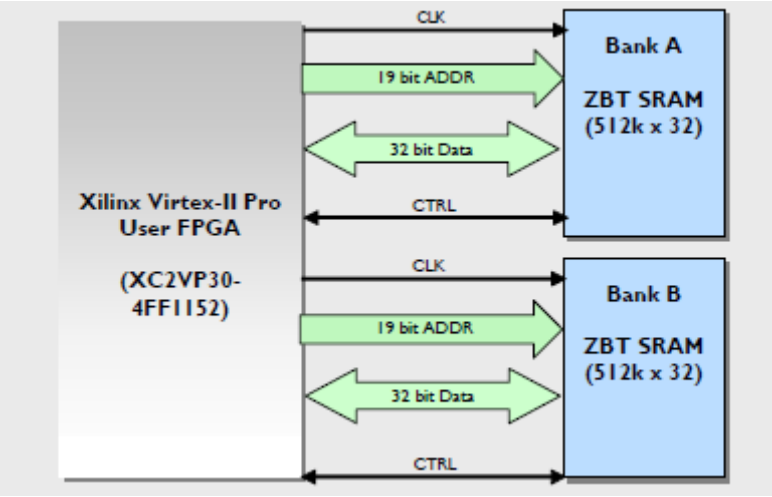

Figure 5-7. ZBT SRAM interface.

5.4 Optimizations

To further improve the performance and reduce the hardware cost of a single-channel ECG processor, there are some architecture-level optimizations that may be considered. For example, the study on how to determine the optimum number of rows in cache has been described in Chapter 2. Nonetheless, there are some parameter settings that need to be investigated.

5.4.1 FIFO size

FIFOs in the QRS detector are used to store detected beat waveforms. The size of FIFO is mainly determined by typical beat width and ADC digitization sampling rate. The beat widths vary between 100 ms (QRS-interval) to 600 ms (PR-interval + QT-interval), which are equivalent to 25 samples to 150 samples using 250 Hz sampling rate. A typical beat waveform is shown in Figure 5-1.

Larger FIFO contains more noise than the targeted waveform, while smaller FIFO might lose some important features in a complete beat waveform such as P-wave and U-wave. From a hardware perspective, smaller FIFO consumes less power. There is a need for a quantitative study on the relationship between FIFO size and the beat classification accuracy.

5.4.2 Cluster Size

The cluster size largely affects the accuracy of beat classification. Larger cluster size results in unwanted mix of two different beat shapes. Smaller cluster size produces more clusters than necessary. A fixed-size cluster scheme is used in Chapter 3. However, an adaptive and optimized cluster size could potentially achieve better accuracy. Quantitative study on the Euclidean distance variation will be conducted to get the optimal initial cluster size.

5.4.3 Number of Templates

A beat shape is located in a feature space by calculating its Euclidean distances with pre-selected templates. The more templates are used to locate a beat, the more dimensions a feature

space has, thus the more variability for a beat shape to differentiate itself. For example, in the case of two templates, the coordinate of each detected beat is considered as two Euclidean distances with templates or values along two axes of a two-dimension plane.

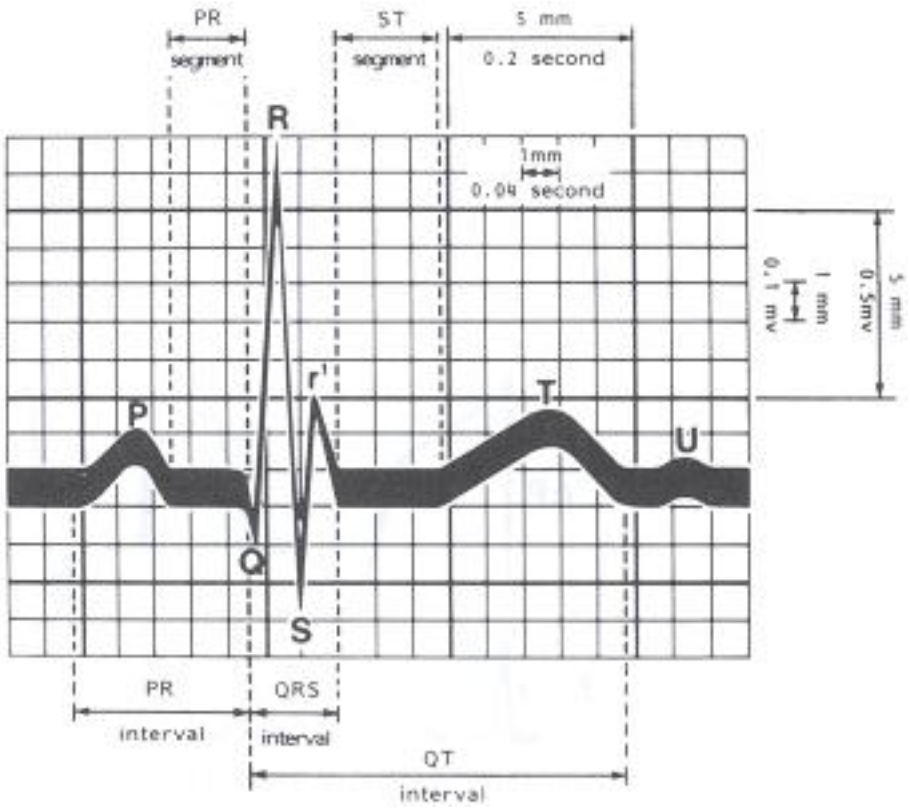

Figure 5-8. Typical heart beat waveform.

CHAPTER 6
CONCLUSION

6.1 Conclusive Comments

Wearable devices allow the monitoring of vital signs at home, and enable wirelessly transmitting of physiological data to a remote diagnostic center. In this work, we focus on monitoring the ECG signal, which is a crucial tool for cardiologists to diagnose the condition of a heart. The electrocardiogram (ECG) measures the electrical activity of the heart, and is probably the most representative and noninvasive test to diagnose cardiac disorders. The identification of an arrhythmia event involves detecting heart beats automatically, discriminating abnormal beats from normal beats, and identifying the type of arrhythmia.

For an automatic ECG diagnosis algorithm, retrieving characteristic points is essential. The QRS complex is the most significant characteristic waveform set of the cardiac cycle and corresponds to the depolarization of the ventricles in the heart. We evaluated the performance of different QRS detection algorithms, and selected one of the algorithms for our system.

We proposed a heart beat classification architecture, Heart Beat Cache, that benefits from the cache concept in Computer Architecture. The idea is to maintain a small table with low power such that it can fit into the small medical devices. The information recorded in the cache provides necessary matching attributes to clustering the heart beats.

Finally, the complete system of an autonomous single-channel processor for ECG monitoring is presented. The VLSI implementation with the pipeline datapath is described and a cycle-based timing diagram is given. The RTL implementation was functionally verified and was used for the generation of the FPGA synthesis report.

6.2 Future Lines of Research

6.2.1 Explore More Databases

To further test the performance of the architecture, we plan to use more arrhythmia databases from PhysioBank, such as *MIT-BIH Supraventricular Arrhythmia Database*, *MIT-BIH Malignant Ventricular Arrhythmia Database*, and *MIT-BIH Atrial Fibrillation Database*.

6.2.2 Intervals and Waves

To further distinguish different types of abnormal beats, characteristics that are not mentioned previously need be considered, including P-wave, PR-interval, QRS-interval, QT-interval, and QTc-interval. For example, APB (Atrial Premature Beat) has slightly prolonged PR-interval, and the RR-interval between two QRS enclosing APB is less than twice the normal RR-interval.

6.2.3 Heart Rate Variability

The rhythm of a healthy heart is actually surprising irregular even under resting conditions. Heart rate variability (HRV) has been widely studied as an indicator of the entrainment between brain and heart, as well as of cardiac performance after severe cardiac diseases and operations.

Figure 6-1. Sample plot for APB.

LIST OF REFERENCES

[1] B.-U. Kohler, C. Hennig, and R. Orglmeister, "The principles of software QRS detection," *Engineering in Medicine and Biology Magazine, IEEE*, vol. 21, no. 1, pp. 42-57, 2002.

[2] A. Armato, E. Nardini, Antonio Lanata, Gaetano Valenza, C. Mancuso, E. P. Scilingo, and D. De Rossi, "An FPGA based arrhythmia recognition system for wearable applications," *ISDA*, pp. 660-664, 2009.

[3] L. Senhadji, G. Carrault, J. J. Bellanger, and G. Passariello, "Comparing wavelet transforms for recognizing cardiac patterns," *IEEE Eng. Med. Biol. Mag.*, vol. 14, no. 2, pp. 167–173, Mar./Apr. 1995.

[4] Y. H. Hu, W. J. Tompkins, J. L. Urrusti, and V. X. Afonso, "Applications of artificial neural networks for ECG signal detection and classification," *J. Electrocardiol.*, vol. 26, pp. 66–73, 1993.

[5] Y. H. Hu, S. Palreddy, and W. J. Tompkins, "A patient-adaptable ECG beat classifier using a mixture of experts approach," *IEEE Trans. Biomed. Eng.*, vol. 44, no. 9, pp. 891–900, Sep. 1997.

[6] E. Patterson and B. J. Scherlag, "Decremental conduction in the posterior and anterior AV nodal inputs," *Journal of Interventional Cardiac Electrophysiology*, vol. 7, pp. 137-148, Oct. 2002.

[7] S. S. Barold, "Willem Einthoven and the birth of clinical electrocardiography a hundred years ago," *Cardiac Electrophysiology Review*, vol. 7, pp. 99-104, Jan 2003.

[8] E. Besterman and R. Creese, "Waller: Pioneer of electrocardiography," *British Heart Journal*, no. 42, pp. 61-64, 1979.

[9] M. Rivera-Ruiz, C. Cajavilca, and J. Varon, "Einthoven's string galvanometer: The first electrocardiograph," *Texas Heart Institute Journal*, vol. 35, no. 2, pp. 174-178, 2008.

[10] A. R. Perez Riera, C. Ferreira, C. F. Filho, M. Ferreira, A. Meneghini, A. H. Uchida, E. Schapachnik, S. Dubner, and L. Zhang, "The enigmatic sixth wave of the electrocardiogram: The U wave," *Cardiology Journal*, no. 5, pp. 408-421, 2008.

[11] R. C. Bourge, W. T. Abraham, P. B. Adamson, M. F. Aaron, A. Magalski, M. R. Zile, A. L. Smith, F. W. Smart, M. A. O'Shaughnessy, M. L. Jessup, B. Sparks, D. L. Naftel, and L. W. Stevenson, "Randomized controlled trial of an implantable continuous hemodynamic monitor in patients with advanced heart failure: The COMPASS-HF Study," *Journal of the American College of Cardiology*, vol. 51, no. 11, pp. 1073-1079, 2008.

[12] F. Braunschweig, B. Kjellstorm, M. Sodehall, N. Clyne, and C. Linde, "Dynamic changes in right ventricular pressures during haemodialysis recorded with an implantable haemodynamic monitor," *Nephrology Dialysis Transplantation*, vol. 21, no. 1, pp. 176-183, 2006.

[13] D. W. Reynolds, N. Bartelt, R. Taepke, and T. D. Bennett, "Measurement of pulmonary artery diastolic pressure from the right ventricle," *Journal of the American College of Cardiology*, vol. 25, no. 5, pp. 1176-1182, 1995.

[14] S. C. Malpas, "Neural influences on cardiovascular variability: possibilities and pitfalls," *American Journal of Physiology - Heart and Circulatory Physiology*, vol. 282, no. 1, pp. 16-20, 2002.

[15] C. Guger, G. Edlinger, R. Leeb, G. Pfurtscheller, A. Antley, M. Garau, A. Brogni, D. Friedman, and M. Slater, "Heart-rate variability and eventrelated ECG in virtual environments," in *Presence 2004: The 7th Annual International Workshop on Presence*, pp. 240-245, 2004.

[16] N. Thakor, J. Webster, and W. Tompkins, "Estimation of QRS complex power spectrum for design of a QRS filter," *IEEE Trans. Biomed. Eng.*, vol. 31, no. 11, pp. 702-706, 1984.

[17] S. Ding, X. Zhu, W. Chen, and D. Wei, "Derivation of respiratory signal from single-channel ECGs based on source statistics," *International Journal of Bioelectromagnetism*, vol. 6, no. 1, 2004.

[18] G. B. Moody, R. G. Mark, A. Zoccola, and S. Mantero, "Derivation of respiratory signals from multilead ECGs," *Computers in Cardiology*, vol. 12, pp. 113-116, 1985.

[19] J. O. Wisbeck, A. K. Barros, and R. G. Ojeda, "Application of ICA in the separation of breathing artifacts in ECG signals," *IEEE Trans. Biomed. Eng.*,1998.

[20] M. Costa, A. L. Goldberger, and P. C.-K., "Multiscale entropy analysis of biological signals," *Physical Review E*, vol. 71, 2005.

[21] L. A. Nunes Amaral, A. L. Goldberger, P. C. Ivanov, and H. E. Stanley, "Modeling heart rate variability by stochastic feedback," *Computers in Cardiology*, 1999.

[22] H.-X. Zhang, Y.-S. Zhu, and Z.-M. Wang, "Complexity measure and complexity rate information based detection of ventricular tachycardia and fibrillation," *Medical and Biological Engineering and Computing*, vol. 38, pp. 553-557, 2000.

[23] F. Gritzali, "Towards a generalized scheme for QRS detection in ECG waveforms," *Signal Processing*, vol. 15, pp. 183-192, Sept. 1988.

[24] E. Skordalakis, "Syntactic ECG processing: A review," *Pattern Recognition*, vol. 19, no. 4, pp. 305-313, 1986.

[25] R. Poli, S. Cagnoni, and G. Valli, "Genetic design of optimum linear and non-linear QRS detectors," *IEEE Transactions on Biomedical Engineering*, vol. 42, pp. 1137-1141, Nov 1995.

[26] L. Sornmo, O. Pahlm, and M.-E. Nygards, "Adaptive QRS detection: A study of performance," *IEEE Transactions on Biomedical Engineering*, vol. BME-32, pp. 392-401, Jun 1985.

[27] R. Murray, S. Kadambe, and G. F. Boudreaux-Bartels, "Extensive analysis of a QRS detector based on the dyadic wavelet transform," in Time-Frequency and Time-Scale Analysis, 1994., *Proceedings of the IEEE-SP International Symposium*, pp. 540-543, Oct 1994.

[28] N. Arzeno, Z.-D. Deng, and C.-S. Poon, "Analysis of first-derivative based QRS detection algorithms," *IEEE Transactions on Biomedical Engineering*, vol. 55, pp. 478-484, Feb. 2008.

[29] M. Aboy, J. McNames, T. Thong, D. Tsunami, M. S. Ellenby, B. Goldstein, and A. Member, "An automatic beat detection algorithm for pressure signals," *IEEE Transactions on Biomedical Engineering*, October 2005.

[30] M. Okada, "A digital filter for the QRS complex detection," *IEEE Transactions on Biomedical Engineering*, vol. BME-26, pp. 700-703, Dec 1979.

[31] F. Chiarugi, V. Sakkalis, D. Emmanouilidou, T. Krontiris, M. Varanini, and I. Tollis, "Adaptive threshold QRS detector with best channel selection based on a noise rating system," in *Computers in Cardiology*, pp. 157-160, October 2007.

[32] I. I. Christov, "Real time electrocardiogram QRS detection using combined adaptive threshold," *BioMedical Engineering OnLine*, vol. 3, no. 1, p. 28, 2004.

[33] W. A. H. Engelse and C. Zeelenberg, "A single scan algorithm for QRS detection and feature extraction," *Computers in Cardiology*, vol. 6, pp. 37-42, 1979.

[34] J. Pan and W. J. Tompkins, "A real-time QRS detection algorithm," *IEEE Transactions on Biomedical Engineering*, vol. 32, pp. 230-236, March 1985.

[35] P. Baldi, S. Brunak, Y. Chauvin, C. A. F. Andersen, and H. Nielsen, "Assessing the accuracy of prediction algorithms for classification: an overview," *Bioinformatics*, vol. 16, no. 5, pp. 412-424, 2000.

[36] J. Thomas, J. Lewis, K. W. Clark, C. N. Mead, K. L. Ripley, B. F. Spenner, J. Oliver, and G. Charles, "Automated cardiac dysrhythmia analysis," *Proceedings of the IEEE*, vol. 67, pp. 1322-1337, Sep 1979.

[37] M. Botsivaly, C. Koutsourakis, and B. Spyropoulos, "Evaluation of a new technique for the detection of ventricular fibrillation and ventricular tachycardia," in *22nd Annual EMBS International Conference*, pp. 938-941, 2000.

[38] J. Millet-Roig, J. Lopez-Soriano, A. Mochol, R. Ruiz-Granell, and R. Garcia-Civera, "An additional and easy algorithm based on morphological analysis of unipolar electrogram: Missclassification in implantable cardioverters-defibrillators," *Computers in Cardiology*, vol. 25, pp. 561-564, 1998.

[39] M. Engin, "ECG beat classification using neuro-fuzzy network," *Pattern Recognition Letters*, vol. 25, pp. 1715-1722, 2004.

[40] M. Bahmanyar and W. Balachandran, "Beat to beat classification of long electrocardiograms using entropies and hierarchical clustering," in *IEEE Engineering in Medicine and Biology 27th Annual Conference*, pp. 5579-5581, 2005.

[41] J. Nolan, P. D. Batin, R. Andrews, S. J. Lindsay, P. Brooksby, M. Mullen, W. Baig, A. D. Flapan, A. Cowley, R. J. Prescott, J. M. Neilson, and K. A. Fox, "Prospective study of heart rate variability and mortality in chronic heart failure: Results of the united kingdom heart failure evaluation and assessment of risk trial (UK-Heart)," *Circulation*, vol. 98, no. 15, pp. 1510-1516, 1998.

[42] G. Zuanetti, J. M. Neilson, R. Latini, E. Santoro, A. P. Maggioni, and D. J. Ewing, "Prognostic significance of heart rate variability in post-myocardial infarction patients in the fibrinolytic era: The GISSI-2 results," *Circulation*, vol. 94, no. 3, pp. 432-436, 1996.

[43] H. V. Huikuri, T. Seppanen, M. J. Koistinen, K. J. Airaksinen, M. Ikaheimo, A. Castellanos, and R. J. Myerburg, "Abnormalities in beat-to-beat dynamics of heart rate before the spontaneous onset of life-threatening ventricular tachyarrhythmias in patients with prior myocardial infarction," *Circulation*, vol. 93, no. 10, pp. 1836-1844, 1996.

[44] J. Bigger, J. Thomas, J. L. Fleiss, R. C. Steinman, L. M. Rolnitzky, R. Kleiger, and J. Rottman, "Frequency domain measures of heart period variability and mortality after myocardial infarction," *Circulation*, vol. 85, no. 1, pp. 164-171, 1992.

[45] J. Bigger, J. Thomas, R. C. Steinman, L. M. Rolnitzky, J. L. Fleiss, P. Albrecht, and R. J. Cohen, "Power law behavior of RR-interval variability in healthy middle-aged persons, patients with recent acute myocardial infarction, and patients with heart transplants," *Circulation*, vol. 93, no. 12, pp. 2142-2151, 1996.

[46] H. V. Huikuri, T. H. Makikallio, K. E. J. Airaksinen, T. Seppanen, P. Puukka, I. J. Raiha, and L. B. Sourander, "Power-law relationship of heart rate variability as a predictor of mortality in the elderly," *Circulation*, vol. 97, no. 20, pp. 2031-2036, 1998.

[47] K. K. L. Ho, G. B. Moody, C.-K. Peng, J. E. Mietus, M. G. Larson, D. Levy, and A. L. Goldberger, "Predicting survival in heart failure case and control subjects by use of fully automated methods for deriving nonlinear and conventional indices of heart rate dynamics," *Circulation*, vol. 96, no. 3, pp. 842-848, 1997.

[48] H. V. Huikuri, T. H. Makikallio, C.-K. Peng, A. L. Goldberger, U. Hintze, and M. Moller, "Fractal correlation properties of R-R interval dynamics and mortality in patients with depressed left ventricular function after an acute myocardial infarction," *Circulation*, vol. 101, no. 1, pp. 47-53, 2000.

[49] R. W. Glenny, H. T. Robertson, S. Yamashiro, and J. B. Bassingthwaighte, "Applications of fractal analysis to physiology," *J Appl Physiol*, vol. 70, no. 6, pp. 2351-2367, 1991.

[50] P. C. Ivanov, L. A. Nunes Amaral, A. L. Goldberger, S. Havlin, M. G. Rosenblum, H. E. Stanley, and Z. R. Struzik, "From 1/f noise to multifractal cascades in heartbeat dynamics," *Chaos*, vol. 11, no. 3, pp. 641-652, 2001.

[51] U. Rajendra Acharya, K. Paul Joseph, N. Kannathal, C. M. Lim, and J. S. Suri, "Heart rate variability: a review," *Med Biol Eng Comput*, vol. 44, pp. 1031-1051, December 2006.

[52] A. Amann, R. Tratnig, and K. Unterkoer, "Reliability of old and new ventricular fibrillation detection algorithms for automated external defibrillators," *BioMedical Engineering OnLine*, vol. 4, no. 1, p. 60, 2005.

[53] L. J. T. Jr., K. W. Clark, C. N. Mead, K. L. Ripley, B. F. Spenner, and G. C. O. Jr., "Automated cardiac dysrhythmia analysis," *Proceedings of the IEEE*, vol. 67, pp. 1322-1337, september 1979.

[54] T. Dahan and A. Sade, "Application of ICA in removing artifacts from the ECG," Master's thesis, Israel Institute of Technology, 2004-2005.

[55] N. Thakor, Y. Zhu, and K. Pan, "Ventricular tachycardia and fibrillation detection by a sequential hypothesis testing algorithm," *IEEE Trans Biomed Eng*, vol. 37, no. 9, pp. 837-843, 1990.

[56] G. Ersoy and M. Holewijn, "Development of a QRS detector algorithm for ECG's measured during centrifuge training," in *Proceedings of the 18th Annual International Conference of the IEEE*, vol. 4, pp. 1390-1391 vol.4, Nov 1996.

[57] C. M. van Ravenswaaij-Arts, L. A. Kollee, J. C. Hopman, G. B. Stoelinga, and H. P. van Geijn, "Heart rate variability," *Ann Intern Med*, vol. 118, pp. 436-447, March 1993.

[58] C.-K. Peng, S. Havlin, J. Hausdor, J. Mietus, H. Stanley, and A. Goldberger, "Fractal mechanisms and heart rate dynamics: Longrange correlations and their breakdown with disease," *Journal of Electrocardiology*, vol. 28, no. Supplement 1, pp. 59-65, 1995. Research and Technology Transfer in Computerized Electrocardiology.

[59] A. Shukla and L Macchiarula, "A Fast and Accurate FPGA Based QRS Detection System," in *30th Annual EMBS International Conference*, pp. 4828-4831, 2008.

[60] M. Cvikl and A. Zemva, "FPGA-based System for ECG Beat Detection and Classification," *IFMBE Proceedings 16, Medicaon 2007*, pp. 66-69, 2007.

[61] Elmore, Kimberly L., Michael B. Richman, "Euclidean distance as a similarity metric for principal component analysis," *Monthly Weather Review*, 129, 540-549.

[62] J. L. Hennessy and D. A. Patterson, "Computer architecture: A quantitative approach (third edition)", *Morgan Kaufmann Publishers*, San Francisco, CA, USA.

[63] F. Castells, P. Laguna, L. Sornmo, A. Bollmann and J. M. Roig, "Principal component analysis in ECG signal processing," *URASIP Journal on Advances in Signal Processing*, Vol. 2007.

[64] K. Beyls and E. H. D'Hollander, "Reuse distance as a metric for cache behavior," *Proceedings of PDCS'Ol*, pages 617-662, Aug 2001.

[65] M. Zeng, J.-G. Lee, G.-S. Choi and J.-A. Lee, "Intelligent sensor node based a low power ECG monitoring system", *IEICE Electron. Express*, Vol. 6, No. 9, pp.560-565, 2009.

[66] Al-Nashash, "A dynamic Fourier series for the compression of ECG using FFT and adaptive coefficient estimate," *Medical Engineering and Physics*, 17, 197-203.

BIOGRAPHICAL SKETCH

Chung-Ching Peng was born in Taipei, Taiwan, ROC. The older of two children, he grew up mostly in Taipei, Taiwan, graduating from Affiliated Senior High School of National Taiwan Normal University (HSNU) in 1997. Chung-Ching received the B.S. degree in Electrical and Control Engineering from National Chiao Tung University (NCTU), Hsinchu, Taiwan, in June 2001.

In July 2001, Chung-Ching enlisted in the Navy as an Ensign for his mandatory military service. During his service in the Navy (1 year and 8 months), Chung-Ching was a battalion-level human resource and computer system officer in charge.

Upon completion of his military duty in March 2003, Chung-Ching was then enrolled in the Computer and Information Science and Engineering Department (CISE) at University of Florida as a teaching assistant, in August 2003, and Electrical and Computer Engineering Department (ECE) as an Alumni Fellowship recipient, in August 2006. His research interests are computer architecture, low-power VLSI and biomedical signal processing. His research advisor is Dr. Jih-Kwon Peir.

Chung-Ching received the M.S. degree in Computer and Information Science and Engineering (CISE), and the Ph.D. degree in Electrical and Computer Engineering (ECE) from University of Florida, in August 2006 and April 2011 respectively. He will work at MaxLinear Inc., in Carlsbad, CA with their ASIC group as a Member of Technical Staff.